Integrated Terrestrial Simulations over Europe: Groundwater-Atmosphere Feedbacks with Altered Water Tables Including the Effect of Recent Droughts

Dissertation

zur

Erlangung des Doktorgrades (Dr. rer. nat.)

der

Mathematisch-Naturwissenschaftlichen Fakultät

der

Rheinischen Friedrich-Wilhelms-Universität Bonn

vorgelegt von

Carl Martin Hartick

aus

Darmstadt

Bonn 2023

Angefertigt mit Genehmigung der Mathematisch-Naturwissenschaftlichen Fakultät
der Rheinischen Friedrich-Wilhelms-Universität Bonn

1. Gutachter: Prof. Dr. Stefan J. Kollet, Forschungszentrum Jülich
2. Gutachter: Prof. Dr. Clemens Simmer, Rheinische Friedrich-Wilhelms-Universität Bonn

Tag der Promotion: 26.06.2023
Erscheinungsjahr: 2023

Abstract

The groundwater flow is an essential part of the terrestrial system encompassing the atmosphere, land surface, and subsurface. In past research, there was usually no focus on water in the subsurface because climate models worked with simplified free drainage assumptions. However, recent research has shown that the groundwater table has a vital memory function, especially in hydrometeorological extremes. Droughts are remembered for long timescales, but surpluses in groundwater can also mitigate current water deficits. Groundwater can also interact in feedback loops altering the water and energy cycle.

Suited to investigate these research questions in a modeling environment is the Terrestrial Systems Modeling Platform (TSMP). TSMP couples an atmospheric, land surface and subsurface model to simulate the whole water cycle from the bedrock to the cloud top. Three studies exploring groundwater interactions utilizing TSMP over Europe are combined in this thesis. First, groundwater memory and predictability are investigated by combining three states of recent droughts with past atmospheric boundary conditions leading to a model ensemble with varying drought initial conditions. The ensemble was simulated for one year resembling atmospheric uncertainty and natural variability. The results show the increased probability of ongoing drought conditions and the dominant influence of the initial condition on the timescale of one year over atmospheric forcing.

Secondly, the results of the drought ensembles are compared to the original realization of the years not influenced by drought conditions. The comparison reveals changes in the energy cycle with more available energy at the surface. Together with changes in cloud properties, the results indicate a drought feedback loop where the persisting water deficits contribute to higher and thinner clouds leading to increased incoming shortwave radiation at the ground.

Lastly, potential feedback processes between groundwater and precipitation are further investigated, showing that a climatology with a shallower water table due to changed parameters also influences rainfall at the continental scale. This feedback connecting groundwater and precipitation makes calibration impossible in a fully coupled system. Furthermore, the feedback highlights the potential influence of altered water tables due to climate change in the future.

The results of this thesis highlight the importance of incorporating groundwater in climate models, especially in hydrometeorological extremes. Significant interactions are observed between all components of the terrestrial system, which would otherwise be overlooked. While including a complex groundwater representation is connected to additional computational costs, feedback processes strongly influencing atmospheric processes are essential for climate projections. Further improvement of the physical representation of numerical models and increased resolutions might additionally emphasize the connections in the future.

Contents

Chapter 1

Introduction

1.1 The Terrestrial System

The terrestrial system - stemming from the Latin word for earth, *terra* - includes all processes that occur over the land mass. Although the continents are only a fraction compared to other components of planet earth, they are the site of human life and socioeconomic well-being. Most (70%) of the earth's surface is covered by water, mainly oceans with salt water (Tang and Oki, 2016). The seas reach a depth of up to $11\,\mathrm{km}$ and are essential for regulating the air temperature and CO_2 levels (David et al., 2004). The other central component is the atmosphere, which covers the surface by up to $100\,\mathrm{km}$ with diminishing density at higher levels.

Land masses are crucial for life and thus for the terrestrial system's development. Flora and fauna developed in the oceans, but a new evolution began when plants and animals first populated the land. Widespread photosynthesis changed the composition of the atmosphere through the release of free oxygen (Lyons et al., 2014). The increasingly many animals on earth breathed oxygen and exhaled CO_2, changing the balance of the carbon cycle.

Today, the most influential aspect of the ecosystem on land is humans. Since the evolution of modern humans, we have interfered with the ecosystem to increase the growth of our species. With the beginning of the industrial age, this interference by humans was greatly increased, especially through the release of greenhouse gases, which have raised mean temperatures globally. The impact of humanity might become so extensive that the start of a new geologic epoch, the Anthropocene, might become a reality (Waters et al., 2016).

The influence of the land surface on the carbon cycle, which in turn affects radiation in the atmosphere and the acidity of oceans, is an example of the interaction between major components of the earth. Another example is the global water cycle, which directly connects the land surface, the subsurface, the oceans and the atmosphere. The crucial connecting processes are evaporation and precipitation. Over the oceans, there is a net flux of water to the atmosphere, initiating the transport process of water to the land because evaporation outweighs precipitation. The water flux to the land surface is accelerated by general atmospheric circulation that is created by the temperature differences between the tropics and the poles.

Overland precipitation, such as rain, snow, hail or graupel, falls in various forms. The canopy intercepts the total rainfall by storing small amounts of water, while the throughfall reaches the ground. Water can infiltrate the subsurface at the ground or may be carried directly to river systems as runoff. At the surface, the water may instantly evaporate or transpire from the stomata of plants. The term evapotranspiration refers to overland processes that combine to transport water back to the atmosphere. Usually, precipitation exceeds evapotranspiration at the land surface. Therefore, the water cycle is completed by continental river systems transporting water back to the ocean.

Each component in the water cycle has water reservoirs, the biggest being the oceans. Small amounts of water are stored in the atmosphere as water vapor. Within the land surface are relatively small stores such as lakes, soil moisture interception water and large reservoirs in the form of ice, along with glaciers, snow and permafrost (Tang and Oki, 2016). Groundwater stored in the subsurface is a large reservoir that far exceeds smaller stores like freshwater lakes. Groundwater can influence land processes by serving as a water source in dry periods through - for example - capillary rise for vegetation or groundwater abstraction to provide for human needs. While deep storage in the earth's crust can be up to millions of years old and remains largely untouched, groundwater up to $2\,\mathrm{km}$ deep is actively involved in the water cycle (Gleeson et al., 2016).

Because of the various interactions occurring on and across the land surface, analyses of the terrestrial system must consider processes in the low levels of the atmosphere, the subsurface (with variably saturated groundwater) and the land surface itself. The ocean also influences the terrestrial system through the sea level and surface temperatures.

This work focuses on the terrestrial system encompassing the atmosphere, the land surface and the subsurface. It does not consider the oceanic influences. More precisely, it aims to understand feedbacks from the groundwater to the atmosphere, as simulated with numerical modeling. This chapter lays out the context and background, and the research questions are presented at the end of the chapter.

1.1.1 The Atmosphere

The atmosphere covers the earth from its surface to around $100\,\mathrm{km}$ into space, with an approximately exponential decrease in density with increasing altitude. Due to this rapid decline, the most critical processes influencing the surface happen in the troposphere, within the first $10\,\mathrm{km}$. Within this range, a distinction exists between the boundary layer, which is heavily influenced by the roughness of the surface of earth (located within the first few kilometers) and the free atmosphere.

In percentage of volume, the atmosphere consists of 78% N_2, 21% O_2, 0.93% AR and around 0.5% H_2O. Additionally, it contains a current concentration of approximately $415\,\mathrm{ppm}$ CO_2 as well as noble gases (Marshall and Plumb, 1989). Water is thus a rather small atmospheric component.

Water displays a high-frequency exchange between the ocean and the surface. Averaged globally, water has a residence time between 8 and 10 days, with variations across regions and seasons. In winter, the residence times are shorter than in summer; residence times are also generally lower over the ocean than overland (Van Der Ent and Tuinenburg, 2017). The age of water in the atmosphere can be connected to typical timescales in the atmosphere. Standard frontal systems exist within a timescale of several days, whereas for meteorological timescales they are longer-lived. Only baroclinic waves or long waves such as planetary Rossby waves have a time scale of up to a month or a year, respectively (Orlanski, 1975). They influence the development over large spatial

scales of several thousand kilometers. Smaller in scale than frontal systems are local thunderstorms, tornadoes, deep convection and turbulence in the form of small eddies close to the surface. Most of these convection processes must be parameterized in numerical models.

The fact that processes in the atmosphere primarily operate at relatively small time scales and are rapidly evolving makes it difficult to predict the state of the atmosphere over longer time scales. Furthermore, the atmosphere is a chaotic system, and small errors in observations and the model employed may lead to substantial differences in predictions. Rigorous global evaluation has shown that skillful weather predictions are only possible up to 10 days (Krishnamurthy, 2019). For specific regions, useful information can be obtained from forecasts of up to 14 days, and the theoretical limit is assumed to be around 15 days (Stern and Davidson, 2015). Nevertheless, forecast quality has improved vastly over the years and might continue to improve.

1.1.2 The Land Surface

The land surface is diverse. There exist regions covered with rocks, sand, grassland, crops and forests, along with wetlands and urban areas. These regions differ in how they handle precipitation, evapotranspiration and energy partitioning. If plants cover the land surface, the characteristics often vary greatly during the year according to the growing season and harvesting of crops and the fall of leaves in deciduous forests. Furthermore, within one plant category - such as crops - there can be significant differences in plant characteristics, such as the leaf area index or the stomatal conductance.

Land cover changes initiated by events such as economic change, anthropogenic influence or climate change have a considerable impact on the atmosphere. The changes can be local, such as clearing a small forest, ranging to continental-level changes, such as the political collapse of the Soviet Union.

Land cover changes associated with ancient societies can be studied with climate models (Gilgen et al., 2019). Despite many uncertainties, it can be demonstrated that changes in land cover can lead to significant warming and cooling. Land cover changes associated with widespread change in human societies have extended timescales, ranging from a year to decades, with large spatial extents. When vegetation is constant in smaller timescales, evapotranspiration rates vary on the timescale of a few minutes to one day due to the small storage capacity of interception water on the land surface.

The land surface influences the atmosphere in various ways. First, plant cover alters the CO_2 cycle; second, the available water determines evapotranspiration; and third, the energy budget and the surface roughness alter the momentum flux. CO_2 plays an essential role in global warming and is critical for photosynthesis. To take up CO_2, plants open their stomata, which are otherwise closed to limit the water loss from transpiration. Therefore, plant uptake of CO_2 increases transpiration, which in turn increases the water flux to the atmosphere, constituting a critical link between CO_2 and the water cycle. In

dry conditions, plants reduce their water loss and open fewer stomata, limiting their gross primary production (Gentine et al., 2019).

The subsurface also influences the available water for root water uptake and evapotranspiration. Shallow water tables can replenish soil water via capillary rise, and additional human influence occurs through irrigation in agricultural regions. Modeling has shown that the extra water introduces a cooling effect and has a regionally varying impact on the energy budget and precipitation rates (Cook et al., 2011). The energy budget and the surface roughness of the land surface further influence local weather. Both are important for the planetary boundary layer's extent and stability, altering regional wind patterns (Mahmood et al., 2014).

1.1.3 The Subsurface

Water is found everywhere in the continental crust, although it can be disconnected from processes at the surface. For example, groundwater reservoirs can be up to millions of years old (Gleeson et al., 2016). These reservoirs are relatively insensitive to recharge variability in the short term and present the most extended timescales for subsurface water, at around 10,000 years (Cuthbert et al., 2019). Regions with a shallow water table are closely connected to land surface processes; in such areas, seasonal variations of groundwater or droughts have timescales of a few months up to a year. The soil moisture close to the surface and the streamflow, which are standard variables to forecast, have even shorter timescales of a few days (Brutsaert, 2005).

Overall, water in the subsurface operates at longer timescales than in the atmosphere. Nonetheless, in hydrology, highly local processes can play an important role even at the pore scale. For example, the number of pores of a few mm established by roots and earthworms can determine soil moisture transport during and after heavy precipitation events (Vereecken et al., 2022). Other typical hydrological scales are also smaller than typical atmospheric timescales - such as the hillslope scale, which is between $1\,\mathrm{m}$ and $100\,\mathrm{m}$, and the catchment scale, which starts at a few hundred meters and can reach up to a few hundred kilometers. However, large continental river systems like the Danube, the Amazon or the Nile span several thousand kilometers and have a continental impact.

Many authors propose a categorization of the subsurface into distinct zones. For example, Robinson and Ward (2017) offered the following zones: the soil zone, the intermediate zone, the water table and the fully saturated zone above an impermeable bedrock. The zones are differentiated by the most influential process, such as the interactions with the root system for the soil zone. Other authors describe only two categories, the unsaturated or vadose zone and the saturated zone (Stumpp and Kammerer, 2022). The lack of consensus stems from the fact that research on the subsurface is interdisciplinary and researchers are interested in different aspects. Examining the subsurface from the perspective of the terrestrial water cycle leads to a continuum approach, in which all water - from surface water through the soil to the water table - is connected, without strict borders (Kumar et al., 2009). This approach also allows for connecting subsurface

water to vegetation and the atmosphere.

1.2 Major Feedbacks in the Coupled Terrestrial Water and Energy Cycle

The connections of the terrestrial system through the energy and water cycle lead to various feedback mechanisms. In the case of hydroclimatic extremes, such as heatwaves and droughts, these mechanisms are most apparent. Figure 1.1 provides a schematic overview of feedback during droughts, adapted from Miralles et al. (2019). Reduced evaporation and transpiration by plants due to water limitation exert positive feedback on temperature, such that temperatures rise because of reduced evaporative cooling.

In more detail, soil moisture-temperature coupling involves three main relationships. The first is the strong connection between soil moisture and evapotranspiration in transitional zones. Second, reduced evapotranspiration leads to an increase in sensible heat, which increases the air temperature. Lastly, high temperatures raise the demand for water through a water pressure deficit, leading to additional evapotranspiration (Seneviratne et al., 2010). Evidence for the connection between soil moisture and evapotranspiration has been documented in observational studies (Teuling et al., 2006) and in modeling (Koster et al., 2006; Barlage et al., 2021; Furusho-Percot et al., 2022). Reduced evapotranspiration may also negatively impact precipitation through reduced convection and less local moisture recycling. Processes related to both temperature and rain may lead to further continental desiccation, prolonging and strengthening the drought and initiating a feedback loop.

An additional layer of complexity is added if groundwater interacts in the feedback loops. With a shallow groundwater table, surface soil moisture can be recharged with water even if precipitation is lacking. By contrast, prolonged droughts eventually affect groundwater storage, leading to deeper water tables and reduced capillary rise toward the root zone and land surface.

Figure 1.1 simplifies the feedback loop in several regards. For example, plant physiological processes involve additional factors, such as interactions with atmospheric CO_2 concentrations. Concerning atmospheric processes, changes in evapotranspiration do not always impact precipitation. Local moisture recycling may be negligible if local rainfall mainly depends on marine-influenced large-scale weather patterns. However, changes in the energy budget can have various other influences on the atmosphere, such as changes in the boundary layer height, which in turn affects clouds and incoming solar radiation. Another aspect of importance is the teleconnection of drought events. Potentially, droughts create water deficits downstream of the leading wind patterns if the downstream region depends on evaporated water in the original drought region. This teleconnection is challenging and needs additional research (Miralles et al., 2019). The following subsections present a detailed discussion of examples of feedback mechanisms.

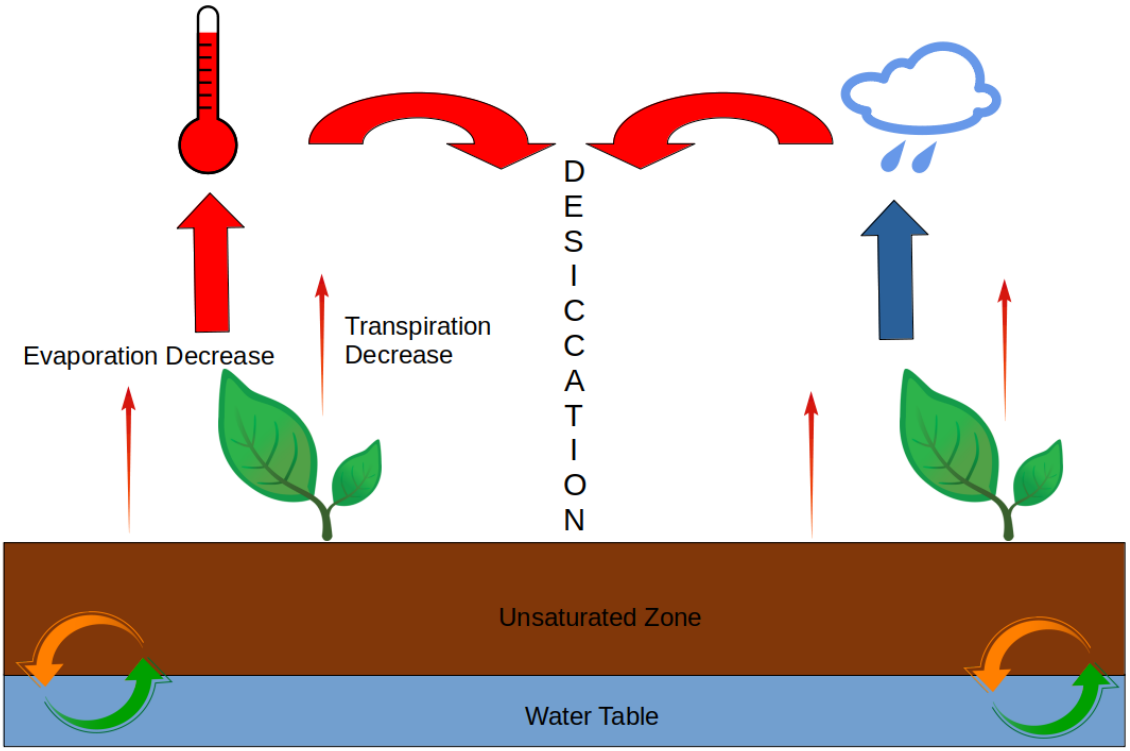

Figure 1.1: Feedback mechanisms during drought. Red arrows indicate positive feedback on temperature and desiccation; blue arrow depicts negative feedback on precipitation. Adapted from Miralles et al. (2019).

1.2.1 Groundwater Memory

Two major hydrologic storage systems impact the availability of water at the surface and streamflow generation, namely snow and groundwater. Snow melt is recognized as a freshwater resource; roughly 1.5 billion people worldwide depend on freshwater from mountains (Viviroli et al., 2020), and 53% of the streamflow in the western United States stems from snow melt (Li et al., 2017). In mountainous regions, water from snow melt is even more dominant, at 70%.

Brooks et al. (2021) showed that including groundwater storage in a model significantly improved streamflow prediction, even for mountainous regions. The reason is that groundwater abundance indicates that rain is routed efficiently to streamflow. Overall, groundwater is essential for many ecosystems, including lakes, swamps and rivers. The amount of regulation it provides varies seasonally and regionally. For example, a river can gain water from groundwater if the river's water level is below the groundwater level. In the reversed case, water infiltrates from the river into the soil (Kløve et al., 2011). The ability of groundwater to influence rain routing and river levels demonstrates its importance beyond the immediate impact on water availability.

One approach to groundwater memory is not solely dependent on how much water can

be stored in a soil column but also the system's response time to return to an equilibrium state (Cuthbert et al., 2019). A common formula for this approach is the groundwater response time (GRT),

$$\text{GRT} = \frac{L2s}{\beta T}$$

where L is the spatial scale of the system [L], s is the storativity $[-]$, β is a dimensionless constant and T is the transmissivity $[\text{L}^2\text{T}^{-1}]$. With the inclusion of L, this approach includes the size of the groundwater system, enabling the comparison of different catchments. Researchers often assume that the volume of groundwater is modeled with a cosine function to apply this equation. In the case of stooped recharge, the groundwater decays exponentially, determined by the GRT. Under these assumptions, β is equal to π^2.

The basis of the above approach dates to the early 1970s (Downing et al., 1974). Other approaches might be useful, such as applying a transfer function (Opie et al., 2020):

$$H(t) = \int_{\infty}^{t} p(\tau)\theta(t-\tau)d\tau$$

where H is the output state at time t, p is the input state, τ is the delay time between input and output and θ is the transfer function. The parameters for the transfer function are derived from convolutional modeling (Long and Mahler, 2013) or with a linear transformation time series model (Von Asmuth and Knotters, 2004). A more straightforward approach for calculating the response time of groundwater is to determine the point in time needed to diminish a groundwater anomaly to $1/e$ of its value (Lo and Famiglietti, 2010).

The presented mathematical expressions need sufficient data to measure groundwater memory. That is hard to accomplish on a continental scale or even a regional scale, such as for Central Europe. However, groundwater memory can be determined in hydrological modeling by initializing one model with multiple initial conditions and one forcing, according to Wood and Lettenmaier (2008). Under the same forcing, the multiple initial conditions converge to one state; the timespan to reach this state can then be used to estimate groundwater memory. The estimation depends on the hydraulic parameters of the hydrologic model (MacLeod et al., 2016).

Groundwater memory has various impacts on hydrologic response and prognostic modeling. For example, comparison of different catchments shows that varying hydrologic memory significantly influences predictability and the success rate of early warning systems for droughts (Sutanto and Van Lanen, 2022). In specific catchments, abundant groundwater can increase evapotranspiration rates in summer by up to 30% for several years. However, groundwater memory is often assumed to be most influential in arid regions (Opie et al., 2020). In humid regions, water resources are strongly correlated to recent precipitation. Nonetheless, the occurrence of droughts with marked anomalies highlight the importance of groundwater memory. Even oceanic regions like Scotland

experienced groundwater deficits in the summer of 2017, with continuing effects until late 2018 (Soulsby et al., 2021). Due to short response times in relatively humid regions in Europe, the impact of groundwater memory can quickly diminish.

1.2.2 Energy Balance Feedbacks

The following equation describes the basic land surface energy balance:

$$RNET=LH+SH+GH$$

where RNET is the net downward radiation, partitioned into latent heat (LH), sensible heat (SH) and ground heat (GH) flux. Hence, RNET is the sum of net values of shortwave and longwave radiation at the surface. Clouds determine the incoming parts of these net values in the atmosphere. Dense cloud cover reduces incoming shortwave radiation but reflects emitted longwave radiation from the ground

Cloud properties can be altered by the surface energy fluxes, connecting the incoming energy from the atmosphere and the land energy balance. An increase in sensible heat increases cloud height, which leads to less dense clouds, whereas an increase in latent heat has the opposite effect (Betts, 2004). The available water strongly influences the energy balance at the surface. When water resources are sparse, evapotranspiration is soil moisture limited. The opposite case is energy limitation. Here, the incoming energy determines the latent heat flux, which provides evaporative cooling or could influence precipitation (Koster et al., 2004). In both regimes, energy balance feedback mechanisms often play a minor role. Under conditions of energy limitation, large-scale weather systems are highly influential and relatively resistant to an altered latent heat flux from the surface

In dry regions, the soil moisture controls evapotranspiration; however, compared to wet regions, the overall flux is too small to affect the local climate. Therefore, strong soil moisture-evapotranspiration coupling often occurs in transitional regions between soil moisture and energy limitation (Seneviratne et al., 2010). The Mediterranean region and California are typical transitional regions. In addition, the categorization of a region can vary over time; for example, California may experience a dry, transitional or wet regime within a single year (Ryu et al., 2008).

1.2.3 Moisture Recycling

Moisture recycling describes the principle that water evaporating from the land surface contributes to regional precipitation, thereby establishing a regional water cycle. The cloud-building process relies not only on surface water vapor but also on atmospheric stability and the large-scale weather situation. The latter dynamics influence air parcel lifting, which is key in cloud- and precipitation-forming processes.

Global modeling studies (Koster et al., 2006) and regional climate modeling have doc-

umented the positive feedback between evapotranspiration and precipitation (Pal and Eltahir, 2001; Su and Dickinson, 2017). Various studies have shown that mesoscale circulations favor the development of clouds over relatively dry soils because of increased moisture convergence (Taylor et al., 2007; Lee et al., 2019). A recent study illustrated this process on a global scale using model and reanalysis data (Zhou et al., 2021). The results indicated that the water availability in drylands was reduced by negative feedback between the soil moisture and precipitation. However, large discrepancies occurred between the different models used in that study, and the correlations obtained were significant only in a few areas. Overall, the complexities are ubiquitous: the heterogeneity of spatial moisture availability, the parametrization of convective processes in modeling and the influence of atmospheric conditions all interfere with local moisture recycling. At the moment, a general answer cannot be given whether feedbacks between evapotranspiration and precipitation are negative or positive.

Like soil moisture-temperature feedback, precipitation feedback can be categorized into three processes. Close to the soil moisture-temperature coupling, the first process is the connection between soil moisture and evapotranspiration. This link is most important in transitional regions between water and energy limitation. The second process is the influence of evapotranspiration on precipitation, which is an ambiguous relationship. Negative feedback has often been found in local simulations, where the lack of evapotranspiration leads to moisture advection and initiates rainfall. In regional to global simulations, the feedback is positive, with evapotranspiration enhancing precipitation. Regions with substantial positive feedback are also likely to show a strong soil moisture-temperature coupling. The third process is straightforward under many circumstances: precipitation increases the soil moisture. Excessive rainfall is converted to runoff rather than soil moisture only in the case of utterly dried-out soils (Seneviratne et al., 2010).

1.3 Models and Data for Hydrometeorological Extremes

The different time and spatial scales in the terrestrial system pose a challenge for numerical modeling. The rapidly evolving atmosphere cannot be predicted for lengthy time scales, but it provides the essential forcing for slower processes in the land and subsurface. Observations are also not equally available. For example, atmospheric data is available worldwide in nearly real-time and is relatively easy to process from various remote sensing measurements, whereas it is more complex to obtain subsurface parameters, and groundwater measurements are spatially not always representative.

It is advantageous to combine atmospheric, land-surface and hydrologic models. New computer architectures and better scalability of models allow for increasing numbers of applications for fully coupled terrestrial climate simulations to demonstrate the feedback processes. Including the subsurface enables comprehensive assessments because of the slowly changing conditions in the subsurface. The droughts in Europe in 2018 and 2022

and other hydrometeorological extremes have highlighted this demand.

1.3.1 Hydrometeorological Extremes

The primary hydrometeorological extremes are droughts and floods, which are respectively associated with precipitation deficits and extreme precipitation events. Extremes can be particularly complex during compound events, where catastrophic conditions occurring in atmospheric processes interact with anomalies in the land and subsurface. During floods, this can mean increased runoff because the subsurface is already saturated or there is dried-out soil that cannot absorb the water quickly enough. In the case of hot conditions, there may be ongoing drought due to absent precipitation and water deficits in the subsurface (Zhang et al., 2021). The combination of heatwaves with wet conditions in the subsurface can lead to increased heat stress, especially near big cities with high temperatures and relative humidity (Yuan et al., 2020).

The interest in hydrometeorological extremes as compound events provides a compelling argument for investigating terrestrial feedbacks. Droughts and floods are responsible for vast economic loss; for example, in the United States, floods cost an average of 4 billion dollars per year. Droughts accounted for an average loss of 1.6 billion dollars annually between 1996 and 2016. The differences in costs can be explained by the fact that more floods are recorded and losses are more measurable compared to droughts (Zhou et al., 2018). Some droughts last decades, such as the one in south-western United States, with long-term impacts on society and the ecology (Kogan and Guo, 2015).

Central Europe recently experienced a drought originating from the 2018 heatwave, in which 38 Mha of agricultural land was severely affected by drought conditions (Peters et al., 2020). Dry conditions continued in the following years, with damaging impacts on forests. After a wet year in 2021, the situation worsened again in 2022, with the lack of streamflows reducing the energy generation and stopping river transport routes (Toreti A. et al., 2022). The most recent impactful flood occurred in 2021 over the western part of Germany, Belgium, France, Luxembourg and the Netherlands. In Germany, 180 people died and insurance loss estimates reached 7 billion euros. The flood was caused by heavy precipitation with the compound event of an already saturated subsurface. The event was detected in weather prediction models beforehand, but the official warnings did not reach the public in time or with enough influence (Fekete and Sandholz, 2021).

These events have strengthened the need for predictions of the terrestrial water cycle. Furthermore, climate change is likely to increase the challenge, and rising temperatures are expected to increase droughts such as the 2018 event (Hari et al., 2020). Moreover, air has higher water storage capacity at higher temperatures, which enables heavier precipitation (Fischer and Knutti, 2016).

1.3.2 Numerical Modeling of the Terrestrial System

Models of the terrestrial system are usually run independently to provide assessments of hydrometeorological extremes. Atmospheric models are either run as a hindcast to dynamically downscale reanalysis fields (Bowden et al., 2016) or as seasonal forecasts that give an ensemble of possibilities for weather development. After the downscaling, hydrologic and impact models can predict variables concerning water resources at a much higher resolution, taking into account known subsurface parameters (Yuan et al., 2015b). The obtained forecast can be combined with locally measured soil moisture to reach stakeholders in agriculture (Andersson et al., 2020).

The above procedure does not utilize the potential information from terrestrial hydrology for atmospheric reanalysis and seasonal forecasts. Atmospheric reanalysis can be performed through data assimilation of soil moisture, which offers improved land energy fluxes at monthly to seasonal timescales (Draper and Reichle, 2019), or the use of coupled models. Koster et al. (2010) demonstrated that across the United States, the realistic states of the terrestrial system derived from land surface models improved the temperature and precipitation forecasts for up to two months in summer. Nonetheless, the question arises whether these moderate improvements justify the incorporation of coupled terrestrial modeling into already costly seasonal forecasts.

Given the above question, fully coupled modeling systems are a novel approach that could result in better understanding of terrestrial feedback. Coupled models are often limited to regional simulations. Several recent studies have demonstrated that in the case of extreme events, the different regulation of evapotranspiration due to the groundwater component led to a simulation of heatwaves that differed from that of other regional climate models (Keune et al., 2016; Furusho-Percot et al., 2022; Mu et al., 2022). The differences exist because other regional climate models contain land components, where groundwater is usually only considered close to the surface, with a few vertical layers (Gedney and Cox, 2003). Furthermore, typical standalone land models work in 1D columns with no lateral interactions. Practically, that means for groundwater that incoming precipitation on a grid cell is divided into runoff and a portion that is held in the shallow soil. A part of the latter is lost to free drainage, while the stored part contributes to evaporation and transpiration (Fan, 2015). In such a description, many aspects of groundwater are neglected, such as lateral connections, capillary rise and groundwater memory.

One solution to the shortcomings of land models is to replace the groundwater component with a sophisticated groundwater model. These models can be categorized into 1) lumped models with volume-based approaches and 2) distributed models (Collins, 2017). The conceptual approach of lumped models does not enable a lateral flow between grid cells and breaks with the continuum approach of a continuous water cycle. Therefore, distributed models are better suited to simulate the effect of groundwater on evapotranspiration. An example is ParFlow (Kuffour et al., 2019), which solves the 3D Richard's equation in a variably saturated flow and can be integrated into fully coupled terrestrial

systems.

Overall, technologies exist for coupled subsurface, land surface and atmosphere models. Progress is being made in the Coupled Model Intercomparison Project Phase 6 (CMIP6), where participating models have significantly improved their groundwater parametrization, such as ISBA-CTRIP (Decharme et al., 2019). However, computational cost and storage capacity pose a challenge for long coupled simulations on climate time scales. To provide sufficient processing power, graphical processors are used that allow for massive parallelization of calculations and enhance the energy efficiency and computation time. Furthermore, institutions like the European Union are investing in establishing a digital twin of the earth, which includes all parts of the terrestrial and oceanic systems coupled together (Bauer et al., 2021).

1.3.3 Available Observations for Evaluation

Numerical modeling offers excellent opportunities to obtain consistent time series of variables at locations that lack observations. However, modeling results have little value unless they are evaluated against observations. Observations must be made in the atmosphere, land and subsurface to measure the water cycle adequately. This section gives an overview of river discharge, soil moisture and groundwater, all depicting the water content of the terrestrial system and precipitation and evapotranspiration as water transport processes. Many additional variables of the terrestrial system can be evaluated, but the selection presented here is crucial for determining how well the water cycle is represented in a model.

Precipitation is highly variable in space and time but can be measured with rain gauges on the ground and by radars and satellites. Rain gauges offer the longest data record and continuous measurements; however, they are not feasible on open water and in undeveloped regions (Rast et al., 2014). Effort is needed to collect individual measurements and then apply bias correction and quality control.

An example of a global data set is the product from the Global Precipitation Climatology Centre, where data from over 7200 rain gauges is collected (Schamm et al., 2014). Groundbreaking for precipitation rates from satellites was the Tropical Rainfall Measuring Mission (TRMM), which offered a time resolution of $3\,\mathrm{h}$ and maximum spatial coverage of about $4\,\mathrm{km}$, with data covering more than 15 years. Its successor, the GPM-CO mission, provides resolution up to $0.5\,\mathrm{h}$ (Kidd et al., 2020). Radar measurements provide information at a similar temporal scale but even finer resolution, resulting in highly detailed information on precipitation, close to orography (Ramsauer et al., 2018). However, dense radar networks are only available in a few regions, and precipitation signals must be isolated from ground reflections and reflections from other objects such as birds, insects and planes (Germann et al., 2022).

At the land surface, soil moisture can be measured by various techniques. Direct measurement is possible with the gravimetric method. First, soil samples are collected and

weighed; then, the samples are dried until no change in weight can be measured. The execution is simple and resistant to errors, but the sampling is destructive and confined to a small area. A less direct measurement involves determining the soil moisture content related to soil resistivity. With increasing water content, the electric resistance is reduced. Therefore, it is possible to determine the water content with two connected electrodes and a resistance meter, and the method is cheap and transportable. A major constraint is the significant influence of soil temperature and salinity on the results.

Promising noninvasive methods employ ground-penetrating radar; however, this approach faces similar problems to precipitation radars and cosmic-ray neutron sensing (Rasheed et al., 2022). The last method involves the surface continuously being hit by fast neutrons created from galactic radiation interacting with particles of the atmosphere and the soil. There is, again, a relation between the fast neutrons and the amount of water in the soil; therefore, measuring fast neutrons enables a conversion to soil moisture values. The method can measure fields up to $180.000\,\mathrm{m}^2$ at an hourly resolution. The maximum depth depends on the total water content, as wet soils reduce the number of fast neutrons, but can be as much as $83\,\mathrm{cm}$ (Nguyen et al., 2019).

Such scales are impressive for ground-based observations but insufficient to evaluate model results at the continental scale. Continental-scale evaluation can be performed with infrared or microwave observations from satellites, which have been available since the late 1970s. An example of a dataset derived from satellites is the European Space Agency's Climate Change Initiative for Soil Moisture. It merges satellite data from different missions through the years, beginning with Nimbus 7 (started in 1979) until data from ASCAT-C, an ongoing satellite mission. The remote sensing data from such a long period must be harmonized and quality controlled to create a consistent dataset (Gruber et al., 2019).

Remote sensing observations of deep water storages are more challenging to obtain than measurements of soil moisture. The only possibility is measuring gravitational anomalies with the Gravity Recovery and Climate Experiment (GRACE) and its successor GRACE-FollowOn (GRACE-FO). Gravitational anomalies are studied because they can be attributed to significant shifts in total water, such as melting glaciers. However, the measured gravity fields must be heavily post-processed by smoothing and filtering because of noisy shortwaves, which are visible as stripes (Swenson and Wahr, 2006). Over the years, various processing chains have been developed. For example, Watkins et al. (2015) applied spherical harmonic solutions, including the use of background geophysical models and parametrizations. Ultimately, post-processing provided a total water storage anomaly at 0.5° resolution with monthly timesteps, which helped to determine the total water loss during droughts (Boergens et al., 2020). However, it remains a challenge to separate the changes in groundwater from changes in soil moisture, surface water or snow cover.

Furthermore, groundwater is hard to measure. Compared to temperature measurements, the continuous operation of wells requires more effort, and the results are harder to in-

terpolate to a larger region because of the spatial heterogeneity of soil (Adams et al., 2022). Deep learning methods might be suitable to utilize existing measurement methods, as they can learn from observations without knowledge of the soil properties (Wunsch et al., 2022; Ma et al., 2021). If the soil properties are known with high certainty, groundwater can be calculated from classic hydrological models. An example of a dataset for subsurface parameters that is publicly available and covers large parts of the earth is the GLobal HYdrogeology MaPS 2.0 (GLHYMPS 2.0) (Huscroft et al., 2018). GLHYMPS 2.0 consolidates data from the Global Unconsolidated Map (GUM) (Börker et al., 2018), SoilGrids (Shangguan et al., 2017) and its predecessor. GUM provides the sediment types of the soil gathered by many national geological services and post-processed images. Information about the properties of deeper soil is obtained from SoilGrids, where soil profiles and borehole data combined with expert estimations are harmonized. GLHYMPS 2.0 combines these sources into a global map of permeability values for the near surfaces and the bedrock. The chain of steps necessary to assemble GLHYMPS 2.0 and the various origins of the data lead to good coverage associated with high uncertainty.

River discharge is an essential flux for closing the terrestrial water cycle. River discharge is widely measured, because the streamflow of rivers has a major impact on ship traffic, energy generation and water supply. However, measurements are primarily managed locally and considered partly confidential. Additionally, water flow can be complex in large rivers or inaccessible areas (Durand et al., 2019). The challenge of collecting and quality-controlling discharge data was recognized as early as the 1980s. Currently, the Global Runoff Data Center (GRDC) collects data from 10,000 stations in 159 countries and compiles it into a single database for scientific, non-commercial applications (www.bafg.de/GRDC/EN/Home/homepage_node.). Europe is particularly well monitored by GRDC, with daily and up-to-date data. By contrast, other large river systems, especially on the Indian subcontinent, lack data (Durand et al., 2019). There is the possibility of using remote sensing. For example, Papa et al. (2012) utilized the radar instrument of the satellite Jason-2 to infer river discharge. However, the derivation requires in-situ measurements for calibration, and the results have an error margin up to 20%.

Evapotranspiration is measured in-situ with various methods, which are categorized into groups. The first group is oriented to soil moisture measurement and a soil water balance formulation. To apply the formulation, incoming precipitation and soil moisture content must be measured. Then evapotranspiration can be calculated assuming the conservation of mass. However, if there is strong drainage or a lateral flow of groundwater, the system is open and the mass of water is not conserved. Another group of measurements uses the micrometeorological approach. Wind speed, humidity and temperature are measured at different heights to calculate the evapotranspiration rate. These methods produce high-frequency outputs but are executable only for terrains without disrupting wind measurements. Lastly, evapotranspiration can be measured using methods from plant physiology, such as the measurement of heat fluxes inside plants.

For assessments at large scales, remote-sensing data must be utilized along with statis-

tical models, energy balance models, data assimilation or the Penman-Monteith model (Chao et al., 2021). The latter is recommended by the Food and Agricultural Organization of the United Nations and requires observations of the ground heat, irradiance and surface pressure. Because evapotranspiration estimation depends on so many observations, land models are an alternative as they can estimate evapotranspiration from reanalysis products.

Overall, the rapid development of remote sensing and data assimilation technologies makes it possible to capture the earth system accurately. However, limitations remain in terms of temporal and spatial resolution, and an exact representation of the whole terrestrial system with a limited number of observations is impossible. Even high-resolution observational data might not be sufficient for the needs of local stakeholders. Special attention must be given to water resources in the subsurface, as these may be hidden from public observation and can undergo critical changes unnoticed (Famiglietti and Ferguson, 2021).

1.4 Research Questions

The memory effect of groundwater, which is connected to water and energy fluxes at the surface - which in turn influence clouds and precipitation - indicates the importance of feedbacks in the terrestrial system. Recent hydrometeorological extreme events, in which feedbacks are pronounced, highlight the need to include these events in numerical simulations.

This thesis contributes to the understanding of feedback mechanisms through a fully coupled terrestrial model that simulates the entire water cycle, from groundwater to cloud top and beyond. The first two chapters present an overview of land-atmosphere feedbacks and the simulation framework, which provides the basis for chapters 3 to 5, covering the following research questions:

- How does the groundwater memory affect three exceptional droughts under uncertain weather conditions on the interannual time scale? Is knowledge about the correct initial condition more important than accurate atmospheric forcing?
- Can persistent drought conditions influence the energy cycle and cloud characteristics at the interannual time scale, through feedback processes?
- How sensitive is precipitation over continental Europe to groundwater table alterations that result from changes in subsurface parameters in terrestrial simulations?

Concerning the first question, chapter 3 presents the results of an interannual probabilistic assessment of water resources after droughts, highlighting groundwater memory. Chapter 4 investigates the results of the assessment in terms of the energy cycle and cloud properties, revealing a drought feedback loop. Chapter 5 focuses on groundwater precipitation interactions, demonstrating the influence of the water table on rainfall.

Lastly, the results are summarized and discussed in chapter 6, together with limitations and an outlook for future work.

1.5 List of Publications

Parts of this thesis have been published in peer-reviewed journals:

- Hartick, C., Furusho-Percot, C., Goergen, K., & Kollet, S. (2021). An Interannual Probabilistic Assessment of Subsurface Water Storage Over Europe Using a Fully Coupled Terrestrial Model. Water Resources Research, 57(1).
  https://doi.org/10.1029/2020WR027828
  An extended abstract of the published version is included in Chapter 3.2 of the thesis.
- Hartick, C., Furusho-Percot, C., Clark, M. P., & Kollet, S. (2022). An Interannual Drought Feedback Loop Affects the Surface Energy Balance and Cloud Properties Geophysical Research Letters. Geophysical Research Letters, 49(22).
  https://doi.org/10.1029/2022GL100924
  Chapter 4 includes a combined version of the main article and its supplement.

Chapter 2

Terrestrial Modeling with TSMP

2.1 Terrestrial Systems Modeling Platform

Atmospheric, land surface and groundwater models have different development histories due to their various tasks and timescales. Therefore, connecting them in a framework to enable a physically consistent simulation is difficult. Creating a new model that explicitly focuses on the water cycle would be possible. Still, such a model would need an enormous development time to reach adequate results for the separate parts of the terrestrial system. By connecting models with proven capabilities in their compartment, the development can focus on exchanging variables and rely on proven technology.

The Terrestrial Systems Modeling Platform (TSMP) is a platform that achieves a physically consistent simulation by connecting the atmospheric model COSMO, the land surface model CLM and the subsurface model ParFlow with the Ocean Sea Ice Soil (OASIS3) coupler. The initial version was described in Shrestha et al. (2014) and Gasper et al. (2014) and is continuously in development to include newer versions of model components. This thesis concentrates on version v1.1 with COSMO v5.01, CLM v3.5 and ParFlow v3.2, which is used in various studies. TSMP is also used with the Parallel Data Assimilation Framework (PDAF) (Kurtz et al., 2016) and is operated for continuous forecasts of the terrestrial system (Kollet et al., 2018).

Figure 2.1 gives an overview of the involved models and the variables that are exchanged. Starting in the atmosphere, COSMO provides shortwave (SW) and longwave radiation (LW) directed to the ground, the temperature at the lowest level close to the surface (TAS), pressure (PS), horizontal wind (U), precipitation (PR) and humidity (Q) to each gridcell in CLM. CLM calculates the land energy budget with sensible (SH) and latent heat (LH), momentum flux (τ), outgoing LW and shortwave energy (α). The rain simulated by COSMO is intercepted by vegetation (Q_{rain}) in CLM and is sent to the soil layers of ParFlow. CLM also handles the removal of water from ParFlow by evaporation and transpiration through plants (ET). To calculate these fluxes, water pressure (PRESS) and saturation (SAT) of the soil layers are sent to CLM. The Following chapters provide additional details about the individual models and the coupling process.

2.1.1 The COSMO Model

At the beginning of the new millennium, numerical atmospheric models made significant progress towards higher resolutions and longer forecasting periods. At the German weather service, the model chain consisted of the global model GME running at $30\,\mathrm{km}$ resolution (Majewski et al., 2002), and the regional models COSMO-EU at $7\,\mathrm{km}$ and COSMO-DE at $2.8\,\mathrm{km}$ (Baldauf et al., 2011). Very recently, the whole model chain has been replaced by different configurations of the ICON model, which already has a non-hydrostatic dynamical core on the global scale (Zängl et al., 2015). Nevertheless, the COSMO model in its different versions has been applied for nearly 20 years for local weather forecasts over Europe and Germany and for climate modeling activities in a European-wide consortium, the CLM-Community (COSMO-model in CLimate Mode),

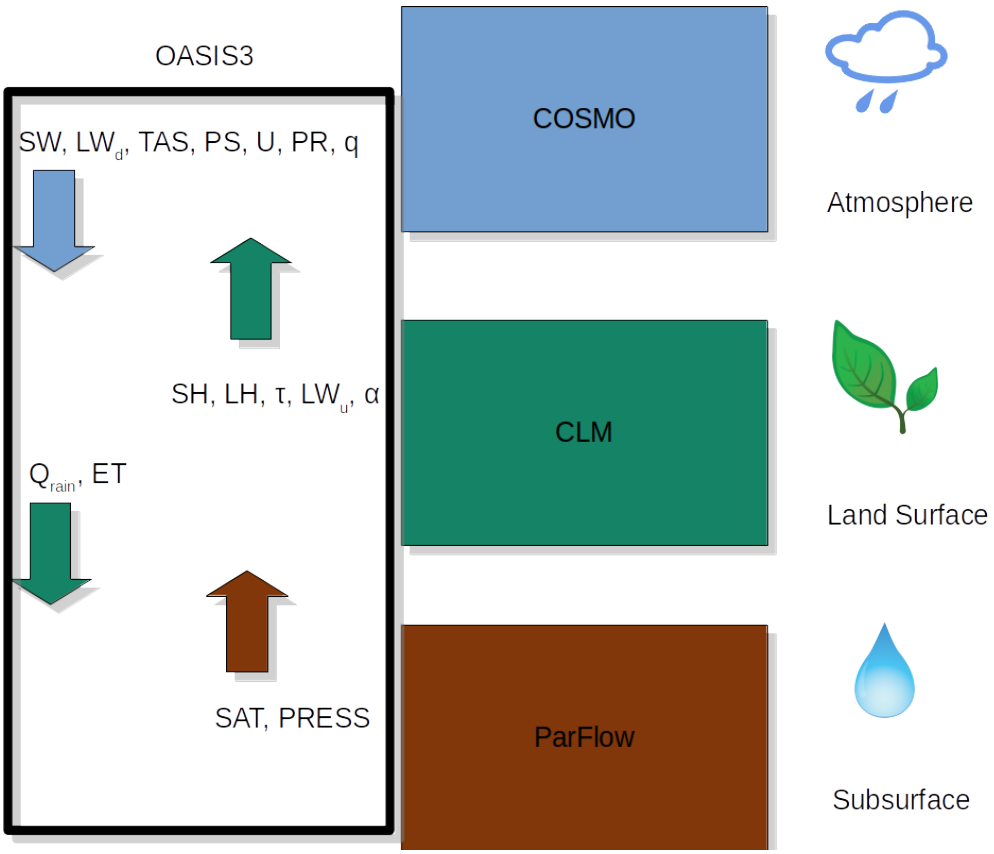

Figure 2.1: Schematic of TSMP with the component models COSMO, CLM and ParFlow and the exchanged variables.

which helped with its development (Rockel et al., 2008). COSMO is variable in its resolution allowing for explicit convective processes around 3 km and coarser resolutions which are more feasible in coupled modeling with TSMP. In this thesis, the COSMO version v5.01 released in 2015, is used.

At the core, the COSMO model solves the primitive equations in their compressible form to obtain solutions for the three wind directions, temperature, humidity and pressure. In detail, this includes a lot of processes, including filtering of sound waves not important for meteorological processes. Additional details can be found in (Doms and Baldauf, 2021). Some details about physical parametrizations, including clouds and radiation, are essential for this thesis and are briefly explained here according to (Doms et al., 2021).

The modeling studies in this thesis are performed with a two-category ice scheme, including the following categories of water in the atmosphere:

- Water vapor
- Cloud water and cloud ice
- Precipitable water in form of snow and ice

Between most of the categories, there are transformation processes described by equations. The starting process is the condensation or deposition of water vapor into cloud

water and cloud ice with the condition that relative water saturation reaches values beyond 100%. The saturation pressure is lower over ice. Therefore, cloud ice can form earlier than cloud water, given temperatures below the freezing point. In case of enough water supply by, for example, rising air masses, cloud water can also grow together with the ice particles resembling the development of mixed-phase water and ice clouds. However, cloud ice and water are treated as monodisperse reservoirs, with their diameter only depending on their mass. Compared to other forms of water in the model, they are of low quantity, which changes quickly. However, they are still crucial for the calculation of radiation through clouds. Besides the mentioned condensation and deposition forming a cloud, transformation to all states of water is possible, as shown in Figure 2.2. Only deposition and condensation are explicitly mentioned in the picture to keep readability. An abrupt transformation happens when the local temperature crosses the threshold of 0 °C. Within one time step, all ice particles melt and turn into the liquid phase.

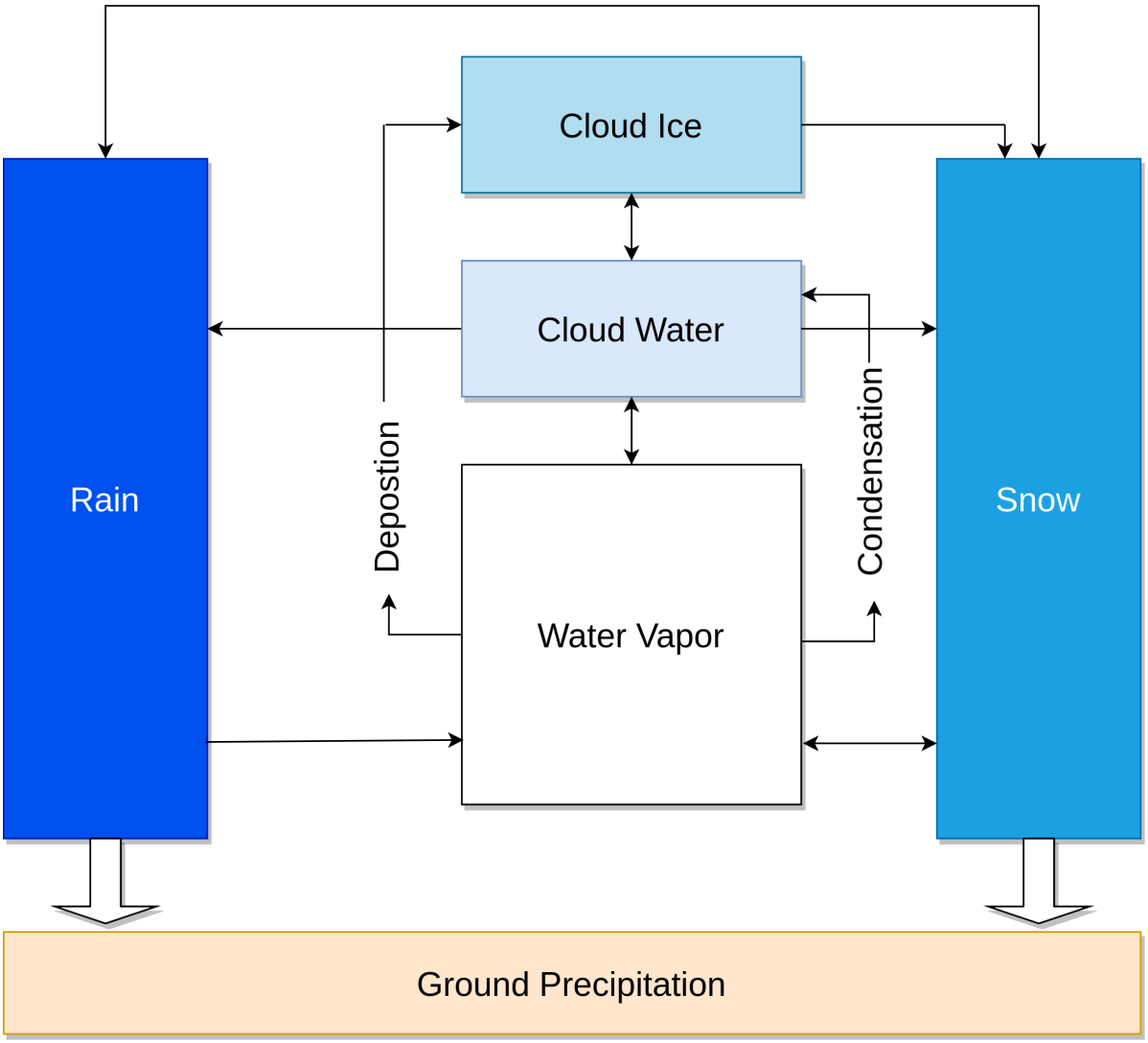

Figure 2.2: Schematic of the two-way ice scheme used to simulate precipitation in COSMO. Adapted from Doms et al. (2021).

Another process in the atmosphere that needs adequate parametrization is radiation. It depends on cloud physics, greenhouse gas concentration and interactions with the surface. In COSMO, radiative processes are described with a radiative transfer equation explained in detail in Ritter and Geleyn (1992). In reality, radiation passes through the atmosphere with different angles, is scattered by components, enters interactions with atmospheric components like ozone and finally is reflected and absorbed at the surface. The radiative equation would need to be integrated over all angles to capture all processes of radiative interactions. Such a calculation is not computationally feasible. Therefore, the COSMO model assumes horizontal homogeneous structures in a grid box, splits the radiation into three solar spectral and five thermal intervals, and calculates radiative fluxes only in certain configurable time intervals. The split between solar spectral and thermal intervals is called the two-stream method. It simplifies the computation as scattering involving air molecules is only included in the shortwave radiation, while the emission of radiation by particles is only relevant to the thermal spectrum.

The assumption of horizontal homogeneous structures allows the radiation to be calculated column-wise for each grid cell. Nevertheless, grid cells can still have variable cloudiness under the condition that there is continuous vertical cloudiness. Having two cloud layers separated by an utterly cloud-free zone is not allowed by the model. For resolutions coarser than $10\,\mathrm{km}$, a column-wise calculation is a fair assumption; for very high resolutions, it becomes a problem as it is not realistic that the radiation processes of two neighboring clouds do not interact with each other.

2.1.2 The Community Land Model

The Community Land Model (CLM) v3.5 (Oleson et al., 2004, 2008) serves as an interface between the atmosphere and the subsurface. In TSMP, CLM is mainly responsible for energy partitioning and determining evapotranspiration, considering the land cover, including plants and available soil moisture. It also can be run offline with atmospheric forcing data or only coupled to an atmospheric model. Without a subsurface model, CLM also handles river routing and groundwater processes, which are very simplified. Different groups develop CLM at the National Center of Atmospheric Research (NCAR) with contributions and software forks from worldwide within the current version 5.

In its newest iterations, CLM can become a dynamic vegetation model with plants growing according to ecosystem conditions and competing against each other. Such more sophisticated vegetation dynamics are much more computationally extensive and currently unfeasible in a fully coupled context. Therefore, plants are characterized in plant functional types (PFT) in CLM v3.5, which are used in TSMP. Specifically, each gridcell has one PFT assigned with plant characteristics and prescribed monthly variables like the leaf area index. Plant characteristics are essential for the interception of precipitation reaching the ground and turbulence in the boundary layer. Zipper et al. (2019) have shown that a widespread change in land cover can significantly impact atmospheric processes even with prescribed plant characteristics and a limited number of PFTs.

CLM simulates each gridbox individually, including the energy balance. Although no direct lateral interaction exists, they occur via the subsurface flow in ParFlow and the atmospheric process. The fundamental equations for momentum, energy and water vapor fluxes between the surface and the atmosphere in CLM are

$$\tau_x = -\rho_{atm}\frac{u_{atm} - u_s}{r_{am}}$$
$$\tau_y = -\rho_{atm}\frac{v_{atm} - v_s}{r_{am}}$$
$$H = -\rho_{atm}C_p\frac{\theta_{atm} - \theta_s}{r_{ah}}$$
$$E = -\rho_{atm}\frac{q_{atm} - q_s}{r_{aw}}$$

With τ being the momentum flux in x- (u-wind) and y- (v-wind) direction, ρ_{atm} the density of atmospheric air, r the aerodynamic resistances to momentum r_{am}, heat r_{ah} and water r_{aw} transfers, θ the potential temperature, H the sensible heat, C_p the heat capacity of air, E the water vapor flux and q specific humidity with r_s denoting surface values. The equations are solved using Monin-Obukhov similarity theory according to (Zeng et al., 1998). This formulation depends on the stability of the atmosphere and soil moisture availability and plant characteristics have various influences on the resistances and surface variables. For example the resistance r_{aw} depends on the leaf stomatal resistance r_s for vegetated zones

$$\frac{1}{r_s} = m\frac{A}{c_s}\frac{e_s}{e_i}P_{atm} + b$$

m is a PFT specific parameter, A is the leaf photosynthesis limited by the available soil moisture, c_s is the CO_2 concentration at the leaf surface, e_s is the vapor pressure at the leaf surface, e_i is the saturation vapor pressure inside the leaf, P_{atm} is the atmospheric pressure and b is the minimum stomatal conductance in CLM. More details can be found in the technical description of CLM.

2.1.3 ParFlow

The subsurface model ParFlow (Ashby and Falgout, 1996; Jones and Woodward, 2001; Kollet and Maxwell, 2006; Maxwell, 2013) simulates variably saturated groundwater flow solving the 3D Richards equation and overland flow at the surface with a kinematic wave approximation. ParFlow developed from its initial release as a watershed model initiated by the Lawrence Livermore National Laboratory and the Center for Applied Scientific Computing into an open-source project with various contributions from US and German institutions. Developed in C, ParFlow was ready for massive parallel computing from the start. Recent developments enable the efficient usage of graphical processing units, which offer even more parallel processing and have a speed advantage over classical computation with CPU in many cases (Hokkanen et al., 2021). However, compared to

lumped models, the numerical solution of the Richards equation in the mixed form is more costly. The main equations are

$$S_s S_w(p)\frac{\partial p}{\partial t} + \phi\frac{\partial(S_w(p))}{\partial t} = \nabla\mathbf{q} + q_s$$
$$\mathbf{q} = -k_s k_r(p)\nabla(p - z)$$

This mixed form of the Richard's equation depends on the pressure head p with S_s being the specific storage, S_w the relative saturation, t is time, ϕ is the porosity, $\mathbf{q}$ is the Darcy flux and q_s is a general source-sink term which comes from CLM in the case of TSMP. k_s is the saturated hydraulic conductivity tensor, k_r is the relative permeability and z is the depth below the surface. Separate equations are used for the simulation of overland flow. They are derived from the two-dimensional shallow water equation

$$\frac{\partial \psi_s}{\partial t} = \nabla(\boldsymbol{v}\psi_s) + q_s$$

with ψ_s as the surface ponding depth and $\boldsymbol{v}$ as the mean velocity vector. Applying the kinematic wave approximation which means that the friction terms are equal to gravitational forcings leads to following velocities in x- and y-direction

$$v_x = \frac{\sqrt{S_{f,x}}}{n}\psi_s^{\frac{2}{3}}$$
$$v_y = \frac{\sqrt{S_{f,y}}}{n}\psi_s^{\frac{2}{3}}$$

$S_{f,x}$ and $S_{f,y}$ are the mentioned friction terms that are given to ParFlow by slope files. The slopes determine the river routing by directing the flow from one cell to only the steepest neighboring cell. n is the Manning roughness coefficient, which is inferred from empirical studies. Especially in flood situations, it has a high impact on the correct simulation of a flood (Lumbroso and Gaume, 2012). In TSMP, ParFlow and CLM share the first soil layers (ten in this study). All hydraulic processes are performed by ParFlow while CLM calculates evaporation and transpiration.

2.1.4 Coupling with OASIS3

The main accomplishment of TSMP is coupling three independent models with the help of OASIS3 (Valcke, 2013). OASIS was developed at CERFACS, a French scientific center for scientific computing. Development started at the beginning of the 1990s, intending to couple oceanic and atmospheric models. The goal was an external coupler to exchange data with minimal modifications to the original models. In a so-called multiple-executable approach, which is applied in TSMP, OASIS3 initializes and terminates TSMP's component models to manage the coupling process.

Initially, all models are set up from cold-start or restart values. After that, COSMO and ParFlow run parallel until the first coupling step, where variables are exchanged to CLM.

During the relatively quick simulation of CLM, COSMO and ParFlow idle. When the computations of CLM are finished, it sends variables to COSMO and ParFlow, which run parallel again while CLM idles. This procedure leads to idle times of all models in one coupling step but is still more efficient than a sequential run of all models (Gasper et al., 2014).

The first data exchange sends shortwave and longwave radiation, precipitation, pressure, humidity, and temperature at the lowest level from COSMO to CLM. No modifications have to be made because this is the same way CLM would receive atmospheric data in an offline simulation. In the next step, ParFlow sends CLM relative saturation and pressure of the soil layers both models share. Based on the two inputs, CLM simulates energy and momentum fluxes which are sent back to COSMO. The transfer is performed by calculation of exchange coefficients. The formulation is similar to the main equations of CLM in chapter 2.1.2 with some modifications

$$
\begin{aligned}
C_{ah} &= -\frac{H}{\rho_{atm} c_p U (T_s - \frac{T_{atm}}{\Pi})} \\
\Pi &= \frac{p}{p_0}^{\frac{R_d}{c_p}} \\
C_{aw} &= -\frac{E}{\rho_{atm} H_{vap} (q_s - q_{atm})} \\
C_{am} &= -\frac{\tau}{\rho_{atm} U u}
\end{aligned}
$$

The resistances - here called transfer coefficients - for heat C_{ah}, moisture C_{aw} and momentum C_{am} are all influenced by the mean wind speed in zonal and meridional direction U. Between the land surface in CLM and the lowest level of the atmosphere in COSMO exists a height difference that has to be corrected with the Exner function Π. Here p is the pressure of the lowest level, p_0 is the pressure at the surface and R_d is the specific gas constant for dry air. Because the transport of moisture from CLM to COSMO includes a phase change, the enthalpy of vaporization H_{vap} is included. For the momentum coefficient, the focus lies on the zonal wind component u.

After sending the transfer coefficients to COSMO, CLM sends ParFlow the rain flux to the top soil layer and evaporation fluxes for the shared layers.

2.2 Configuration, Domain and Workflow

2.2.1 Model Configuration

Many factors determine the outcome of a complex model system. Following aspects are important:

- Model versions

- Namelist settings
- Initial and boundary data
- Static parameter fields

This study uses TSMP in version v1.1, which includes COSMO v5.01, CLM 3.5 and ParFlow 3.2. Each of the three models has its namelist, and defines its grid and timestep. Most crucial is the timestep with COSMO using 60 s and CLM-ParFlow 900 s, which is also the coupling timestep. The full namelists of TSMP used in this study are publicly available on GitHub: https://github.com/HPSCTerrSys/TSMP/tree/master/bldsva/setups/cordex.

Initial data is vital for the land component of TSMP. The use of reanalysis datasets can initialize the atmosphere, but the subsurface in ParFlow needs at least several years to reach an equilibrium state. A spin-up period is usually performed by forcing CLM-ParFlow with averaged atmospheric data in offline simulations. In the study of Furusho-Percot et al. (2019), a spin-up was conducted over 20 years. Once an equilibrium is reached, the states of the surface and subsurface can be used in a fully coupled simulation with COSMO. Additional simulation time in the fully coupled setup is necessary for the subsurface to reflect the atmosphere's forcing correctly. A change of subsurface parameters can break the equilibrium, again initiating an adaption period. The initial state obtained by the spin-up is also essential for the lower boundary condition of ParFlow. On the bottom at 57 m depth, an assumed impermeable bedrock prevents water loss. Therefore, some water is always present at the bottom of the column. The initial spin-up determines the extent of this water column or aquifer. Water can be lost at the coast of the domain. Here, the water tables are always right below the surface, allowing lateral flow into the ocean. This assumption prevents realistic simulation of groundwater near the coasts, as many processes are involved in a sea-groundwater exchange, for example, the sea level (Ketabchi et al., 2016).

In fully coupled TSMP, atmospheric boundary data is only necessary at the lateral borders of the simulation domain. Still, it dominates the development of large-scale weather systems in the domain and ensures that the outflow matches the boundary conditions. Static fields include the orographic height for COSMO, the plant functional types in CLM and subsurface parameters in ParFlow. More details of the used datsets are found in chapter 2.2.3

2.2.2 Model Domain

Inherited from previous studies (Keune et al., 2016; Furusho-Percot et al., 2019) the modeling domain follows the European Coordinated Regional Downscaling Experiment (CORDEX) domain (Giorgi et al., 2009) for simulations with 0.11° (≈ 12.5 km) resolution and 424x412 gridcells ranging from 27° N to 72° N and 22° W to 45° E. In the simulation, the domain is slightly larger for COSMO with 444x432 gridcells and CLM and ParFlow with 436x424 gridcells compared to CORDEX. The additional ten pixels at each side of the domain should allow a transition zone between the CORDEX domain and the direct

influence of the atmospheric boundary data of ERA-Interim. Four of the ten pixels are run with constant fluxes from the surface, replacing CLM-ParFlow. The inner 436x424 are dynamically fully coupled. A longitude-latitude grid with a rotated pole at 162° W and 39.25 N ensures a nearly homogeneous gridcell area. Figure 2.3 shows the modeling domain, including the sponge zone. Inside the CORDEX domain are subdomains called

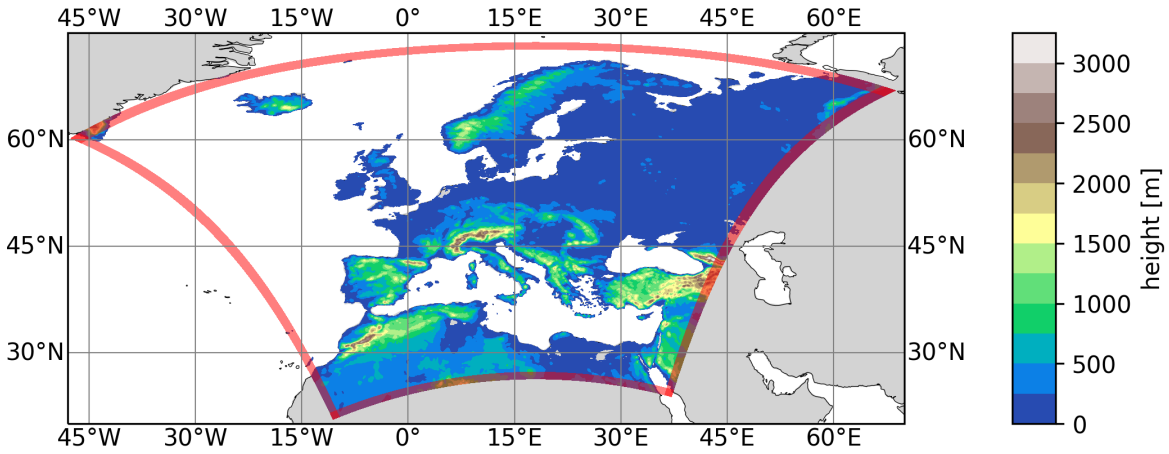

Figure 2.3: Simulation domain of TSMP over Europe with orographic height. The shaded red area depicts the sponge zone, which is cut for the analysis.

PRUDENCE regions used for regional analysis (Christensen and Christensen, 2007). Most of the studies shown in this thesis focus on the region Mid-Europe ME. ME consists of Germany and parts of the neighboring countries. The vertical resolution is variable and terrain following. The atmosphere ranging up to 22 km is equally segmented into 50 layers. The subsurface ranging down to 57 m consists of 15 layers. The first ten subsurface layers up to 2 m depth are shared by CLM and ParFlow.

2.2.3 External Datasets

To define the elevation in ParFlow, slopes in x- and y-direction are derived from the USGS GTOPO30 (DAAC, 2004) digital elevation data set. Soil parameters are vertically homogeneous and are derived from the Food and Agricultural Organization of the United Nations database (Carballas et al., 1990) and categorized into 15 types. To account for spatial aggregation at a resolution of 12.5 km the horizontal permeability values are scaled by the factor 1000. The upscaling has proven to improve the results of the simulation of runoff and soil moisture content (Fang et al., 2016). The distribution of 16 plant functional types for CLM was derived from the MODIS database (Friedl et al., 2002).

To initialize COSMO and to create boundary data, pre-processing has to be done with the program int2lm, which comes with COSMO. The basic requirements are an external parameter file containing surface characteristics. Many surface parameters are redundant when using COSMO coupled to CLM but are required to get the model running. Parameter files for COSMO are provided by the CLM-Community (not to be confused with the CLM model) or the Deutsche Wetterdienst. More critical are the atmospheric

conditions of a global circulation model that are interpolated as initial and boundary conditions. This thesis uses the reanalysis product ERA-Interim (Dee et al., 2011). Necessary variables are

- Temperature
- Wind
- Humidity
- Pressure
- Cloud water content
- Temperature of the snow surface
- Snow water content
- Specific humidity at the surface

For a first initialization more variables describing soil temperatures and water content are needed. Boundary conditions of ERA-Interim were applied every 3 h at the borders of the sponge zone in Figure 2.3. At the time of the publication of this thesis, ERA-Interim was already outdated and ended production in August 2019. The predecessor ERA5 (Hersbach et al., 2020) improved in resolution, model physics, time-span and corrects precipitation by incorporating remote sensing products. However, ERA5 was not available when the simulations of Furusho-Percot et al. (2019) started, which is the basis of the thesis.

2.2.4 The Supercomputer JUWELS

All simulations in this thesis were carried out on the supercomputer JUWELS located at the Forschungszentrum Jülich. JUWELS consists of a cluster module of more than 2300 compute nodes assembled of 48 compute cores each and the JUWELS booster, which has 3744 GPUs especially suited for artificial intelligence research (Kesselheim et al., 2021). Both are embedded in a network and file system connecting all supercomputers in Jülich. Each job at the supercomputer needs to request a certain amount of nodes and wallclock time. The fully coupled version of TSMP was run at the cluster module with 8 nodes spread between COSMO (4), ParFlow (3) and CLM (1). Initially, the runs were set up in monthly steps, meaning that the model stops at the end of each month, reproducing restart files. These files enable to continue the simulation at this point in time. Simulating one month usually takes around 5 h of wallclock time on the supercomputer.

On the one hand, restarting the simulation every month creates a safety net. On the other hand, a relatively small amount of nodes with a short wallclock time compared to the limit (24 h) is ineffective. In the case of heavy system usage, each new request job leads to queuing times, while requesting one longer job only leads to one queuing time. Therefore, later runs covered four months of simulation, reducing the number of job requests from twelve per year of simulation to three.

The amount of data produced by TSMP also proposes a challenge with $2.6\,\mathrm{TB\,year^{-1}}$ for COSMO, $73\,\mathrm{GB\,year^{-1}}$ for CLM and $130\,\mathrm{GB\,year^{-1}}$ for ParFlow. These are the storage requirements for the output variables for the raw output with the variables used in Furusho-Percot et al. (2019). Not saving temperature or humidity data on atmospheric model levels in COSMO can massively reduce the storage requirements.

Chapter 3

An Interannual Probabilistic Assessment of Subsurface Water Storage Over Europe Using a Fully Coupled Terrestrial Model

3.1 Publishing Information and Individual Contribution

The following chapter is published in *Water Resources Research* (Hartick et al., 2021). Co-authors are Carina Furusho-Percot, Klaus Goergen, and Stefan Kollet. Carina Furusho-Percot contributed to developing the experimental setup. Klaus Goergen helped with the initial analysis and edited and reviewed the paper. Stefan Kollet supervised me and contributed to designing visuals, writing the original draft and editing. I carried out the simulations, performed the analysis, and did the visualization and the main writing. In the following, the paper is summarized with an extended abstract.

3.2 Summary

Central Europe experienced a massive heatwave in 2018, significantly impacting public health and agriculture. Yet, the previous year of 2017 was comparably wet and water deficits only developed later in the year. The following year 2019, was dry again and Central Europe was under ongoing drought conditions with deficits up to $-145\,\mathrm{Gt}$ (Boergens et al., 2020). The prolonged water deficits raised awareness for drought assessment and prediction. It is essential to know the probability of a continued drought for adaptation strategies to adjust to the fact that the deficits might not be replenished over winter. In Germany, droughts are assessed through the German drought monitor (Zink et al., 2016), but predicting droughts on longer timescales is difficult. The main obstacle is the uncertainty of the atmospheric forcing (Miralles et al., 2019). However, additional information might be drawn from groundwater memory and the slow-moving processes in the subsurface and land surface to extend the prediction period (Dirmeyer, 2000).

Water flow must not be simplified to utilize groundwater memory in modeling. For example, using a free drainage approach in which water can leave the soil column at the bottom prevents an explicit water table. On a continental wide-scale, common climate models as well as most hydrological models use simple groundwater dynamics. This study uses the fully coupled Terrestrial Systems Modeling Platform (TSMP) (Shrestha et al., 2014; Gasper et al., 2014) to prevent this. It combines the atmospheric model COSMO (Baldauf et al., 2011), the landmodel CLM (Oleson et al., 2004, 2008) and the subsurface model ParFlow (Ashby and Falgout, 1996; Jones and Woodward, 2001; Kollet and Maxwell, 2008; Maxwell, 2013) coupled together with OASIS3-MCT (Valcke, 2013). For TSMP already exists a terrestrial climatology (Furusho-Percot et al., 2019) including the evolution of water storage in the subsurface over continental Europe with matching boundary conditions from ERA-Interim. This data will be utilized for the interannual probabilistic assessment of subsurface water storage.

The assessment is proposed in the following way: The conditions of the land and subsurface are extracted from a long-running climate simulation to initialize a forward ensemble with boundary conditions from all available previous years. The ensemble is run for a full water year. In the end, the probability for a continuing water deficit is calculated with the Weibull plotting position formula (Hao et al., 2016)

$$P(x < 0) = \frac{n_0}{n+1}$$

$P(x < 0)$ is the probability P for a subsurface water deficit smaller than 0, n_0 is the number of ensemble members that fulfill that condition and n is the total number of ensemble members. The assessment was executed with the initial conditions of August 31st 2011, 2018 and 2019, which all showed high water deficits over Central Europe.

The main assumption of the probabilistic assessment is that the information stored in groundwater memory outweighs the lack of information on the atmospheric evolution

on the interannual timescale. A so-called reverse assessment can help to prove this thesis: The basic idea of the probabilistic assessment is already known in classical hydrologic modeling (Day, 1985; Wood et al., 2002; Wood and Lettenmaier, 2008) to predict streamflow. In a reverse assessment (Wood and Lettenmaier, 2008), all available initial conditions are paired with one perfect atmospheric forcing. For both assessments, an error is calculated compared to the actual evolution in the continuous climatology. Naturally, the error of the assessment increases over time. In the reverse assessment, the error gets smaller because the perfect meteorological forcing brings the variety of initial conditions more and more together.

Results show that in the case of the 2018 drought, the initial condition is more influential than the atmospheric forcing for nearly the whole time span of one water year. This proves that the probabilistic assessment helps to determine the probability of a continuous water deficit. The percentages for the three initial conditions were 70% for 2011, 70% for 2018 and 65% for 2019, all well above the value of no predictability ($P \sim 50\%$).

All in all, the interannual probabilistic method has proven valuable in the case of dry and wet anomalies. No useful results can be obtained if subsurface water resources are close to the long-term average. Comparing assessment and reverse assessment shows that the initial condition in the case of droughts leads to long predictability on the interannual time scale. Previous studies (Shukla et al., 2013; Staudinger and Seibert, 2014; Arnal et al., 2018) determined that the initial condition is relevant on a much shorter timescale.

Chapter 4

An Interannual Drought Feedback Loop Affects the Surface Energy Balance and Cloud Properties

4.1 Publishing Information and Individual Contribution

The following chapter is published in *Geophysical Research Letters* (Hartick et al., 2022). Co-authors are Carina Furusho-Percot, Martyn Clark, and Stefan Kollet. Prof. Stefan Kollet supervised me and contributed to designing visuals, writing the original draft and editing. Carina Furusho-Percot contributed to parts of the simulation, the feedback scheme's visual design, and the editing of the writing. Prof. Martyn Clark helped to edit and review the paper. I carried out the simulations, performed the analysis, and did the visualization and the main writing.

For this thesis the content of the main paper and the supplement are condensed into one chapter to expand on the original submission.

Abstract

Long-term groundwater droughts are known to persist over timescales from multiple years up to decades. The mechanisms leading to drought persistence are, however, only partly understood. Applying a unique terrestrial system modeling platform in a probabilistic simulation framework over Europe, we discovered an important positive feedback mechanism from groundwater into the atmosphere that may increase drought persistence at interannual time scales over large continental regions. In the feedback loop, groundwater drought systematically increases net solar radiation via a cloud feedback, which, in turn, increases the drying of the land. In commonly applied climate and Earth system models, this feedback cannot be simulated due to a lack of groundwater memory effects in the representation of terrestrial hydrology. Thus, drought persistence and compound events may be underestimated in current climate projections.

Plain Language Summary

Depending on the climate zone, droughts can persist for a very long time. In generally dry regions, interactions between the drought and the atmosphere become quickly apparent with a missing moisture supply from the surface. In more humid areas like the mid-latitudes, the effects are more hidden because there is more guarantee for moisture supply from the ocean. Still, some feedbacks prolong droughts that are often overlooked in climate modeling. We show with a model that includes the whole water cycle from the groundwater to the cloud top that drought conditions can change the properties of the clouds with changes in the energy cycle. The clouds become higher and transmit more solar energy to the surface. The surplus of energy at the surface leads to more evaporation and prolonged droughts.

Key Points

- Previously neglected drought feedbacks initiated by water deficits in the subsurface are prolonging water deficits
- The shortfall of subsurface water leads to higher clouds via changes in the sensible heat flux
- Higher clouds let more solar radiation reach the ground contributing to drought persistence

4.2 Introduction

Droughts are part of the observed natural variability of the water cycle acting over large spatial scales and on time scales from weeks to decades (Peterson et al., 2021). Factors that influence hydrologic drought are precipitation deficits, hydrologic memory effects, land use modifications (Staal et al., 2020), human water use (Wada et al., 2013), and climate change (Samaniego et al., 2018). In addition, non-linear feedback loops, for example, the triggering of mesoscale circulations or changed advection patterns may be

critical in connecting hydrologic drought with atmospheric processes in the terrestrial system (Seneviratne et al., 2010).

The feedback of soil moisture with land surface temperature and precipitation via evapotranspiration has been studied previously (Humphrey et al., 2018; Miralles et al., 2019; Zhou et al., 2021), showing connections at the weather and climatological time scales (Guo et al., 2006; Koster et al., 2006). Simulating relevant feedbacks can both rely on complex groundwater formulations (Keune et al., 2016) or high-resolution atmospheric models that enable explicit convective processes (Hohenegger et al., 2009). Both come with additional computational costs.

Central Europe is usually not water-limited (Stegehuis et al., 2013) and local feedback processes are superposed by large-scale atmospheric processes. However, during summer and under drought conditions, the influence of local feedbacks may increase (Phillips and Klein, 2014), because the whole energy balance at the surface is shifted towards dominance of the sensible over the latent heat flux (Rajan et al., 2015). Possible consequences are changes in surface albedo with changed soil color due to decreasing soil moisture and vegetation (Meng et al., 2014). Shifts in the energy balance also increase the sensible heat flux, which can influence the cloud base and cover via interactions with the boundary layer (Betts, 2004; Ardilouze et al., 2019). The upper part of the boundary layer is heated, leading to an extension, which moves the cloud base upwards. Dirmeyer et al. (2014) found a strengthened connection between sensible heat and the cloud base in climate projections of coupled models. Feedback processes like this might not only be critical in future climates but be relevant during current droughts. In this study, with fully coupled groundwater-to-atmosphere simulations, positive feedback mechanisms between groundwater drought and atmospheric processes were discovered at the interannual time scale.

4.3 Data and Methods

The discovery of the positive drought feedback is based on the analyses of numerical ensemble prediction experiments. In the experiment, the integrated modeling system was applied with varying drought initial and uncertain atmospheric boundary conditions over the European continent, which is outlined in sections 4.3.1 and 4.3.2. The statistical analyses of the experiments scrutinize the increments in the hydrologic and atmospheric response to the drought initial conditions at the interannual time scale, which is detailed in sections 4.3.3 4.3.4 and 4.3.5.

4.3.1 Modeling System

The feedbacks between continental-scale groundwater and atmospheric processes are examined using coupled land-atmosphere models (Barlage et al., 2015). In this study, we applied the Terrestrial Systems Modeling Platform (TSMP) consisting of coupled groundwater, land, and atmosphere models (Gasper et al., 2014; Shrestha et al., 2014).

TSMP closes the energy and water cycle from the bedrock to the top of the atmosphere, thus, providing physically consistent simulation results.

The atmospheric part of TSMP is covered by COSMO v5.01, a regional atmospheric model developed by multiple weather services under the leadership of the German Weather Service (Baldauf et al., 2011). It has been used as an operational weather forecast system and in research applications up to the climatic timescale solving prognostic equations for a compressible non-hydrostatic moist atmosphere. In TSMP, COSMO provides precipitation, temperature, humidity, horizontal winds, air pressure, shortwave energy and longwave energy fluxes to the land scheme based on the Community Land Model (CLM version 3.5).

In return, in the coupled framework, CLM (Oleson et al., 2004, 2008) provides COSMO with upwelling longwave and reflected shortwave energy, turbulent momentum, moisture and energy fluxes, which are calculated for individual grid cells. Relevant processes in CLM are evaporation, root water uptake and transpiration, and sensible heat, which are parameterized based on thermodynamic, plant physiologic and similarity theory. In this study, the connection of these processes to shallow soil moisture and groundwater redistribution, which is calculated by the variably saturated groundwater and surface water flow model ParFlow, is key explaining the feedback.

ParFlow (Ashby and Falgout, 1996; Jones and Woodward, 2001; Kollet and Maxwell, 2006; Maxwell, 2013; Kuffour et al., 2019) solves the 3D Richards-equation for a physical representation of variably saturated groundwater flow, which enables the calculation of e.g. total water storage (saturated/unsaturated) and groundwater table depth. Overland flow is represented with a kinematic wave equation in a free surface boundary condition. The equations are discretized via finite differences in space and implicitly in time, and solved by a Newton-Krylov solver. ParFlow covers the shallow soil layers in CLM and is extended with five additional soil layers to include deeper groundwater flow. At the upper boundary, ParFlow receives precipitation after interception and evapotranspiration from CLM. ParFlow provides subsurface water pressure potential and saturation values to CLM. The coupling of the different model components is implemented with OASIS3-MCT (Valcke, 2013). All models are initialized by the coupler and run independently until the user defined coupling timestep. Then coupling variables are exchanged in 2D and 3D arrays in memory, and updated in all models.

4.3.2 Domain and Model Setup and Reference Climatology

The global simulation domain encompasses the official EURO-CORDEX region (Giorgi et al., 2009; Gutowski et al., 2016), including large parts of continental Europe. The horizontal grid spacing is 0.11° on a rotated longitude-latitude grid, roughly equal to a distance of 12.5 km. The vertical grid spacing is variable, with the atmosphere reaching up to 22 km with 50 levels and the subsurface up to 57 m with ten levels shared with CLM and ParFlow and five additional ParFlow layers. The subsurface grid is terrain following with increasing layer thickness with depth. Not resolving convection explicitly,

we operate with the two-category ice scheme of COSMO that includes the categories of water vapor, cloud water (CLW), cloud ice, rain and snow but ignores graupel. The convective parametrization from Tiedtke (1989) is utilized with the addition that mixed-phase clouds of ice and water are accounted for. Calculation of radiative fluxes is done according to Ritter and Geleyn (1992), which enables the calculation of incoming solar radiation to the surface, taking into account partial cloudiness of individual layers and the water content in different forms through all layers. It is assumed that clouds in adjacent levels overlap completely, and the radiative fluxes are calculated only for the timestep used for the coupling process to reduce computational demand. Generally, the timestep of COSMO is 60 s, while the CLM and ParFlow run with a timestep of 900 s, which is also the coupling frequency.

The lateral boundary information for the atmospheric model was obtained from the reanalysis dataset ERA-Interim (Dee et al., 2011), updated every 3 h at the domain's borders. Parameters for PFTs of CLM were obtained from the Moderate Resolution Imaging Spectroradiometer (MODIS) database (Friedl et al., 2002). The individual plant properties were calculated from the CLM surface dataset. The topographic representation in ParFlow is represented by slopes in 2D derived from USGS GTOPO30 (DAAC, 2004), soil properties stem from the Food and Agricultural Organization (FAO) database (Carballas et al., 1990) categorized in 15 soil types with assumed vertical homogeneity. Due to the resolution of 12.5 km, there was the need to scale horizontal permeability by a factor of 1000 (Fang et al., 2016; Niedda, 2004). Along the coastlines, we apply a Dirichlet boundary condition for ParFlow with constant hydraulic pressure and the water table located close to the surface.

Applying ERA-Interim boundary forcing, a continuous climatological time series was simulated from 1996 to 2018 with TSMP, which serves as the reference (REF) in this study. REF constitutes a consistent, transient climatology of all relevant states and fluxes of the terrestrial water and energy cycle from groundwater across the land surface into the atmosphere (Furusho-Percot et al., 2019). We focused on the region of Mid-Europe (ME) defined in Christensen and Christensen (2007), which roughly consists of Germany and the Benelux states (Figure 4.1).

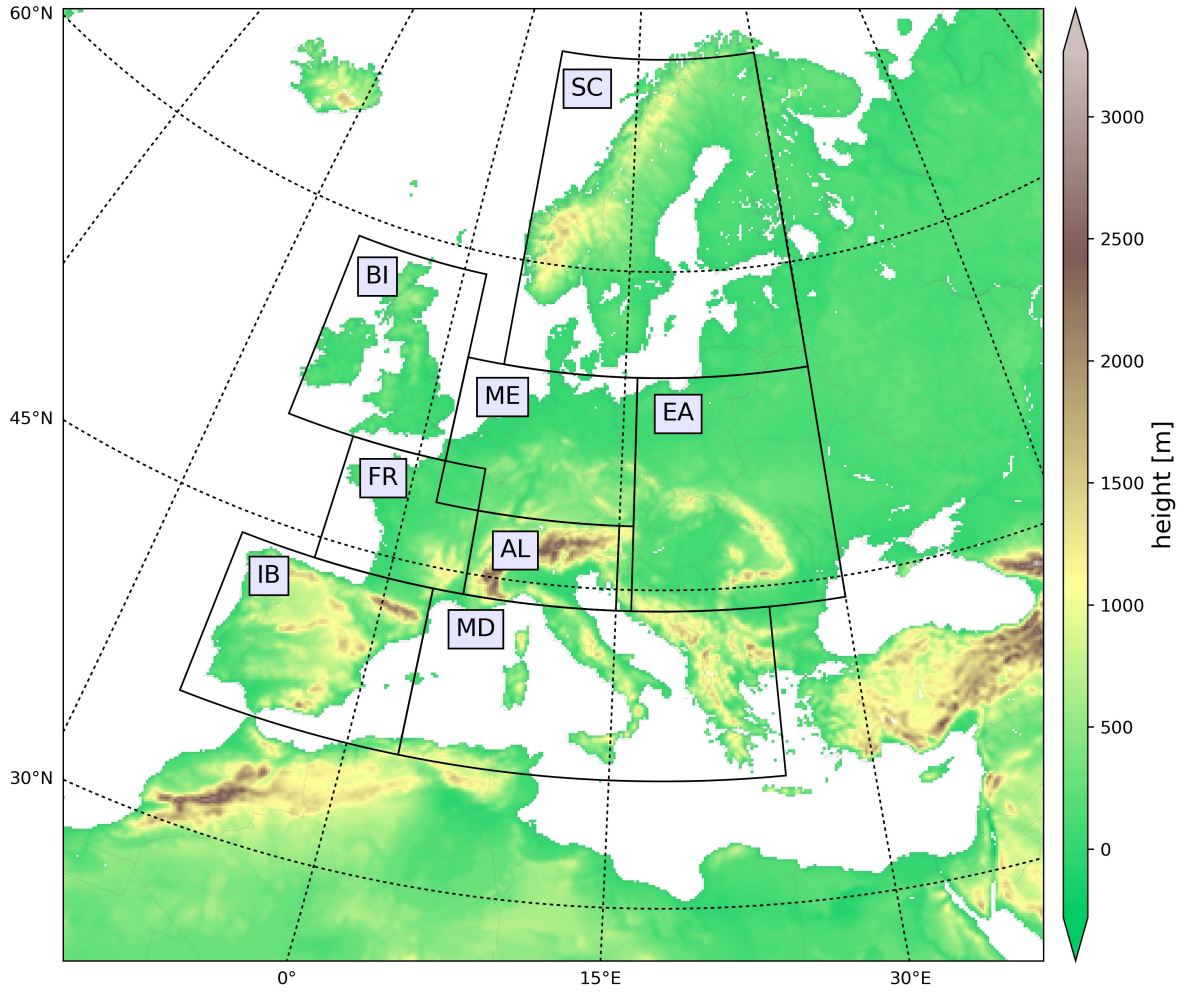

Figure 4.1: Simulation domain over continental Europe including topographic height with PRUDENCE subdomains. The European CORDEX model domain, including the topographic height. Abbreviations are: BI: British Isles; IB: Iberian Peninsula; FR: France; ME: Mid-Europe; SC: Scandinavia; AL: Alps; MD: Mediterranean; and EA: Eastern Europe. Reproduced from Hartick et al. (2021).

4.3.3 Ensemble Construction and Increment Analyses

In the ME focus region, there were three major groundwater drought events in the years 2011, 2018, and 2019 that were identified from anomalies of total subsurface water storage, S. These events were part of previous evaluation studies where water states and fluxes simulated with TSMP underwent a century-long spin up period and were shown to agree well with observations from remote sensing (Furusho-Percot et al., 2019; Hartick et al., 2021).

We applied an established probabilistic ensemble prediction approach (Day, 1985; Wood and Lettenmaier, 2008), which can be summarized as follows: In order to assess the impact of drought conditions at the end of a given water year on the hydrologic and atmospheric system in the ensuing water year (1. September to 31. August), the atmospheric uncertainty must be taken into account at the interannual time scale. Since there is arguably no predictive skill in e.g. precipitation at the interannual time scale, an ensemble of atmospheric conditions must be constructed that covers the full range of atmospheric uncertainty, which encompassed, in the best case, realizations of all possible atmospheres for the ensuing water year. In this study, an estimate of atmospheric uncertainty was obtained by forcing the ensuing water year with atmospheric ERA-Interim boundary conditions of the 22 water years, $y \in Y = \{1996, 1997, ..., 2018\}$ covering the simulated time series of the reference simulation, REF. Thus, for a single initial drought condition at the end of a water year, this resulted in an ensemble of 22 realizations of the hydrologic and atmospheric system in the ensuing water year over the simulation domain. Because three drought years (2011, 2018 and 2019) were considered for initializing the ensemble simulations, the total ensemble size was 66. Note, the initial disequilibrium between the atmospheric and hydrologic system right at the beginning of each simulation after initialization can be neglected because of the strong dynamics and short memory of the atmosphere on the order of hours to days. For more details on the experimental design, the reader is referred to Hartick et al. (2021).

The ensemble results were analyzed based on increments $\Delta_{Y,V}$, where the subscript V is a set of subsurface, land surface, and atmospheric variables

$$v \in V = \{RNET, LH, SH, GH, SSR, LF, CEILING, CLT, LCL, CLW\}$$

defined in Section 4.3.4; and Y is the set of REF forcing years defined above. Individual increments were calculated as the differences between the ensemble members initialized with the drought conditions of the years $i \in I = \{2011, 2018, 2019\}$ and REF simulation results for the years Y (see also Figure 4.2)

$$\Delta_{y,v} = v_{y,i} - v_{y,REF}$$

In the analyses, all $\Delta_{Y,V}$ were seasonally and spatially averaged over the focus region and normalized with the seasonal standard deviation (background atmospheric variability) of

REF over the study region resulting in the averaged increment Δv for a given variable $v \in V$. Thus, Δv reflect the impact of initial drought conditions on land surface and atmospheric variables at the interannual time scale. If the increments, Δv, follow a normal distribution with a mean of zero (essentially white noise), this would suggest that the drought initial conditions do not have a systematic impact on V. Thus, essentially the null hypothesis is tested, which, in case of rejection, suggests that indeed a systematic influence of drought initial conditions on V may exist.

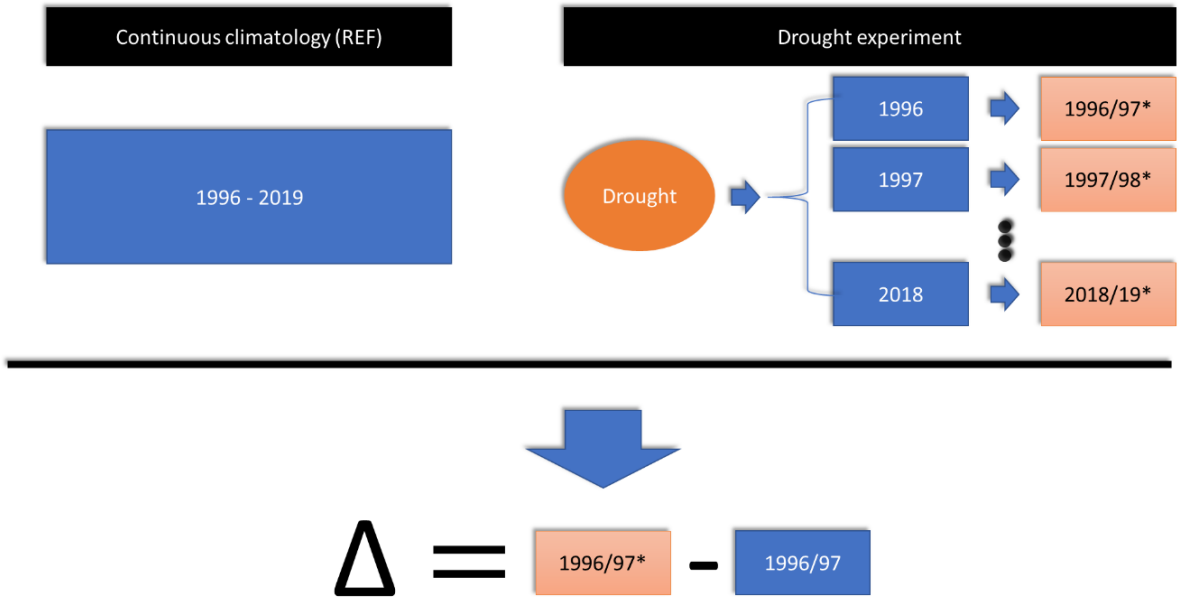

Figure 4.2: Schematic describing the experiment setup. The continuous climatology serves as a reference with a transient evolution of subsurface water and all other variables. The drought experiments consist of parallel initializations of all years of the climatology with drought states for the land- and subsurface. The altered evolutions are simulated for one year then increments are calculated for all years between the reference and the drought-influenced years.

4.3.4 Key Climate Variables

We inspected increments, Δv, defined in Section 4.3.3 of the land surface energy budget for the analyses, including net radiation at the surface (RNET), which is distributed between the sensible heat flux (SH), the latent heat flux (LH), and the ground heat flux (GH). Further, we inspected the net values of incoming shortwave (SSR) and longwave radiation (LF). SSR is determined by the solar radiation coming from COSMO and the ground albedo calculated in CLM. LF is estimated from ground temperature and cloud cover.

It is important to note that other factors than clouds like greenhouse gases and the solar cycle were constant in our configuration. Thus, under clear sky conditions, the same amount of radiation reaches the surface in the different simulations. Overall, SSR simulated by TSMP agreed well with the reanalysis product ERA5-Land (Muñoz-Sabater et al., 2021) (Figure 4.3). To calculate the water deficit in the subsurface, all soil layers are added to the total subsurface water storage (S). For cloud related variables, we analyzed the cloud ceiling height (CEILING), total cloud cover (CLT), lifting condensation level (LCL) and cloud water content (CLW).

Providing a brief explanation of the different cloud related variables, CEILING is the height at which most of the sky is covered with clouds, which can also be observed by ceilometers. COSMO has been evaluated against such observations reaching high values of reproducibility (Bucchignani and Mercogliano, 2021). CEILING is a measure for general cloud height both in convective and high-pressure synoptic situations, where cirrus clouds are formed. Under clear sky conditions, CEILING reaches an arbitrary maximum value which we removed from the analyses. LCL is a useful variable in convective situations describing the level to which an air parcel near the surface needs to be lifted to reach supersaturation and start forming a cloud. LCL does not exist as a direct model output, but Yin et al. (2015) and Romps (2017) made progress toward deriving exact solutions for LCL from pressure, humidity and temperature at the surface. We calculate the LCL with the help of the Python script provided by Romps (2017). In COSMO, CLW is the amount of water stored in clouds with a negligible fall velocity serving as a reservoir for precipitable water. By autoconversion or the interaction with existing rain or snowdrops, CLW is transformed and replenished by condensation of water vapor. Comparisons to observations are difficult because the amount of cloud water is small and difficult to separate from the total amount of water in the atmosphere. Thus, while CLW is observable, the variable is more useful in the modeling realm especially in parametrizations of subgrid scale cloudiness. CLW is also part of widely applied reanalysis products like ERA5 (Hersbach et al., 2020), to which TSMP agrees well (Figure 4.4).

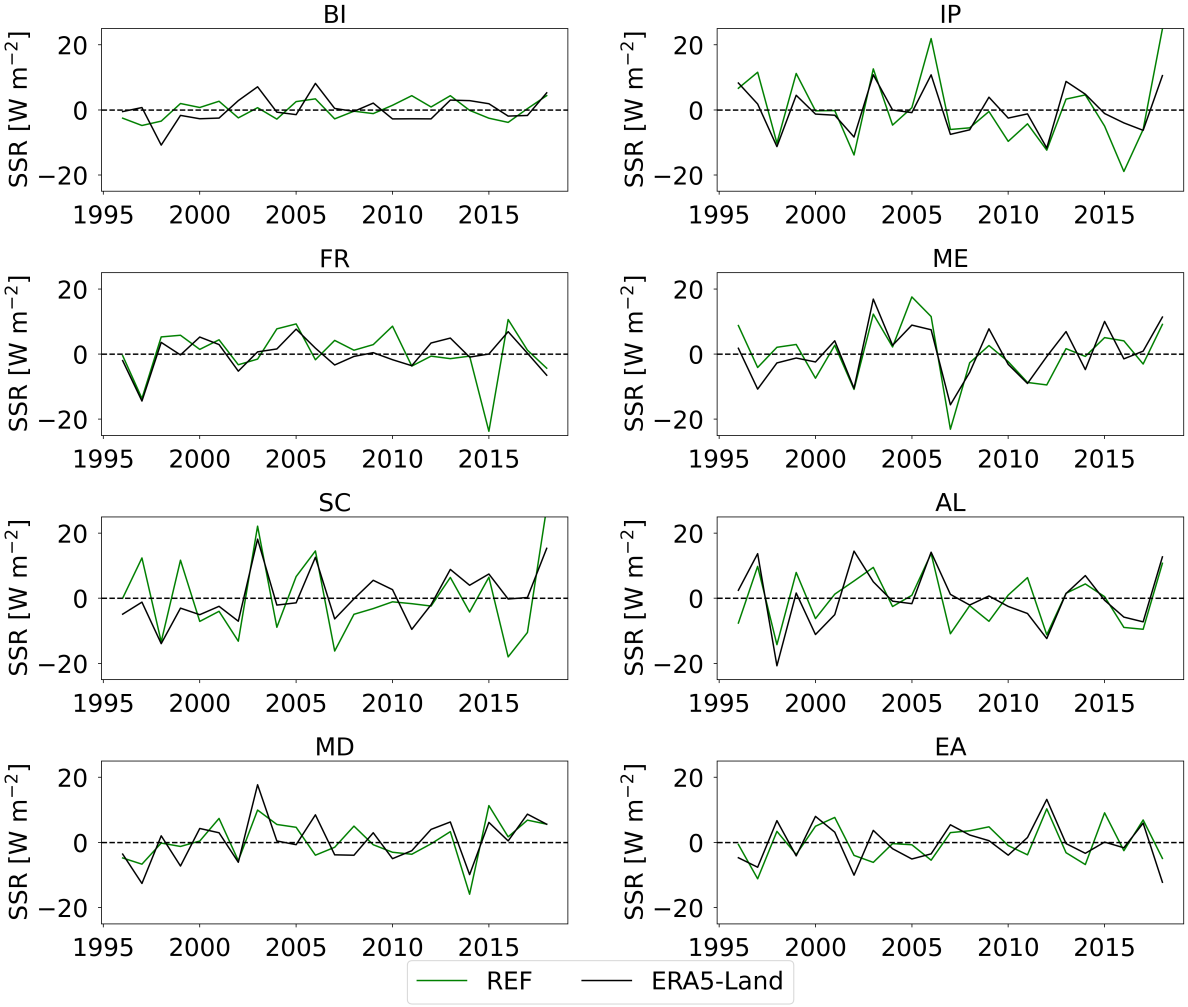

Figure 4.3: Seasonal anomalies in summer of net solar radiation SSR in the reference climatology REF and the reanalysis dataset ERA5-Land. Abbreviations are: BI: British Isles; IB: Iberian Peninsula; FR: France; ME: Mid-Europe; SC: Scandinavia; AL: Alps; MD: Mediterranean; and EA: Eastern Europe.

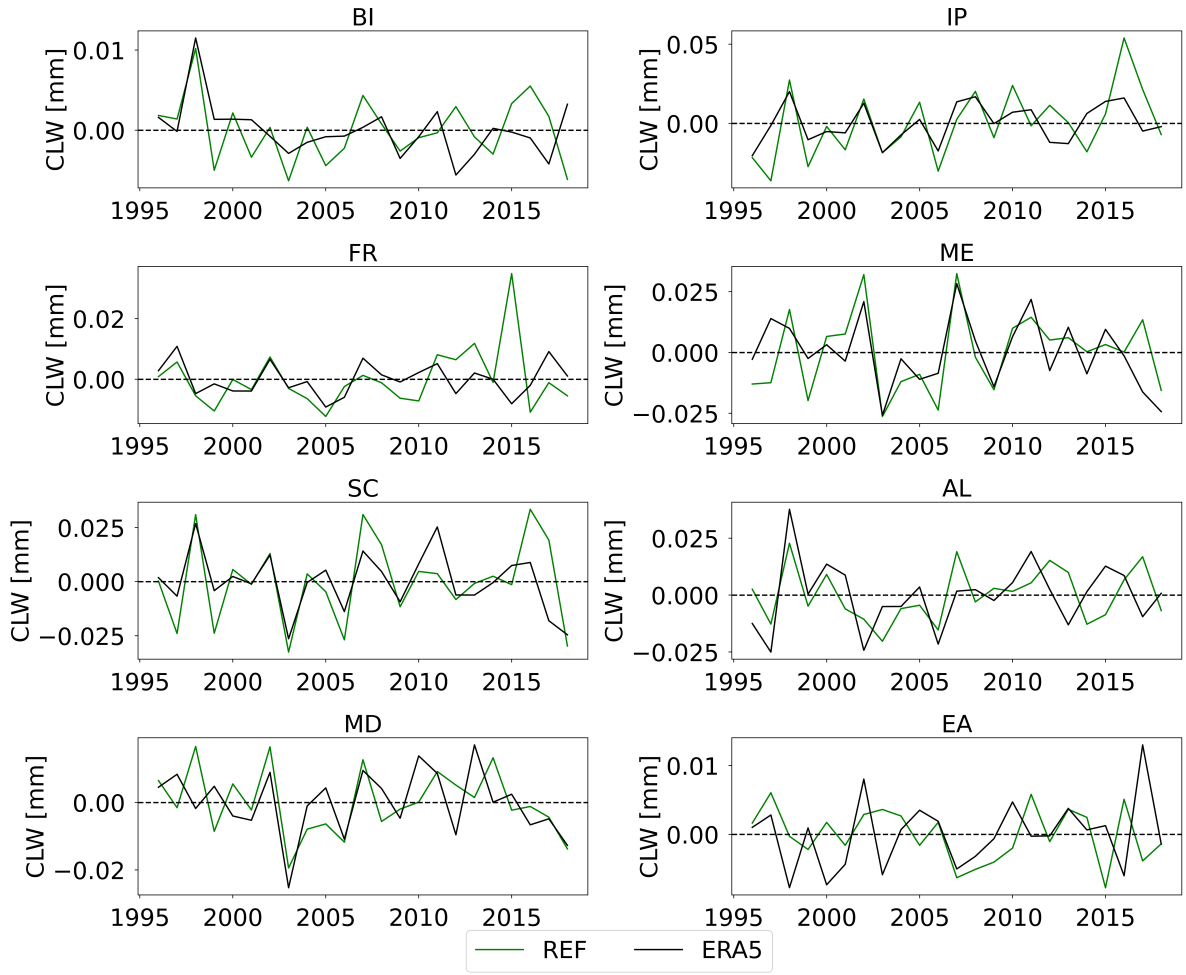

Figure 4.4: Seasonal anomalies in summer of total cloud water CLW in the reference climatology REF and the reanalysis dataset ERA5. Abbreviations are: BI: British Isles; IB: Iberian Peninsula; FR: France; ME: Mid-Europe; SC: Scandinavia; AL: Alps; MD: Mediterranean; and EA: Eastern Europe.

4.3.5 Hypothesis Testing

We applied multiple empirical and statistical techniques in the hypothesis testing, such as a two-sided t-test, Bayesian networks (Salvatier et al., 2016), and bootstrapping. Because applying significant tests on small sample sizes is questionable, all three drought ensembles with the total sample size of 66 were combined in the analyses. We present the p-values in the context of mean and standard deviation of the climatology REF. In the analyses we also consider statistically non-significant but systematic non-zero increments across all experiments (i.e. all initialization years, Y) in the rejection of the null-hypothesis in the scientific sense. To quantify the increased probability for a positive increment in SSR, we apply Bayesian inference. First, we categorize all the results of our drought experiments into two outcomes: a positive increment of SSR in summer (1) and no positive increment (0). We assign them a Bernoulli probability distribution. As prior, we assume a probability percentage of 50% for a positive increment distributed in a beta distribution. Finally, we apply a Markov Chain Monte Carlo simulation with 12,000 drawn samples from our outcomes. Each iteration proposes a modified distribution of the probability that is accepted or rejected depending on if a higher probability is reached and distribution from previous iterations. We perform the Bayesian inference with the python package pymc3. Additionally, to performing t-tests, we used bootstrapping to show the robustness of our results for SSR. Bootstrapping is random sampling with replacement from a given population. We tested our increments with a sample size of 10000 and calculated the 95% confidence interval for the mean.

Zhou et al. (2021) recently investigated coupling strength between soil moisture and precipitation with partial least square regression (PLS) (Geladi and Kowalski, 1986). The method is adapted to investigate the connection between normalized values of S and SSR

$$\Delta SSR = n_0 + n_1 \Delta S$$

n_1 is determined by PLS corresponding to the partial derivative of ΔSSR in summer to ΔS in summer. We use spatially averaged values over the PRUDENCE regions to account for the impact on a larger spatial scale. Naturally, water deficits are often paired with high values of incoming solar radiation in the same season. The dry conditions originate from an accumulation of clear sky days and a lack of precipitation. By focusing on the increments between simulations forced by the same large-scale weather conditions of each year, we exclude this effect and only investigate the influence of the altered water resources.

4.4 Results

4.4.1 Increments in the Energy Fluxes

Figure 4.5 shows the first essential result of the probabilistic numerical experiment. In Figure 4.5A-D, all energy increments, which were normalized by their naturally vari-

ability of one standard deviation, are positive or close to zero. For example, the mean ΔRNET is about 25% of the natural variability with the range reaching 100%. Thus, in the simulations with the dry initial conditions, more energy is absorbed by the land surface than in REF. This energy is mainly partitioned into SH with the mean ΔSH being close to 50% of the natural variability reaching with an even larger range. Analyses of in-situ energy flux observations during the extreme European summer of 2018 also identified sensible heat as the most affected flux of the energy cycle (Graf et al., 2020). Decomposing the net energy balance at the surface into its components ΔSSR and ΔLF (Figure 4.5E-F), the results show an increase in incoming shortwave radiation in the mean sense and a decrease in longwave radiation, in case of drought initial conditions. There is a mean increase of around $2.5\,\mathrm{W\,m^{-2}}$ for ΔSSR in absolute numbers. Compared to the natural variance, this is of considerable magnitude, especially considering the impact can be much higher in individual years.

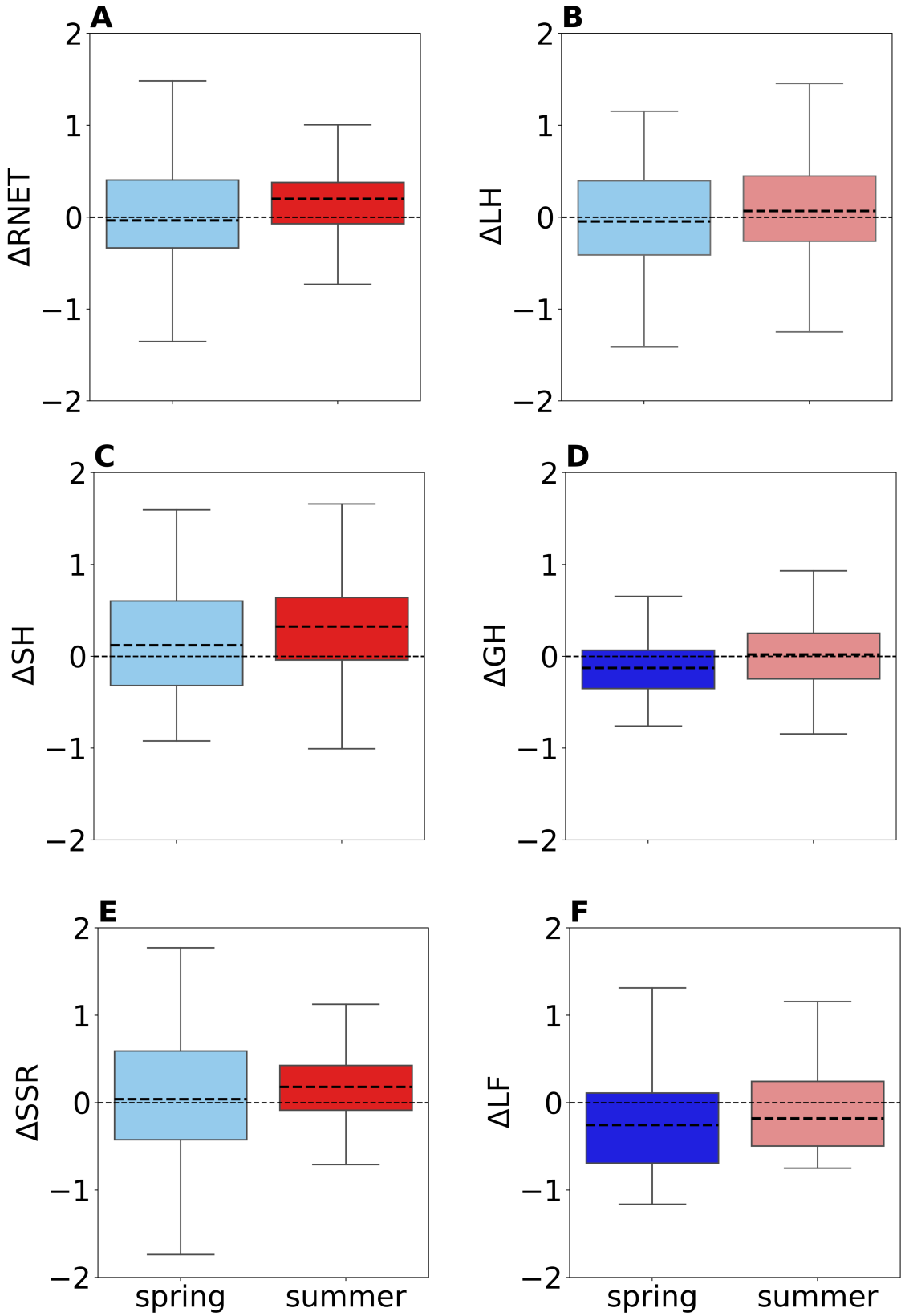

Figure 4.5: Boxplots of the normalized increments of the energy budget in spring and summer of the drought experiments. The net surface energy flux RNET (A) is shown with its components the latent heat flux LH (B), the sensible heat flux SH (C) and the ground heat flux GH (D). E and F show net energy fluxes of shortwave radiation SSR and longwave radiation LF. Light blue and red denote ensembles that did not pass a single mean two-sided t-test (p-value > 0.05). Negative values indicate a deficit in the experiments, positive values a surplus. The dotted line inside the boxes shows the average of the increments.

The darker shaded boxplots in Figure 4.5 denote in which seasons and experiments the results significantly differ in a statistical sense according to a single mean two-sided t-test. The results support the finding that significant, systematic changes are detectable only for SH, RNET and SSR; other components of the energy balance, ΔLH and ΔGH, did not show a systematic change for the different drought initial conditions, *Y*.

The determined probability of a positive increment in SSR using Bayesian inference increases to about 70% shown in Figure 4.6. The posterior distribution obtained by performing Markov Chain Monte Carlo simulation is well separated from the prior distribution with a mean of 0.5. Even the high-density interval where 94% of the experiments are distributed spans from 0.6 to 0.8. The result for the bootstrapping test are shown in Figure 4.7. Through all three experiments, the confidence intervals of the mean of ΔSSR are located above 0, showing a surplus. These results provide additional robustness for the increase of the probability for a surplus in solar radiation.

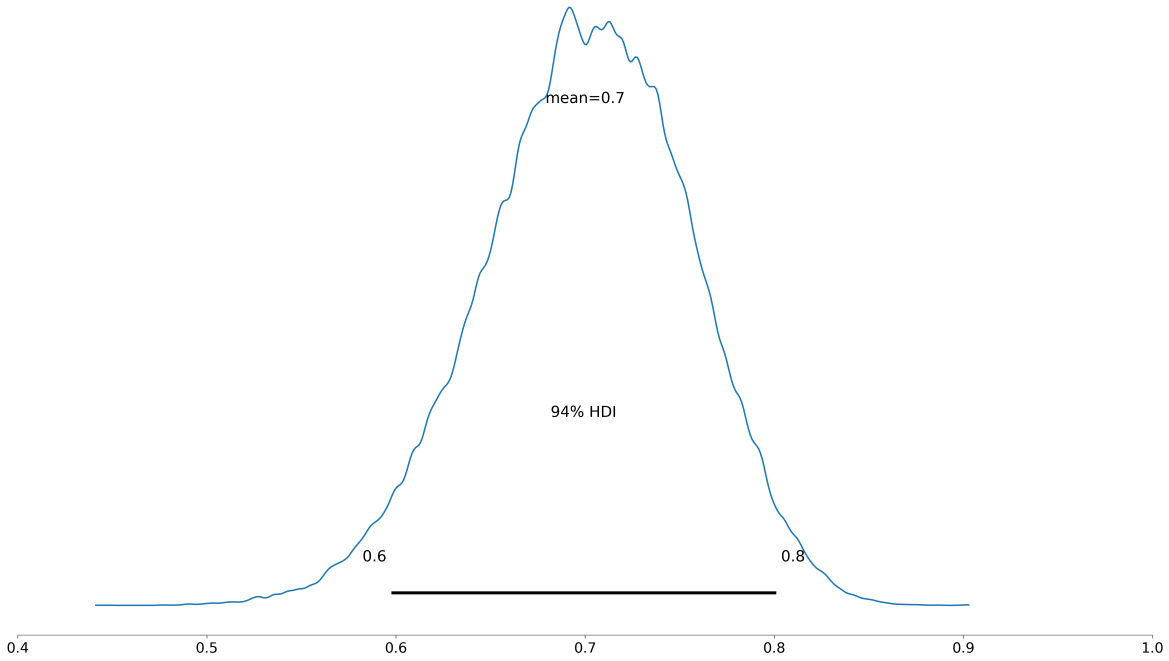

Figure 4.6: The posterior distribution obtained by Bayesian inference for a positive increment in SSR.

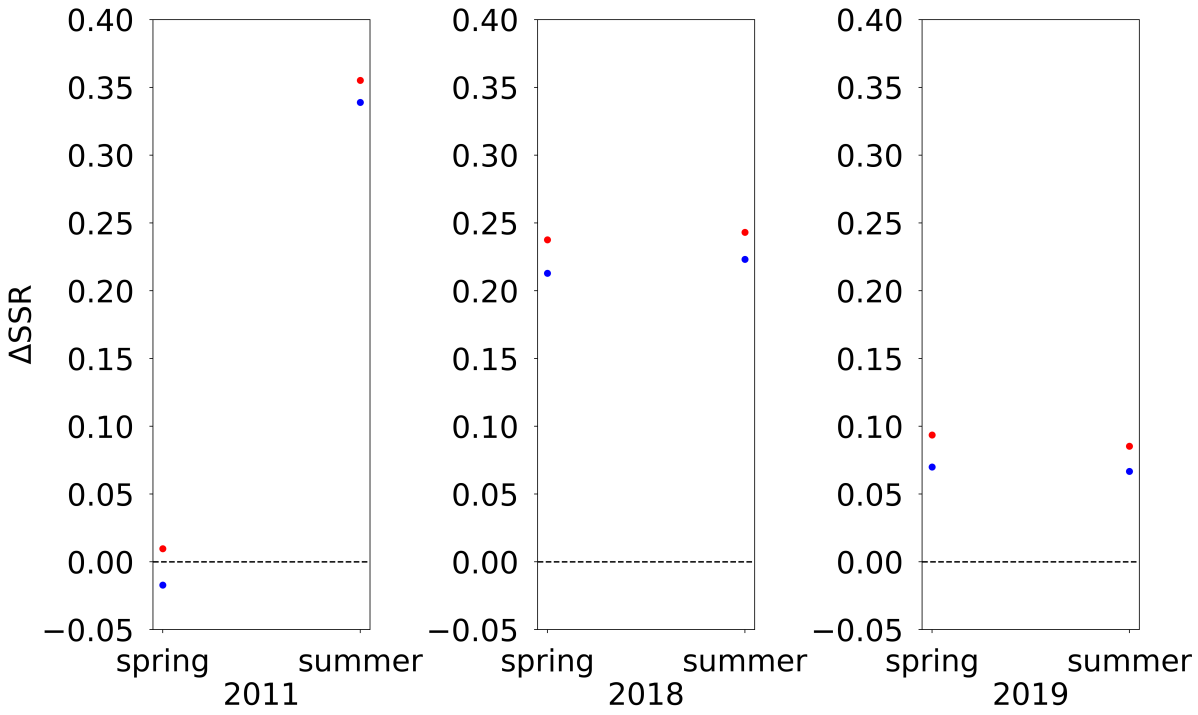

Figure 4.7: Lower bound (blue) and upper bound (red) of the 95% confidence interval of the mean of ΔSSR obtained by a bootstrapping test.

Table 4.1 summarizes the results for the sensitivity coefficient n_1 obtained by PLS for the experiment with the initial conditions of the three droughts. ME and also EA experienced in all three experiments a spatially widespread drought in the leading fall. The negative values in these regions indicate that with a more robust deficit in the subsurface water storage in summer than the original climatology, a higher surplus in net solar radiation can be expected. Therefore, there is an indication that an intense drought can affect solar radiation in the following summer regardless of the generally chaotic evolution of the weather at that time scale. The most significant sensitivity values are found in the strongest initial drought condition of 2018, while the smallest initial drought condition has the weakest coefficients. We see in other regions, which have no distinct initial condition in all three cases, that the sensitivity values fluctuate quite strongly. An aspect not included is the interplay between the regions. Widespread drought in one region could also influence other areas.

Table 4.1: Sensitivity coefficients n_1 of each Prudence region (British Isles (BI); Iberian Peninsula (IP); France (FR); Mid-Europe (ME); Scandinavia (SC); Alps (AL); Mediterranean (MD); and Eastern Europe (EA)) in each drought experiment for the feedback of the summer increment of total water storage to the increment of net solar radiation in the summer.

region	n_1 2011/12	n_1 2018/19	n_1 2019/20
BI	-0.31	-0.24	-0.31
IP	0.04	0.1	-0.03
FR	-0.26	-0.36	-0.23
ME	-0.16	-0.58	-0.38
AL	-0.37	-0.49	-0.19
SC	-0.22	-0.33	0.04
MD	0.22	-0.25	0.11
EA	-0.36	-0.77	-0.43

4.4.2 Increments in Cloud Variables

The identified changes in the energy budget have to be connected to altered cloud properties which are shown in Figure 4.8. Most notably, the cloud height is consistently higher with an average absolute CEILING increment of some $110\,\mathrm{m}$, which is on the order of the natural variability (Figure 4.8A). Total cloud cover is also consistently reduced by about 25% of the natural variability (Figure 4.8B). These two variables include all types of clouds, such as high cirrus clouds, low stratocumulus and convective clouds. The changes in cloud height seem to be the most consistent change in the ensembles with all assembled increments being significant, thus, supporting suggested feedback loop. Inspection of convective processes, Figure 4.8C shows the increments in the lifting condensation level, ΔLCL. Absolute LCL values were calculated for every grid cell individually from relative humidity RELHUM, pressure and temperature TAS and then spatially aggregated and seasonally averaged. However, the initial variables are already daily averages, including nighttime values. Since both LCL values for REF and

the drought experiments are calculated the same way, we assume this to be negligible. The values of ΔLCL indicate that changes in convective cloud generation appear to be especially important in summer with the mean close to 50% natural variability and passing the p-value threshold. We also identified a systematic reduction in total cloud water CLW (Figure 4.8D) showing that the reservoir of water in clouds is reduced.

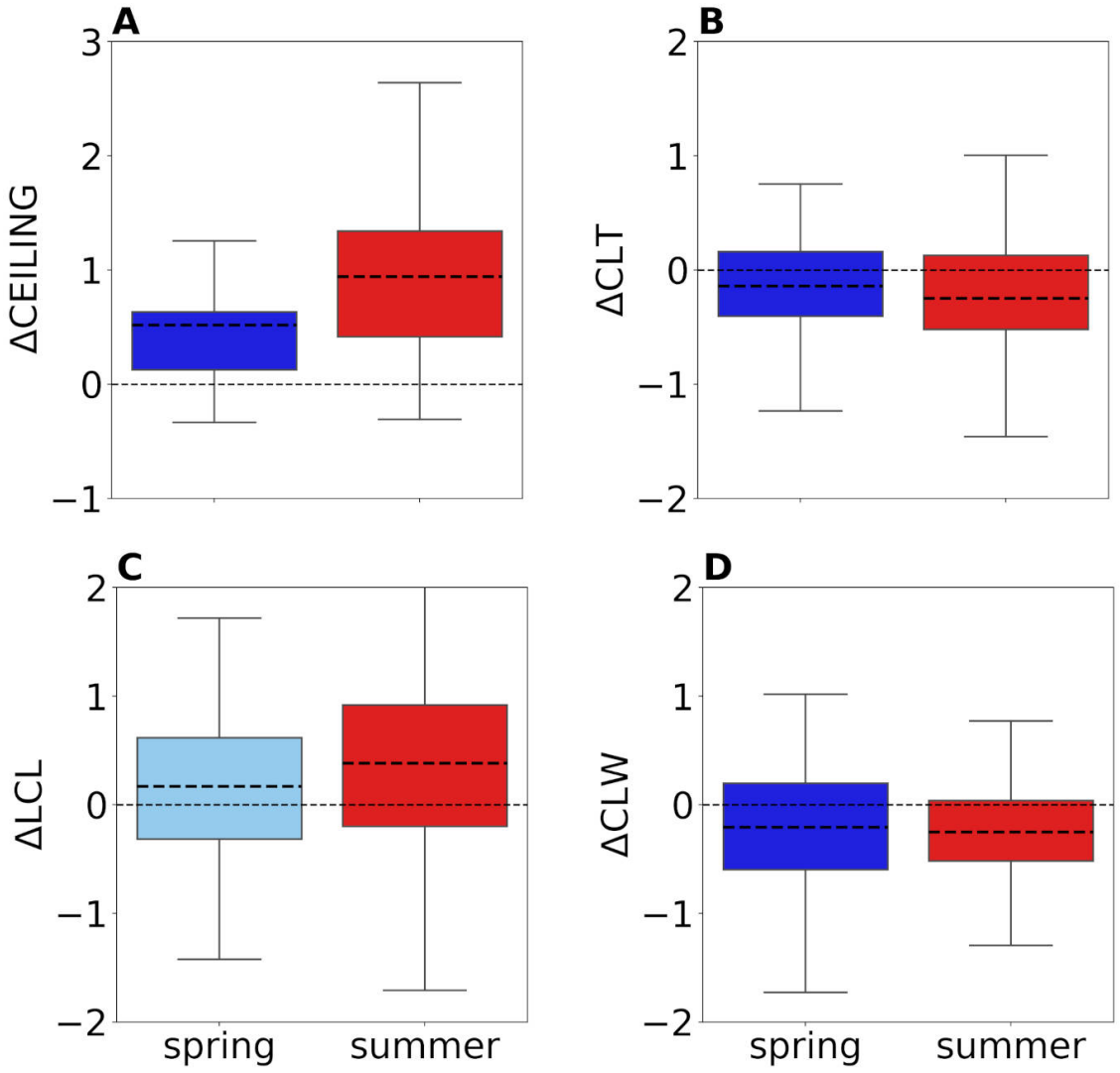

Figure 4.8: Boxplots of the normalized increments of cloud variables including the cloud ceiling height CEILING (A), the total cloud cover CLT (B), the lifting condensation level LCL (C) and total cloud water content CLW (D) of the drought experiments. Light blue and red denote ensembles that did not pass a single mean two-sided t-test (p-value > 0.05). Negative values indicate a deficit in the experiments, positive values a surplus. The dotted line inside the boxes shows the average of the increments.

Previous evaluation of the results of the ensemble in Hartick et al. (2021) has already shown that important meteorological variables like TAS and precipitation (PR) show no visible effect on the timescale of one water year while the memory effect of groundwater is evident. Figure 4.9 shows the results for ΔS, ΔTAS, the relative humidity at 2 m ΔRH and ΔPR as normalized values to strengthen that conclusion. ΔS shows significant increments throughout, while ΔTAS and ΔPR are not significant. The result for PR is exciting, showing that most precipitation processes happen in both REF and the drought ensembles while CLW values are significantly decreased. ΔRH is significant in summer. This significant reduction in RH shows that not ΔTAS is most important for the changes in LCL but the reduction in humidity at the surface.

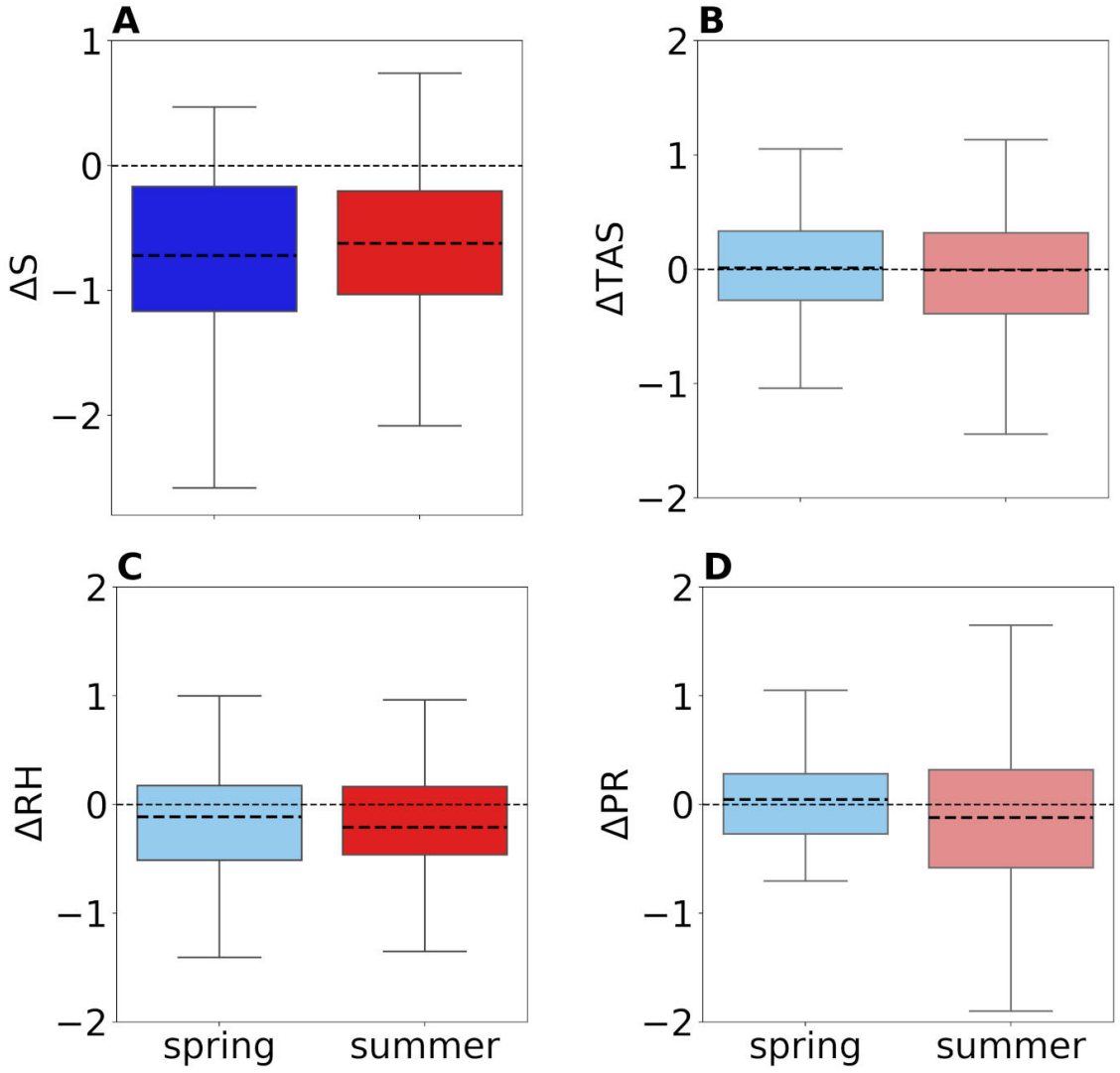

Figure 4.9: Boxplots of the normalized increments of water storage S (A), 2-m temperature TAS (B), relative humidity RH (C) and total precipitation PR (D) of the drought experiments. Light blue and red denote ensembles that did not pass a single mean two-sided t-test (p-value > 0.05). Negative values indicate a deficit in the experiments, positive values a surplus. The dotted line inside the plots marks the average.

4.4.3 The Drought Feedback Loop

These results lead us to the formulation of a positive feedback loop induced by significant groundwater storage deficits at the interannual time scale (Figure 4.10). Strong memory effects of groundwater storage deficits increase the probability of drought persistence in the ensuing year. Drought conditions change the land surface energy balance, increasing mainly the sensible heat due to an initially reduced latent heat flux because of lower water availability. A large-scale increase in sensible heat increases the energy input of the atmosphere, shifting the boundary layer and cloud height upwards to lower temperatures, where clouds have reduced water content. The drought conditions increase the lifting condensation level through lower humidity near the surface. Higher thin clouds with reduced cloud cover transmit more solar radiation to the surface, increasing net solar radiation and lowering downward longwave radiation. Thus, in the positive feedback loop, modification of cloud cover characteristics is key in increasing incoming radiation at the land surface.

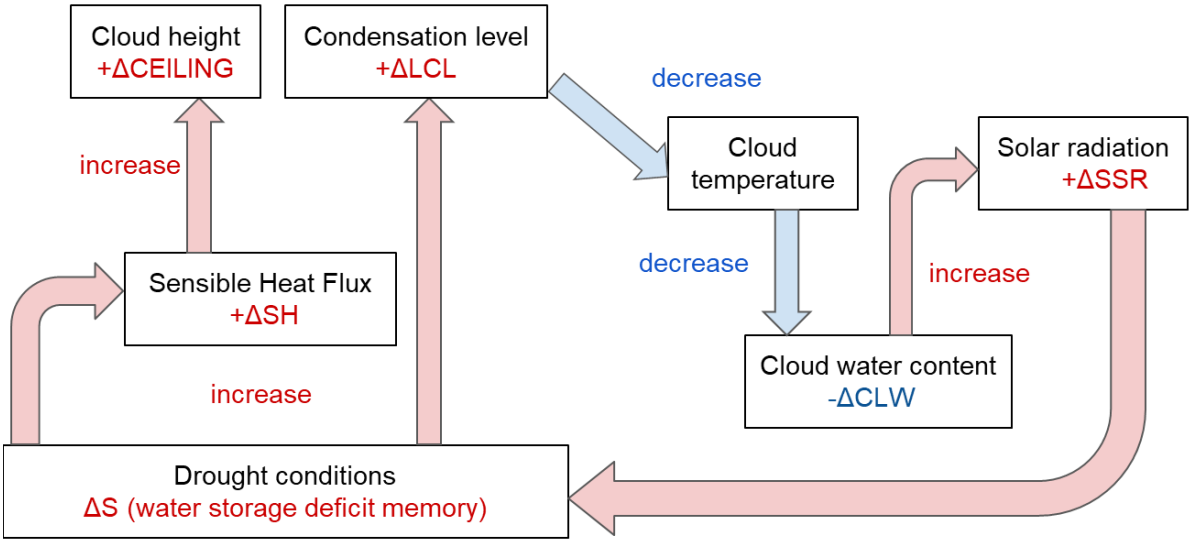

Figure 4.10: Schematic of the feedback mechanism. ΔSH, ΔCEILING, ΔCLW, ΔSSR, and ΔLCL indicate the significant increments of sensible heat flux, cloud height and cloud water content, identified as the long-term effects of drought initial conditions (represented by the water storage deficit ΔS).

The temporal onset of the feedback loop in the water year via an initial change in energy partitioning is not easily detectable at the seasonal timescale. However, there is an indication for the onset of the feedback loop at the daily timescale with opposite development of ΔLH and ΔSH at the beginning of the summer season in June shown in Figure 4.11. ΔSH shows a persistent surplus, while ΔLH increments are mainly negative. Later both fluxes develop similarly under the influence of the feedback loop. The cumulative sum of the mean increments reveals the period of a portioning shift (Figure 4.11B). For 2018/19 and 2019/20, the sum of both fluxes fluctuates until June, then the sum of LH and SH spread in opposite directions. The sum of SH continuously increases while LH stays negative until late summer. Followed by the steady growth of SH, the sum of increments of total cloud water CLW steadily decreases. Anticorrelated to this development is the continued growth of the sum of solar radiation SSR showing the acceleration of the energy cycle. Despite some already positive increments of SSR in spring, the steady decrease in CLW begins after the spread between LH and SH, which is an indication of the feedback loop. The experiment of 2011/12 develops differently; the spread is much less pronounced while there is still a steady increase in all fluxes. Still, there is a significant effect over all ensemble members concerning SSR. The sum of increments in LH is probably too low to impact water transport to the atmosphere.

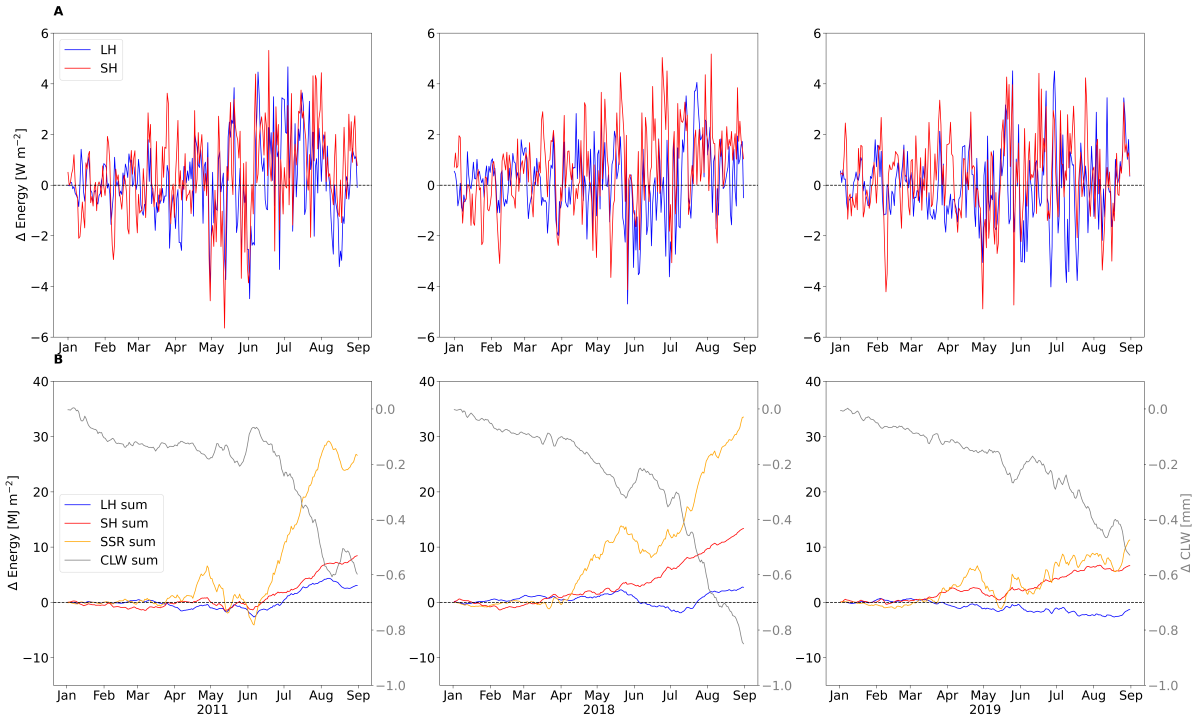

Figure 4.11: Daily mean increments of latent (LH) and sensible heat flux (SH) for each ensemble (A) and the cumulative sums of the increments of LH, SH, net solar radiation (SSR) and cloud water (CLW) over the region ME (B).

To better understand to development for the experiment of 2011, it might be helpful to look at neighboring regions. Figure 4.12 and 4.13 show the development in the regions of France (FR) and Eastern Europe (EA), respectively. Both are partly affected by drought for the three initial conditions. 2011 has an exceptionally dry initial state in FR. For 2011/12 over FR, the partitioning shift and the order of reduction in CLW are much more pronounced than in ME, suggesting that the main feedback loop happens in FR and could have influenced ME. In contrast, no apparent portioning shift is visible in FR for 2018/19, which could mean that the main drought effects shifted to ME. The region EA shows clear effects for 2011/12 and 2018/19 on a smaller level. 2019/20 shows a portioning shift to more LH, which is accompanied by higher values of CLW and less SSR.

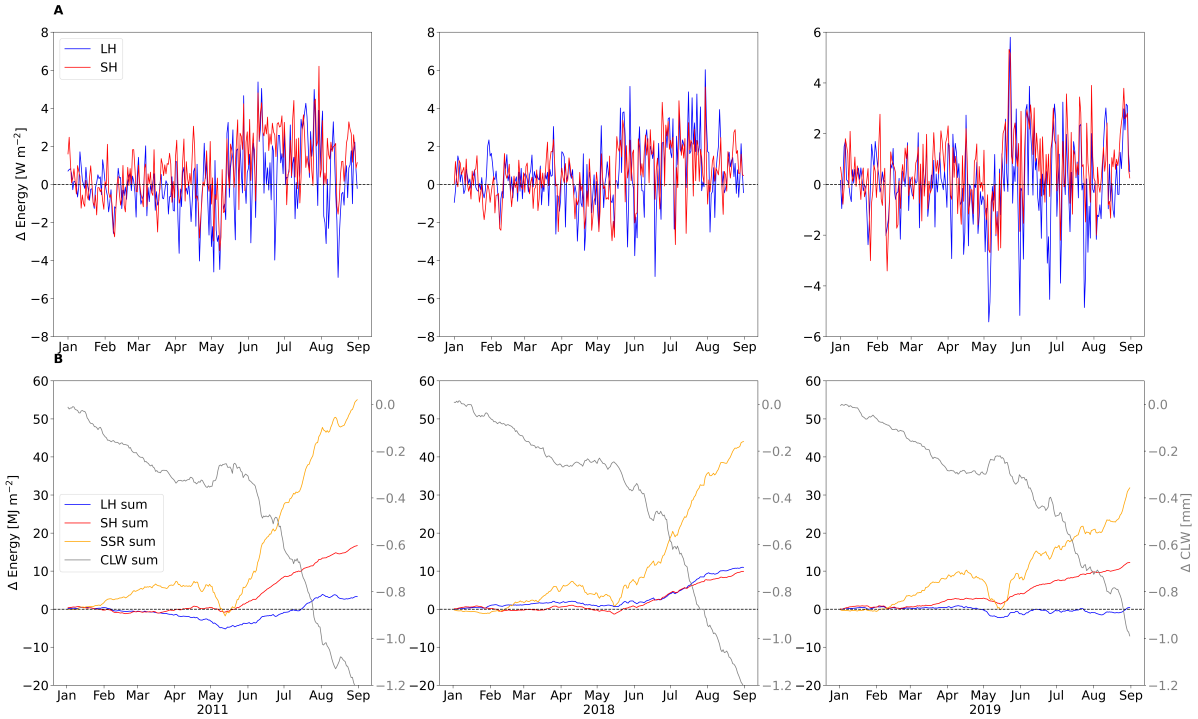

Figure 4.12: Daily mean increments of latent (LH) and sensible heat flux (SH) for each ensemble(A) and the cumulative sums of the increments of LH, SH, net solar radiation (SSR) and cloud water (CLW) over the region FR (B).

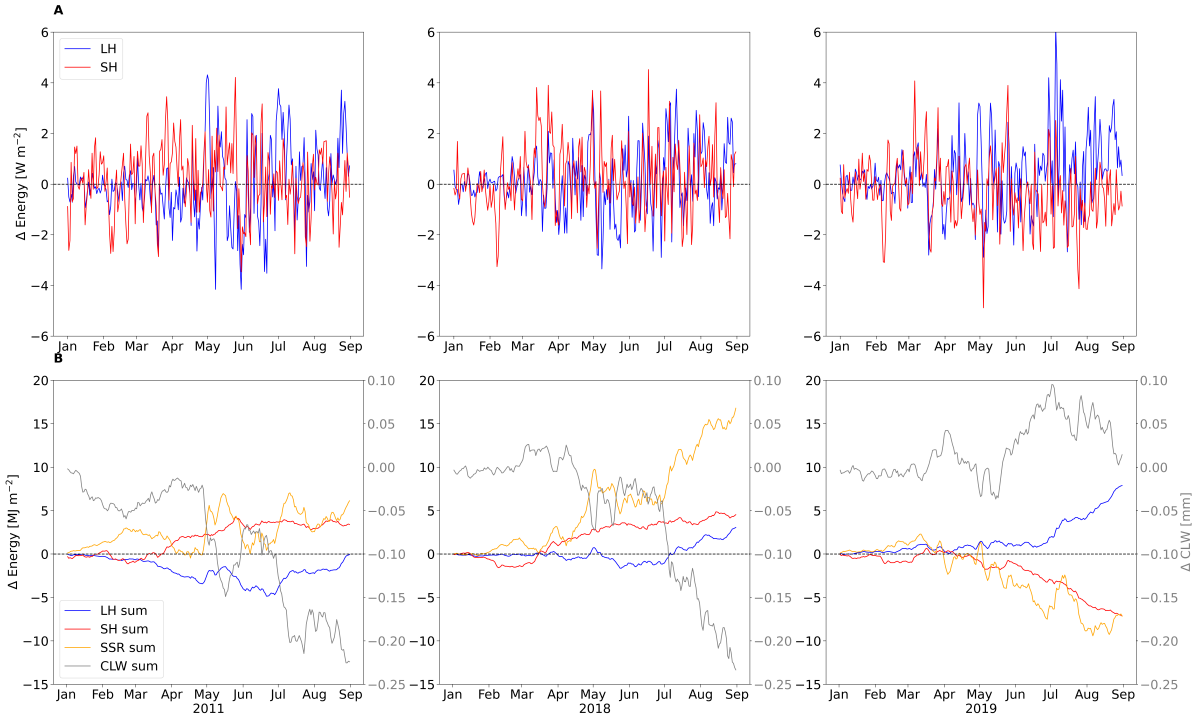

Figure 4.13: Daily mean increments of latent (LH) and sensible heat flux (SH) for each ensemble(A) and the cumulative sums of the increments of LH, SH, net solar radiation (SSR) and cloud water (CLW) over the region EA (B).

To provide context for the increments of all variables, Table 4.2 shows the p-value, the summer mean and standard deviation in REF and the mean increment of all discussed variables. The values are sorted from the lowest to the highest p-value. Inspecting the order of magnitude, CEILING and S have the lowest p-value. The low value for S is intuitive, because it is a direct consequence of the applied drought initial conditions. The other variables in the feedback process (SH, CLW, LCL, CLT, RNET, SSR and RELHUM) are roughly in the same order of magnitude. The low p-value of CEILING could be connected to other unknown atmospheric processes. The p-value of the remaining variables (LF, PR, LH, GH and TAS) are not significant, thus not directly influenced by the drought initial condition at the interannual time scale.

Table 4.2: p-values, summer mean and std of REF and mean increments for every variable. P-values are obtained by sampling all summer increments with a single mean two-sided t-test. The null hypothesis is a mean of 0.

variable	p-value	summer mean	std	MeanΔ
CEILING	6.94e-13	8488.25 m	119.97 m	112.95 m
S	7.57e-09	23687 mm	20.13 mm	-12.54 mm
SH	2.29e-05	29.82 $\mathrm{W\,m^{-2}}$	3.19 $\mathrm{W\,m^{-2}}$	1.03 $\mathrm{W\,m^{-2}}$
CLW	4.43e-05	0.07 mm	0.02 mm	-0.004 mm
LCL	1.30e-03	352.08 m	10.43 m	3.99 m
CLT	1.56e-03	77.0 %	4.0 %	-0.01 %
RNET	2.09e-03	97.67 $\mathrm{W\,m^{-2}}$	6.74 $\mathrm{W\,m^{-2}}$	1.35 $\mathrm{W\,m^{-2}}$
SSR	4.00e-03	146.19 $\mathrm{W\,m^{-2}}$	14.0 $\mathrm{W\,m^{-2}}$	2.51 $\mathrm{W\,m^{-2}}$
RELHUM	2.31e-02	76.93 %	1.57 %	-0.33 %
LF	1.45e-01	50.02 $\mathrm{W\,m^{-2}}$	5.34 $\mathrm{W\,m^{-2}}$	-0.99 $\mathrm{W\,m^{-2}}$
PR	2.00e-01	77.8 mm	12.23 mm	-1.48 mm
LH	3.55e-01	62.97 $\mathrm{W\,m^{-2}}$	3.29 $\mathrm{W\,m^{-2}}$	0.22 $\mathrm{W\,m^{-2}}$
GH	7.36e-01	4.86 $\mathrm{W\,m^{-2}}$	1.57 $\mathrm{W\,m^{-2}}$	0.03 $\mathrm{W\,m^{-2}}$
TAS	9.92e-01	288.11 K	0.97 K	-0.01 K

4.4.4 Spatial Inspection of the Results

In Figure 4.14A, the exemplary spatial inspection of the increments for the drought conditions of 2018 shows that the impact and memory effect of the applied initial drought conditions on ΔS in the following summer are widespread but spatially heterogeneous. Mean ΔSSR (Figure 4.14B) in summer is spatially more homogeneous suggesting modifications of characteristics in atmospheric conditions that cannot be attributed to spatially continuous changes of land surface albedo. The grid cell-wise correlation between ΔS and ΔSSR is negative for most of the domain (Figure 4.14C), corroborating previous conclusions that more negative deficits lead to higher surpluses in net shortwave radiation. Exceptions are positive values near northern coastal regions, which can be explained by shallow groundwater (Figure 4.14D) along the modeled coastlines, which are more likely to experience less deficits and recover faster due to groundwater convergence.

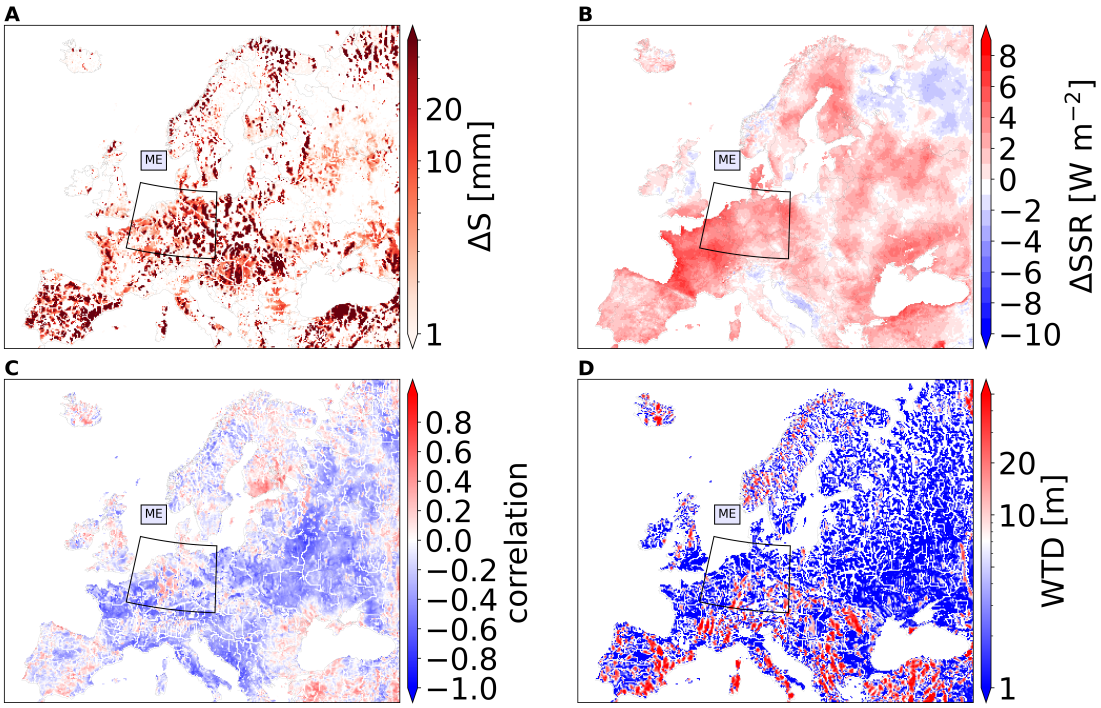

Figure 4.14: Spatial pattern of the mean increment of the 2018 experiment for the subsurface water storage deficits in summer in logarithmic scale (A), incoming solar radiation increment in the summer (B), and Pearson Correlation between the increments (C) and the average water table depth in the domain from the year 1996 to 2018 illustrated on logarithmic scale (D). ME (Mid-Europe) indicates the focus region of the study.

4.5 Conclusion

For the first time, the presented ensemble simulations demonstrate a positive hydrologic drought feedback of groundwater storage deficits on atmospheric processes related to cloud processes and radiation at the interannual timescale in the mid-latitudes. The net solar radiation is systematically larger in the summer months following groundwater drought conditions in the previous fall. Thus, groundwater drought potentially enters a positive feedback loop with cloud forming processes and incoming solar radiation in successive years, increasing the probability of drought persistence. There exists evidence for the proposed feedback loop in observational and reanalysis data for the Canadian great plains (Greene et al., 2011) and China (Zeng et al., 2019), emphasizing the global relevance. Over Europe, similar feedbacks involving reduced soil moisture have been identified in climate projections, however primarily attributed to changes in the latent heat flux (Vogel et al., 2018). In this study, the identified feedback loop is based on simulation results and, thus, impacted by uncertainties related to input parameters, and simplifying model assumptions and parametrizations at the respective spatial resolution on the order of 10 km. While TSMP has been evaluated in previous studies with observations showing good agreement and a high degree of physical realism (Furusho-Percot et al., 2019; Hartick et al., 2021) the proposed feedback loop has not been evaluated directly. Corroboration of the identified feedback loop under widespread drought condi-

tions with observations would require future studies to connect field measurements with remote sensing data. In Earth system modeling, global and most regional climate models do not capture groundwater memory effects. Thus, current climate modeling studies might underestimate the temporal persistence of droughts and compound events.

Chapter 5

New Water Cycle Balance due to Groundwater-Precipitation Interactions in a Fully Coupled Terrestrial Model

5.1 Publishing Information and Individual Contribution

The following chapter is a draft ready to be submitted to a scientific journal. Prof. Stefan Kollet and I developed the initial idea for the simulation setup. Stefan Kollet also gave ideas for the visual representation and provided helpful suggestions for the text. I carried out the simulation, analysis, visuals, and text writing.

Abstract

Groundwater can be a significant source for replenishing soil moisture, indirectly contributing to increased evapotranspiration rates. The contribution's importance depends on the water table's location, which is not well measured on larger scales. Besides missing data, groundwater interactions with the atmosphere are not well represented in climate models. Although the effect is assumed to be insignificant in relatively humid regions in Europe, there could be impactful feedback processes under extreme conditions or due to the effects of climate change. Fully coupled terrestrial models are able to capture these feedbacks, still encountering the problem of sparse groundwater data and obstacles hindering calibrating subsurface parameters. Unlike offline groundwater models, changing subsurface parameters can start a feedback on the incoming precipitation, influencing subsurface conditions. We show that such an interplay between groundwater and atmosphere exists over Continental Europe with the Terrestrial Systems Modeling Platform. Perturbations in subsurface parameters lead to changed groundwater depths of more than one meter compared to a reference climatology. Precipitation is significantly increased in most cases influencing the whole water balance. The altered water cycle can be observed by a different seasonality in water tables and changes in the atmospheric pressure regime over Europe. In extreme precipitation events, this can even alter the circulation so that these events lose strength. The results highlight the sensitivity of long-term atmospheric developments to groundwater levels and stress that standard calibration methods are unsuitable for fully coupled models.

5.2 Introduction

The primary transport process of the water cycle transports water from the oceans to the land in the form of precipitation (PR) (Levizzani and Cattani, 2019). Especially in the mid-latitudes, low-pressure systems are responsible for most of the rainfall during the year. During most of these events, the system is energy limited, where additional water supply is not significant for the PR amount. In summer with more available energy, soil moisture recycling becomes more critical and evapotranspiration significantly contributes to precipitation (Bisselink and Dolman, 2008). In fact, increasing the latent heat release in an air column is the main tool in convective permitting models to correct PR rates according to radar data (Stephan et al., 2008). However, soil moisture - precipitation coupling (SM-PR) is often assessed to be less significant over Central Europe (Koster et al., 2006; Zhou et al., 2021). However, the land-atmosphere coupling (LA) cannot be discarded over Europe in general. For example, the influence of soil moisture on temperature is well proved on climate time scales, especially in the case of heatwaves (Seneviratne et al., 2010; Miralles et al., 2019; Keune et al., 2019). However, the formation of PR is a more complex process and is under the influence of inherent chaos in atmospheric models. Altered pressure and wind fields are essential for changes in PR. Studies are able to identify circulation changes initiated by soil moisture, especially in situations with a lot of convective precipitation (Frye and Mote, 2010; Durkee et al., 2014). There

is also an influence visible on the seasonal timescale. For example, Diro et al. (2021) showed with a principal component analysis that soil moisture alters temperature modes over North America and influences pressure fields. Typically, sea Surface temperatures greatly influence the pressure distribution of the North Atlantic Oscillation, which greatly impacts the continental pressure fields from Northern to South Europe (Wanner et al., 2001; Börgel et al., 2020). But especially during extreme events, local factors can also play a vital role (Boé, 2013). The complexity of PR development is also visible in climate projections over Europe. Extreme precipitation is going to increase and there is a wetting/drying trend in Northern/Southern Europe but especially many uncertainties over Central Europe (Matte et al., 2019; Christensen et al., 2019).

Surface soil moisture is mainly determined by past rates of PR and enables evapotranspiration (ET). Additionally, there is water supply by the groundwater table, which can mitigate heatwaves (Keune et al., 2019) but also remembers recent droughts via groundwater memory (Hartick et al., 2021). Although datasets retrieved from remote measuring enable new insights about the total water stored in the surface, shallow groundwater estimations remain uncertain. For gridded data on the continental scale, modeling techniques are still needed that use many assumptions (Stampoulis et al., 2019). To adequately model the feedbacks from the groundwater table via the land surface to the atmosphere, there are fully coupled terrestrial models (Barlage et al., 2015). For analysis of groundwater feedbacks, terrestrial models with a 3D groundwater component are of importance. All the individual models representing the terrestrial system have their parameters. In typical applications of land models with prescribed atmospheric conditions, calibration is often a must to match observations and to be integrated into forecasting architectures (Pappenberger and Beven, 2006). Although there are new developments in simplifying and automatizing this process with machine learning (Tsai et al., 2021; Maxwell et al., 2021), a fully coupled framework increases the complexity to a level that prevents calibration. In general, machine learning gains knowledge from training datasets, which are limited to a particular region and time period. The transfer of the gained knowledge to another domain under a compactly different influence might be a naive extrapolation. In contrast, physically based models have a higher potential for successful knowledge transfer (Reichstein et al., 2019).

An example of a feedback process that might break calibration is illustrated in Figure 5.1. Increasing the hydraulic conductivity (K) in a subsurface column decreases the water table depth, leading to more precipitation. The increase in PR leads to an even shallower water table which further influences K. In models concentrating on the subsurface, this process does not exist. In fully coupled models, it introduces an additional challenge.

Various studies have investigated SM-PR (Koster et al., 2006; Huang and Margulis, 2011; Zhou et al., 2016; Dirmeyer et al., 2021; Zhou et al., 2021) coupling and studies that work with prescribed soil moisture conditions (Ardilouze et al., 2019). However, these studies often lack a 3D groundwater representation. With TSMP, we are able to conduct a simulation with homogeneous subsurface parameters (HOM) that lead to consider-

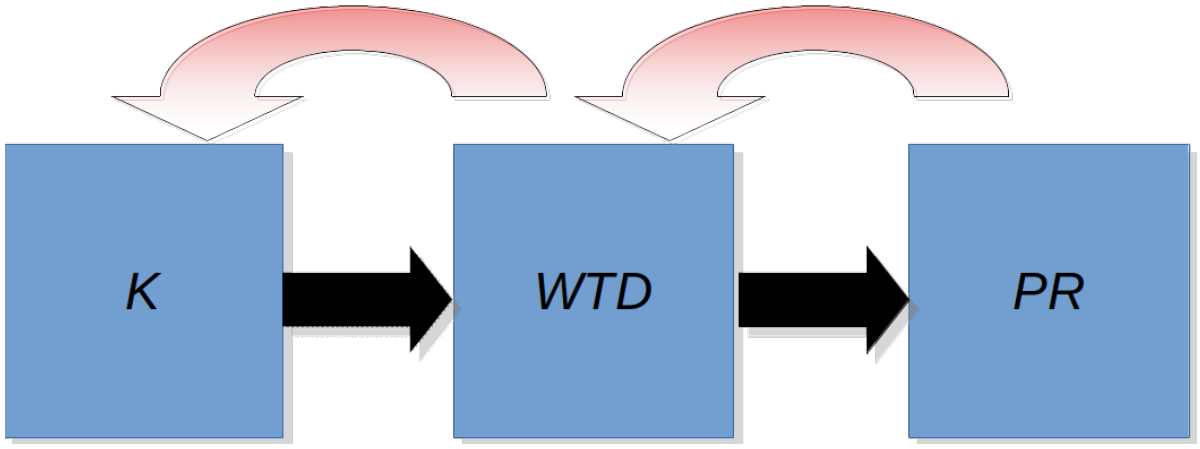

Figure 5.1: Schematic of the two-way feedback between hydraulic conductivity (K), tater table depth (WTD) and precipitation (PR).

ably shallower water tables over Central Europe. The result is not homogeneous soil moisture over Europe but generally more available surface water via a higher supply by groundwater. The decision for these homogeneous parameters may seem somewhat random. However, climate models without a proper subsurface parametrization like a free draining approach (Campoy et al., 2013) also have a rather arbitrary boundary condition.

In contrast, HOM enables the subsurface to interact with the whole water cycle, which makes a new balance possible. The simulation is conducted on a climatic timescale from 1989 to 2018. The experiment enables us to answer the research questions of this paper: Is there a significant influence of the water table depth on precipitation over Europe and the resulting consequences for calibration of the subsurface component? Is the development of water table anomalies altered and are changes in wind or pressure fields visible?

5.3 Methods

5.3.1 Model System and Domain

In this study, TSMP consists of the subsurface model ParFlow v3.2, the land scheme CLM 3.5 and the atmospheric model COSMO v5.01 coupled via the OASIS3-MCT (Valcke, 2013) coupler. To this point, TSMP has been used in various studies (Keune et al., 2019; Furusho-Percot et al., 2019; Hartick et al., 2021). A more detailed description of the model can be found in Shrestha et al. (2014); Gasper et al. (2014). COSMO v5.01 (Baldauf et al., 2011) is a numerical weather forecast model suited for regional modeling on climate timescales. It solves the non-hydrostatic Euler equations with variable vertical and horizontal resolutions. At the land surface, COSMO is coupled to the Community Land Model 3.5 (CLM) (Bonan et al., 2002; Oleson et al., 2008) exchanging wind, humidity, precipitation and temperature. The CLM simulates vegetative, energy and hydrological processes with 16 plant functional types. The simulated sensible and latent heat fluxes are

sent back to the atmospheric model. The groundwater component of CLM is completely replaced by the hydrological model ParFlow (Ashby and Falgout, 1996; Jones and Woodward, 2001; Kollet and Maxwell, 2006; Maxwell, 2013; Maxwell et al., 2021), which solves 3D variably saturated groundwater-surface water flow. The used Richards equation is solved with a Newton-Krylov solver. Overlandflow is simulated with the kinematic wave equation in a finite volume approach. From the coupling process with CLM, ParFlow receives water from precipitation and loses water due to evapotranspiration handled in CLM.

This study relies on the reference climatology (REF) published in Furusho-Percot et al. (2019), where a fully coupled TSMP setup was simulated from 1989 to 2019 with lateral boundary forcing from ERA-Interim (Dee et al., 2011) capturing various variables from the water table to the cloud top. The subsurface component received a spin up over 20 years and the first seven years of the simulation were not used for analysis to provide additional spin up time. The modeling domain is the European Coordinated Regional Downscaling Experiment (CORDEX) domain (Giorgi et al., 2009; Gutowski et al., 2016) with eight subdomains that allow regional analysis in different climatic regimes of continental Europe (Christensen and Christensen, 2007). The grid has a horizontal resolution of $12.5\,\mathrm{km}$ and a vertical extent from $22\,\mathrm{km}$ above ground to a depth of $57\,\mathrm{m}$ into the subsurface. The time step size for COSMO is $60\,\mathrm{s}$, while CLM and ParFlow have a step size of $900\,\mathrm{s}$ equivalent to the coupling frequency. Besides changes in the subsurface parameters, all other settings of the atmosphere and land surface of the simulations in this study are equivalent to REF.

The topographic slopes for ParFlow derived from the USGS GTOPO30 (DAAC, 2004), the Manning's coefficient determined the overlandflow and the Dirichlet boundary conditions with constant pressure at the coasts remain unchanged to REF. The soil parameters for porosity, permeability and constants for the van Genuchten equation change to homogeneous values for the whole domain. However, horizontal permeability values are still scaled by 1000 according to Niedda (2004) and Fang et al. (2016) to compensate for the information loss by the gridscale. This illustrates the fact that the new parameters are not entirely unrealistic but a rough average of all available soil types in REF.

5.3.2 The Homogeneous Run (HOM)

The homogeneous run is started at 1. February 1989, with the first atmospheric restart of COSMO. Initial conditions for the land and subsurface are taken from the end of January 2001, which was neither exceptionally dry nor wet. In contrast to the original values of REF, the homogeneous subsurface parameters for all of Europe lead to a decreased subsurface water storage capacity in large parts of Europe. Mountainous areas and the Mediterranean PRUDENCE region (MD) have a higher storage capacity. Figure 5.2 illustrates this for permeability in the z-direction (A) and the porosity (B). The values from HOM are subtracted by the values of the REF. The new subsurface parameters lead to an adaption process of water resources in the subsurface, which will take several

years. For that reason, we start most of the analysis beginning in the year 1996. For most comparisons, each year in HOM is compared to the original realization of that year in REF. By comparing the results year-wise, the developments are analyzed under the same large-scale atmospheric conditions.

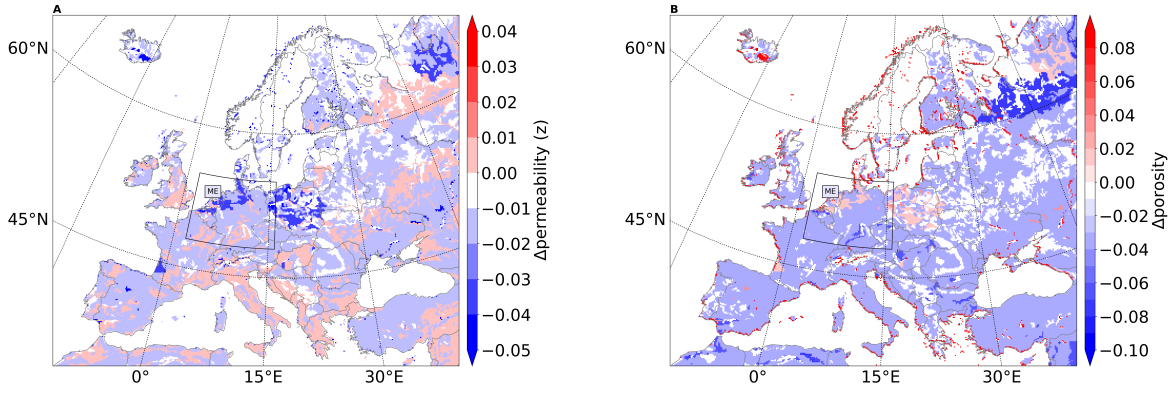

Figure 5.2: Difference in permeability in z-direction (A) and porosity (B).

5.4 Results

5.4.1 Evolution of Water Tables

Figure 5.3 depicts the absolute evolution of water table depth (WTD) in all eight PRUDENCE regions. The adaption to the new subsurface parameters is completed for most regions in 1996. IP still shows spin up effects until the beginning of the 2000s, likely because the difference in water tables is highest with changes around 3 m. For most other regions, including the focus region ME the difference is 1.5 m. There is already some indication that the variance of the seasonal cycle and the reaction to extreme events is less pronounced in HOM. One reason is the lower storing capacity of the subsurface in all regions except MD, but further reasons are changes in PR and evapotranspiration in hot and dry periods. The following chapters will shed more light on this, especially for the region ME.

5.4.2 Evolution of Latent Heat and Precipitation

The significantly shallower water tables provide additional water to the surface. In the case of at least slightly water limited evapotranspiration, latent heat flux should be increased. Going further, this should increase convective precipitation in spring and summer, where local moisture recycling can have an impact. Figure 5.4 shows the cumulative daily increments in all the years of the simulation for LH and PR. LH is consistently increased in nearly all simulation years. Only the first year of simulation, 1989, shows no apparent difference, which is expected. Two years are less impacted with cumulative increases of less than 20 MJ. Another cluster of years has an increase of

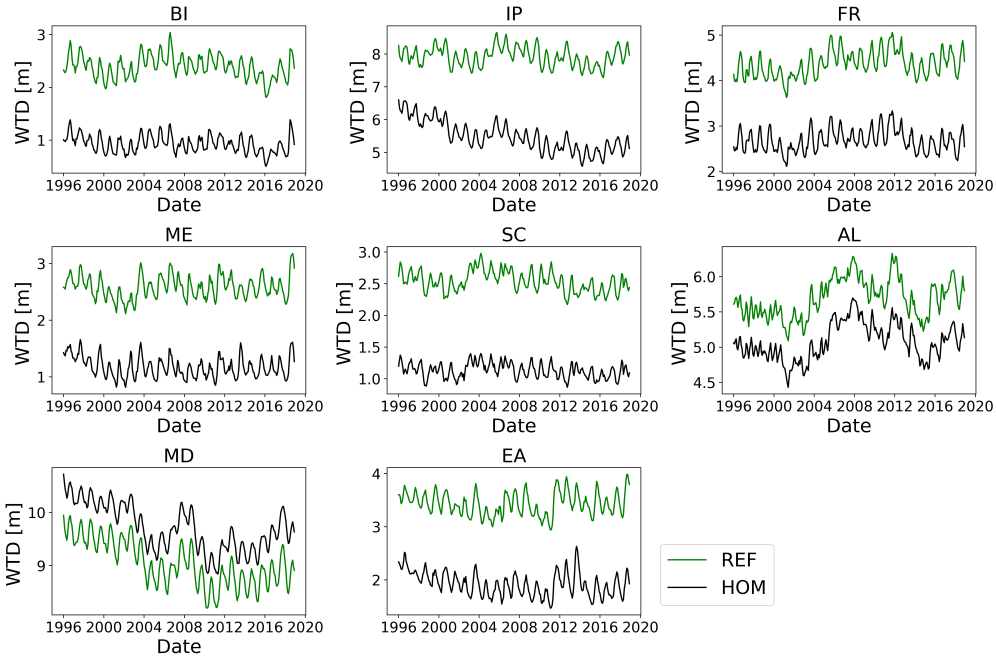

Figure 5.3: WTD evolution in all PRUDENCE regions for the climatology REF and the homogeneous run HOM.

about 40 MJ with some decreases in latent heat later in the year and lastly, there is a cluster with nearly constant increases to around 80 MJ.

The results for precipitation show that the effect of more water transported to the atmosphere is not directly converted to rainfall. Although we can identify relatively steady increases for a cluster of years to end of the year values of around 50 mm per year, another set of years hardly shows an impact. An explanation is the dominant type of precipitation in ME throughout most of the year. Large-scale weather systems from the Atlantic bring most of the PR. These fronts do not take up much local moisture because their lifetime is short, around one or two days, and the atmosphere over ME is too stable. Furthermore, the 2-m temperatures and generally available energy are too low over most of ME through the year. Nevertheless, there are still enough convective precipitation periods where the increase of latent heat can be converted to significant increases of PR.

The long-term average of annual precipitation from 1961 to 1990 in Germany is 789 mm (Brasseur et al., 2017), so an increase of the shown magnitudes can be around 6%. Figure 5.4 reveals that the rise is often pronounced in a few months up to a season. The average seasonal PR in Germany is around 200 mm. Therefore, an increase of about 50 mm translates to 25% more PR. Outstanding are the two years with massive decreases in precipitation, which still have an increase in LH. For such an enormous decrease, the circulation in the two years has to be massively altered. Chaotic developments in the atmosphere could explain it because the two years were comparably wet. However, it is

possible the altered WTD also affected the general circulation. We will take a look at that in later chapters.

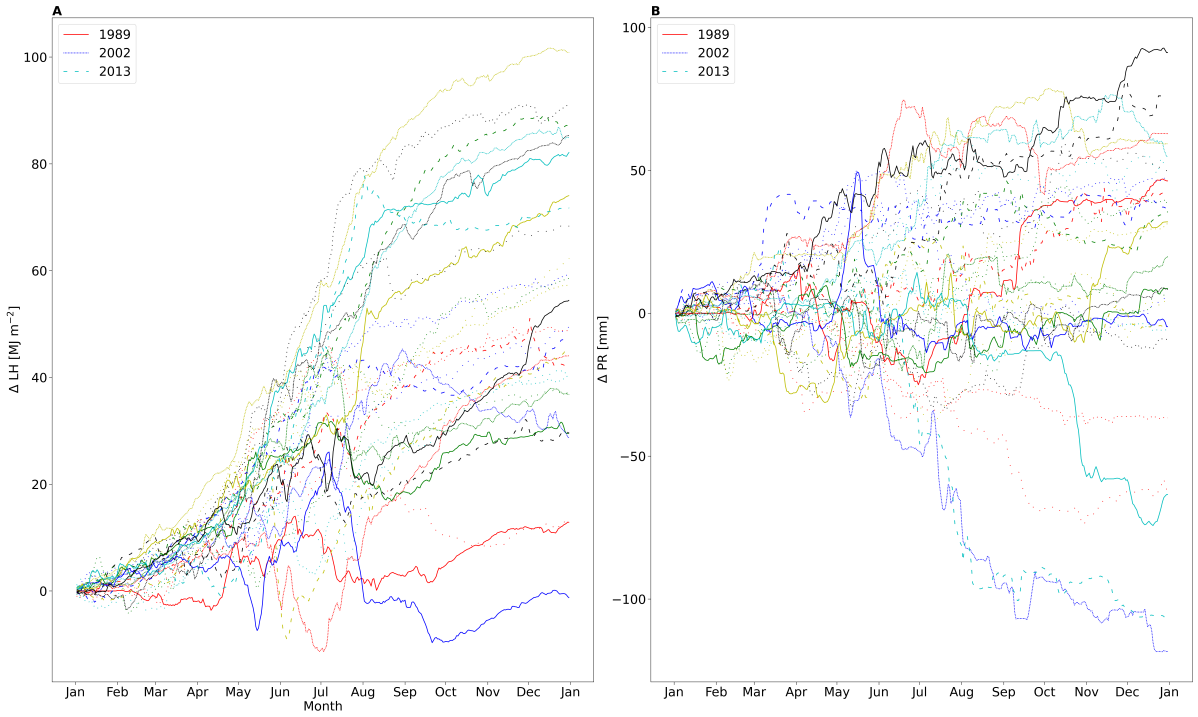

Figure 5.4: Cumulative daily increments of all simulation years (HOM-REF) for LH (A) and PR (B).

Looking at the distribution of increments in each year, it is apparent that the long-time accumulation of PR should reach values that significantly affect the water cycle over Central Europe. We illustrate this in Figure 5.5, which shows the total accumulated difference in the rain from 1996 to 2018. Starting the comparison in 1996 leaves enough room for adaption to the new water balance and the values of REF have also been compared to observations from this year on (Furusho-Percot et al., 2019). The surplus in PR is especially apparent from Central Europe to Eastern Europe with values of more than 1000 mm in these 23 years. Primarily, high values are found in mountainous regions like the alps.

In contrast, the differences over the ocean are spotty showing chaotic patterns likely resembling random perturbations. The influence of the sea is visible in less clear changes in the British Isles, France and the Iberian Peninsula. The existing changes in the subsurface in these regions do not come to light because of the strong oceanic influence from the Atlantic.

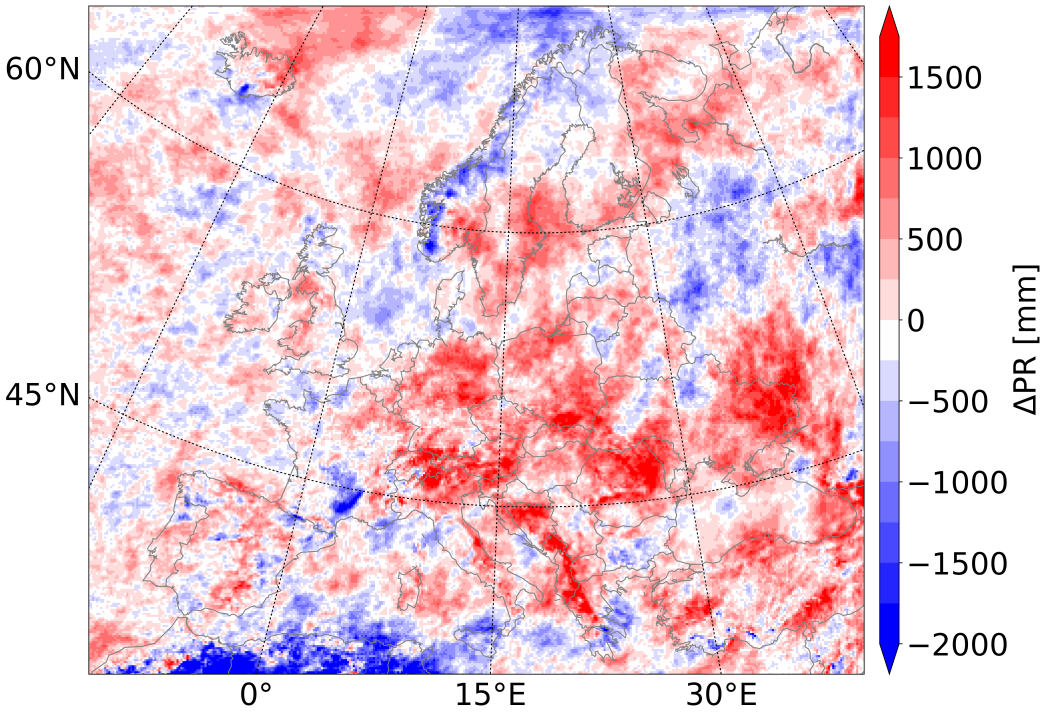

Figure 5.5: Cumulative increments (HOM-REF) for precipitation (PR) from 1996 to 2018.

5.4.3 Distinct Changes in Pressure and Wind Fields

Before investigating extreme deviations from REF in specific years, Figure 5.6 shows the long-term seasonal changes in summer in pressure at sea level (PMSL) and wind direction. The subsurface settings should not influence surface pressure over open water, especially the Atlantic in HOM. The pressure information should be the same originating from the boundary conditions from ERA-Interim. However, over the continental mass we see a dipole. Scandinavia shows increased pressure of up to 0.6 hPa while there is a nearly equivalent increase in pressure in the Mediterranean and Southeast Europe. Matching the pressure changes, we see increased easterly wind over ME, northern wind over West Russia and southern wind at the Norwegian coast. This pattern resembles an increased occurrence of high-pressure systems over North Europe. Overall, the absolute differences are not extremely high, but there can be quite an impact in specific weather events.

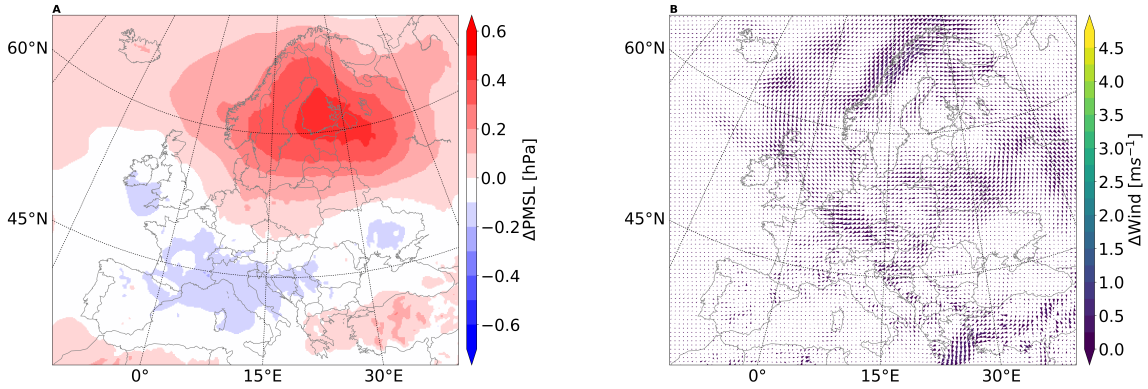

Figure 5.6: Difference maps for mean seasonal sea level pressure (A) and 10-m-wind direction (B).

There must be changes in the height of the boundary layer resulting from additional LH to explain the pressure differences. More water vapor reaching the atmosphere reduces the height of the boundary layer by increasing the stability of the atmosphere. At the same time, the sensible heat flux is reduced. Looking at maps showing the mean changes in LH in Figure 5.7A, we see quite spotty widespread increases in Central and Northern Europe and decreases in the Mediterranean. The pattern is very well anti-correlated with a decrease and increase in boundary layer height (HPBL) in Figure 5.7B. Changes in the boundary layer can influence larger circulation patterns over Europe, which explains why the main differences in atmospheric pressure are not directly found in the regions with the most significant changes in the energy budget.

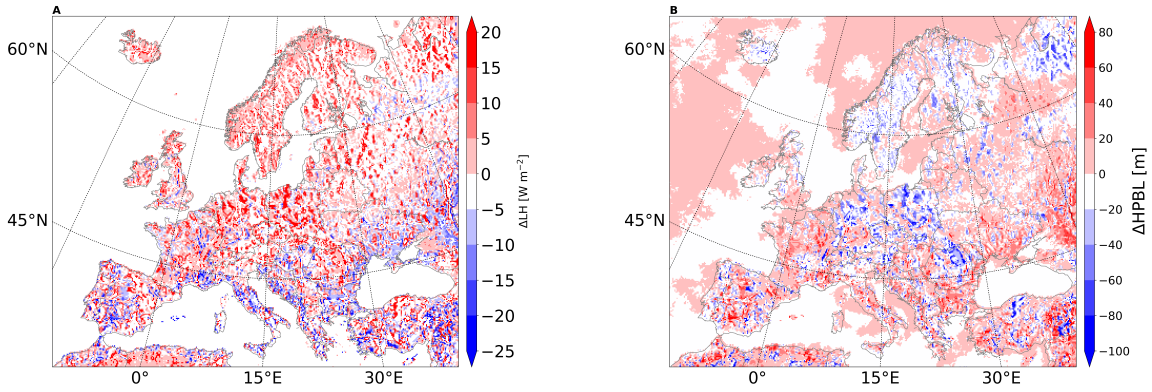

Figure 5.7: Difference maps for mean difference in LH (A) and boundary layer height (B).

5.4.4 Impact on Wet and Dry Events

The massive outliers in terms of missing PR are 2002 and 2013. These years had atmospheric blocking situations with stationary pressure fields over Central Europe and weak easterly winds (Blöschl et al., 2013). In such events, incoming rain fronts from the Atlantic are redirected from their route across Central Europe to the Mediterranean Sea. Over the warm water and influenced by warm air masses of the Sahara, they take up additional moisture and continue to travel Northeast. Reaching the alps or Eastern Germany or Poland, they lose all their water in massive precipitation for several days. This large-scale weather situation is rare but can have massive effects. Figure 5.8 shows that circulation changes initiated by altered water tables can prevent this rather fragile weather phenomenon. The increased easterly winds in Figure 5.8A avert a stable blocking over Central Europe and move precipitation westward. The result is increased rainfall in France and massive deficits over Central and Eastern Europe (Figure 5.8B). The simulation of these two events does not ultimately prove a causal connection between the changed subsurface and the missing rain in 2002 and 2013. Still, it is an indication of the potential influence of specific circulations. More simulations of the events would be needed to show this connection.

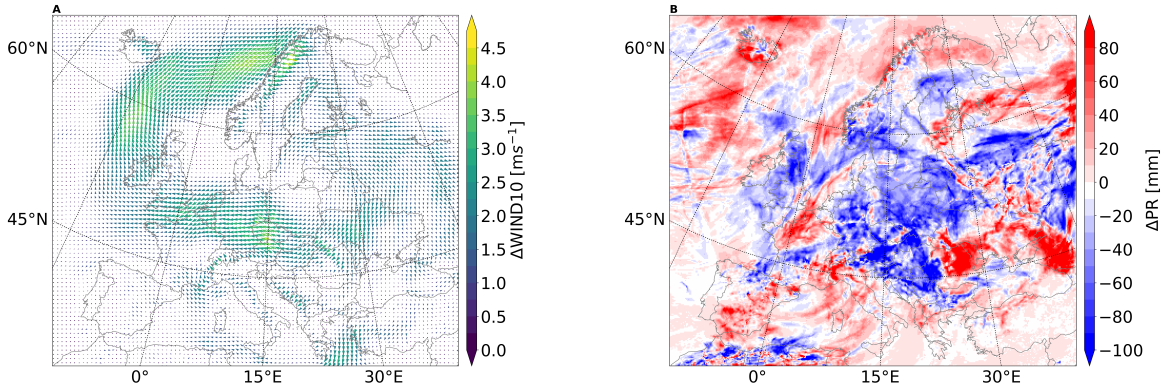

Figure 5.8: Changed wind direction and speed (A) in August 2002 and cumulative PR (B).

In the case of dry years like 2003 and 2018, the increased LH should play an important role because, over many areas, ET is moisture limited. Looking at the difference in PR of 2003 and 2018 combined in Figure 5.9, a consistent increase is visible in the eastern part of Central Europe, where the drought was most pronounced. However, the effect is only dominant in this region, highlighting the chaotic evolution of PR and the strong oceanic influence in Western Europe.

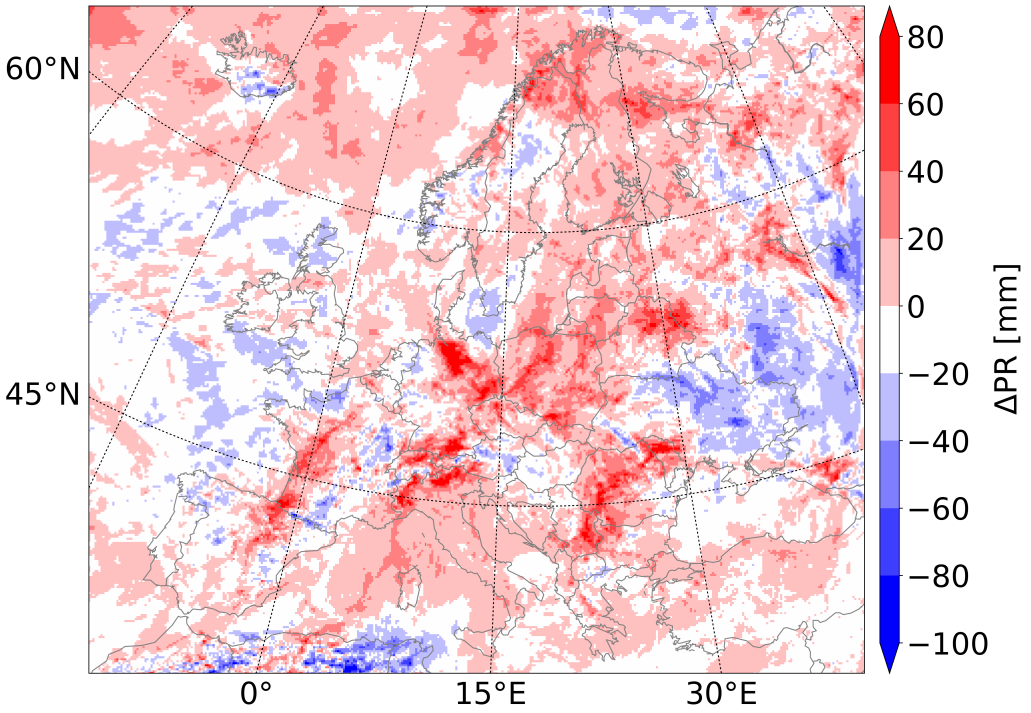

Figure 5.9: Mean difference in summer precipitation during the heatwaves of 2003 and 2018.

5.4.5 The Altered Seasonal Cycle of Groundwater

Previous chapters have shown that changed groundwater properties influence extreme events with massive changes in the incoming water. However, the water cycle seems generally accelerated with bigger exchanges between groundwater and the atmosphere due to less storing capacity of the subsurface. Therefore, the year-to-year groundwater cycle could be affected by changes in seasonality. Figure 5.10 depicts this with the average daily increments of PR, LH and WTD. As expected, latent heat significantly grows in summer, with smaller increments in the other seasons. On average, PR is especially increasing in spring and fall, while there are many fluctuations in summer.

Looking at WTD, this results in a seasonal cycle of differences in WTD. Beginning in winter, water table depths move closer to the values in REF. In late spring, with the most significant increases in PR, the differences increase. Then in summer, with fluctuating changes in PR but also much higher rates of LH, the differences fluctuate around the level reached in late spring. In the fall, we see the most significant differences, with the second substantial increase in PR and fewer increases in LH. Overall, differences in

WTD span only a range of 7 cm. However, this is 20% of the magnitude of an extreme drought event like 2018 in REF.

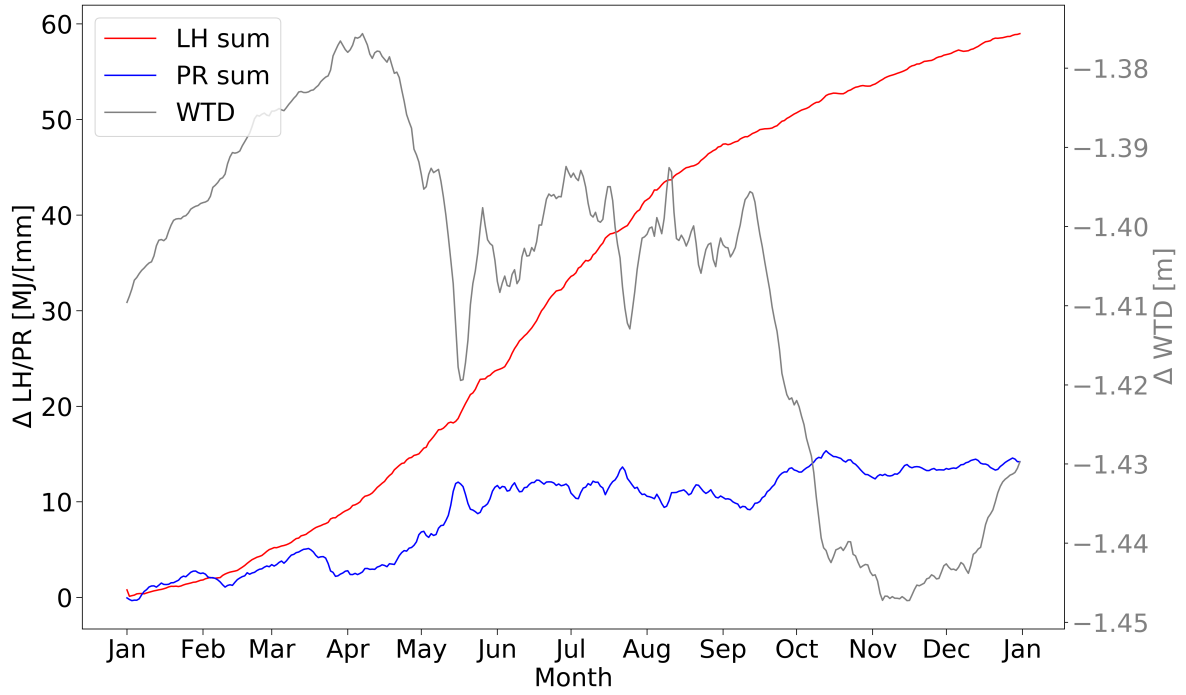

Figure 5.10: Mean cumulative daily increments of latent heat (LH) and precipitation (PR) together with the mean daily increment in water table depth (WTD).

5.5 Discussion and Conclusion

Water table depths are a challenging variable in subsurface modeling. They have high spatial variability, are under human influence, lack widespread observational data and are not easily measured by remote sensing. Still, they are important for mitigating drought and potential feedbacks between water resources in the subsurface and the atmosphere. They significantly contribute to the latent heat flux to the atmosphere, which can contribute to increased precipitation. In terrestrial system models, the groundwater level is determined by topology, in- and out-coming fluxes from the land surface and subsurface parameters like porosity. For standalone subsurface models, these parameters demand calibration to adjust the model to observations. In physically based fully coupled models, the simulation of the whole water cycle can hinder this.

We demonstrated that changed groundwater levels significantly impact precipitation even in regions like Mid-Europe, which are usually regarded to have insignificant SM-PR coupling with a climatological run with homogeneous subsurface parameters. On average, the cumulative differences in PR sum up to 15 mm, with latent heat differences even reaching 60 MJ. These values even include large PR deficits, where the changed water tables potentially alter circulation patterns preventing extreme wet events in a reference simulation. Furthermore, the seasonal cycle of groundwater is altered to a measure of

7 cm on average. These changes resemble a new water balance initiated by changed subsurface properties.

The main limitation of this study is the constraint to a single variation of the subsurface parameters. Several derivations would be necessary to complete a full sensitivity analysis. However, the current setup has the advantage of simulating Europe over a climatologic timespan, enabling the study of extensive time and spatial scales. Accomplishing the same scope for several parameter variations is very compute time intensive. Furthermore, there is no guarantee that the groundwater-precipitation coupling is directly transferable to the real world. The precipitation simulation is one of the most challenging processes in atmospheric models and the influence of latent heat flux is under discussion. Still, drastic changes in water table depths happen in the real world and only a few models can investigate the direct feedback from groundwater to atmospheric processes. The study also highlights the importance of the initial WTD for models that include groundwater.

The results show that calibration is impossible in fully coupled terrestrial models because there is a two-way feedback cycle from subsurface parameters to water table depths to precipitation. Comparing the run with homogeneous subsurface parameters with a reference climatology showed that a somewhat random decision for roughly fitting subsurface parameters can hinder matching simulation of real world events. However, the available solutions for calibration, including newer methods utilizing machine learning, are unsuitable for the whole water cycle. Facing climate change, it is also possible that massive changes in the water cycle occur, for example, human water use or potential evapotranspiration changes. These could start feedbacks and move the water cycle of the real world to a new balance which illustrated this study with changed parameters. Further development on holistic solutions for the whole water cycle are needed in future research.

Chapter 6

Summary and Conclusions

6.1 Summary

In the time of ongoing climate change, some of which is unstoppable, adaptation strategies to face hydrometeorological extremes are increasingly important. To help authorities with adequate planning, simulations of the terrestrial cycle can help determine the magnitude of upcoming extreme events that involve the whole water cycle. Further research is needed on the interactions between subsurface water and the atmosphere and to detect sensitivities such as those regarding continental-scale shifts in water table depths. However, the scientific community must first establish whether feedbacks between groundwater and the atmosphere have a non-negligible impact, at the continental scale; if so, this would justify the considerable computational costs.

Fully coupled simulations over Europe can be performed by TSMP, which connects the atmosphere, the land and the subsurface using a framework with three individual models. Uniquely, water and energy fluxes from below the water table to above the cloud top are consistently modeled physically. Previous work by Keune et al. (2016) and Furusho-Percot et al. (2019) that established the domain and a reference climatology enabled the creation of three studies, which focused on three main research questions. The questions are discussed individually below.

6.1.1 Answer to Research Question 1

How does the groundwater memory affect three exceptional droughts under uncertain weather conditions on the interannual time scale? Is knowledge about the correct initial condition more important than accurate atmospheric forcing?

Central Europe experienced ongoing drought conditions, starting with a heatwave in 2018. Severe impacts were immediately experienced in drinking water shortages and losses in the agricultural sector. On a longer timescale, the 2018 drought damaged the tree population by reducing the water resources in the deeper soil, on which deep roots depend.

Predicting drought conditions is difficult for long time scales, although warning and monitoring systems exist at the national and European levels. The crucial problem is atmospheric uncertainty. Predictions beyond 14 days are not highly accurate, and the maximum timespan covered is seasonal forecasts. However, groundwater memory offers valuable and useful information about the state of the subsurface. During droughts, the water deficits can be so dire that even substantial rainfall cannot replenish groundwater resources.

The simulation of one water year initialized with an intense drought in the subsurface and under the influence of multiple atmospheric conditions can estimate the probabilities of an ongoing drought. Ensembles of one drought and various atmospheric conditions over Europe were simulated with TSMP. Three drought conditions (2011, 2018 and 2019) were used and simulated for one year. The setup was then reversed to assess the value

of the initial condition and its influence on predictability. All three years were simulated with the perfect atmospheric forcing of the relevant year (2011, 2018 or 2019) and an ensemble of all possible conditions of the subsurface. Both setups were compared to the actual development of water resources in a reference climatology. The results showed that the ensemble with multiple atmospheric conditions lost predictability over time as the drought condition diminished. In contrast, the ensemble of initial conditions gained predictability over time, as all ensemble members experienced the same meteorological forcing.

The results also indicated that the initial condition was most important for predictability for nearly a year in the case of droughts. Previous studies assessed the time period to be shorter, especially in regions that were typically not water-limited, such as Central Europe. The current findings highlight the advantage of explicit inclusion of the groundwater component in TSMP. Furthermore, the drought ensembles enabled calculating the probability of an ongoing drought - for example, 70% for 2018. In summary, intense droughts like that of 2018 are likely to prevail for at least one year, with the initial condition outweighing atmospheric uncertainty for almost the whole period.

6.1.2 Answer to Research Question 2

Can persistent drought conditions influence the energy cycle and cloud characteristics at the interannual time scale, through feedback processes?

The first study demonstrated the interannual influence of initial drought conditions on total water resources in the subsurface. However, closer examination of interactions in the terrestrial system was needed. The focus lay solely on the deficits of water in the subsurface. In this second study, increments in variables of the energy cycle and clouds were calculated between the members of the drought ensemble and the reference climatology. At the surface, net radiation increased in summer, indicating more solar radiation reaching the ground. The increases in energy were linked to changed cloud properties. The drought ensembles had consistently higher clouds, which contain relatively little water, which means that substantial shortwave energy is transmitted through them. Abundant available energy at the surface increases the evapotranspiration rate, further prolonging the drought.

In summary, drought conditions of the previous year can influence the energy cycle and clouds in a current year through a feedback loop. The feedback loop can be described as follows. First, the initial drought conditions change the energy partitioning to a greater release of sensible heat in favor of latent heat. Second, this high volume of sensible heat pushes all clouds upwards and increases their transmissivity. Third, the relatively low relative humidity increases the height to which air parcels need to be lifted to form a cloud. Fourth, the changed cloud properties lead to more shortwave radiation reaching the ground, which increases the sensible and latent heat, further prolonging the drought.

6.1.3 Answer to Research Question 3

How sensitive is precipitation over continental Europe to groundwater table alterations that result from changes in subsurface parameters in terrestrial simulations?

In subsurface simulations, soil parameters have high uncertainty, especially at coarse resolutions. The reasons are high spatial heterogeneity and insufficient observations. Therefore, the models are calibrated to fit certain observations, such as streamflow in a catchment, to achieve higher forecasting accuracy. In fully coupled simulations, this approach is unfeasible. In contrast to pure hydrological applications, the atmosphere is not a fixed boundary but dynamically evolves in connection with the subsurface. A water table located at a different depth because of altered subsurface parameters could also influence processes in the atmosphere.

Altered precipitation is especially interesting because it directly affects groundwater recharge. Research in this direction is useful in the context of parameter uncertainty and for shifts in water tables forced by external factors in the real world, such as climate change. In other words, feedback discovered through changed subsurface parameters might also occur under different circumstances.

A transient simulation from 1989 to 2019 across Europe, with homogeneous subsurface parameters, was performed with TSMP. The aim was to study the influence of subsurface parameters and potential feedbacks on precipitation. The altered subsurface had a smaller water storage capacity compared to a reference run, leading to water tables moving closer to the surface, providing more water to the surface. This supply was quickly visible in the simulations, which displayed consistently increased latent heat compared to the reference simulations. Precipitation is a complex and chaotic process; nonetheless, it was vastly increased in most of the studied years, especially in the transition seasons of fall and spring.

Previous studies typically classified Central Europe as a region not very sensitive to the coupling of evapotranspiration and precipitation. By contrast, the current results show that significant changes in water table depth led to a powerful atmospheric impact. It is possible to transfer the results to massive changes in water tables initiated by events such as climate change. In this case, there could also be significant interactions between groundwater and precipitation. In addition, the interactions between groundwater and the atmosphere are not limited to changes in energy flux.

Overall, the studies documented in this thesis have shown that fully coupled simulations provide new insights into feedback processes occurring in the terrestrial system, especially in hydrometeorological extremes. Hence, these models are a valuable tool despite the computational costs. However, this thesis has concentrated on interactions that occur during droughts or are related to water table sensitivity. There are many more possible interactions, including the case of floods, that still require investigation.

6.2 Limitations

The major limitations of the presented simulations with TSMP can be categorized into three areas: model resolution, uncertainties in the input data and simplifications in the models. In the past, a resolution of $12.5\,\mathrm{km}$ was considered high-resolution for atmospheric simulations, but recently there has been a shift to convection-permitting resolutions of about $3\,\mathrm{km}$. The explicit simulation of convection processes might play an essential role in the simulation of soil moisture-atmosphere feedbacks. Furthermore, offline simulations of land-surface models can reach resolutions below $1\,\mathrm{km}$ because the processes are easier to resolve than atmospheric processes.

In principle, it is possible to run the different components at different resolutions, but that introduces a source of errors. For example, an extra step of interpolation is needed to exchange the variables, and the results are less physically consistent. The former challenge is particularly problematic when feedbacks spanning the whole terrestrial system is investigated.

At resolutions around $1\,\mathrm{km}$, the physics-based modeling of ParFlow has not been widely criticized. In the 1980s, researchers assumed that a grid cell should not be larger than $1\,\mathrm{km}^2$ to remain representative of its content (Wood et al., 1988). Physics-based models at that time had far coarser resolutions, but today's state-of-the-art models can simulate the resolutions around $1\,\mathrm{km}^2$ on a global scale (Condon et al., 2021). Other criticisms remain valid: The introduced complexity and the foundation in physics might lead to overconfidence regarding the predictive results and insights about actual hydrologic processes (Grayson et al., 1992). Nonetheless, physics-based models are essential for coupled simulations, as momentum and energy fluxes must be conserved (Fatichi et al., 2016).

At $12.5\,\mathrm{km}$, a problem arises in the overland flow simulation. Due to the low resolution, rivers are widened to $12.5\,\mathrm{km}$ with relatively shallow water depths. In reality, rivers are smaller and have higher velocity and they influence smaller areas through a direct water exchange. A solution is to improve the parametrization of waterways with the scaling of Manning's coefficient, which determines the roughness based on the actual river width (Schalge et al., 2019). In any case, ultra-high resolution for a domain spanning Europe poses significant challenges concerning data management. At a resolution of $3\,\mathrm{km}$, the storage requirements are four times higher and the computational demand is six times higher than for $12.5\,\mathrm{km}$ simulations, because of the explicit simulation of convection. Nonetheless, modeling that includes convection is used in operational weather forecasting over the continental US (James et al., 2022). This achievement indicates that simulations over at least a medium time range, such as a few years, are feasible.

Accurate input parameter sets are essential for high resolution, but they are no less crucial for coarser resolutions. In all simulations in this thesis, the subsurface parameters were vertically homogeneous from the surface to the bedrock at $57\,\mathrm{m}$. Vertical homogeneity significantly simplifies soil characteristics as parameters change with increasing depths. In particular, the upper soil layers - for which data is easily available - can have

varying soil parameters. The deeper layers, close to the bedrock, should be set to the values of the SoilGrids (Shangguan et al., 2017) dataset. The topography in ParFlow could also be improved with the newest topographical data to ensure that all major rivers of the European continent have a matching equivalent and can flow through lakes currently inactive in the simulation.

The land simulation in CLM is limited by static plant cover, where only one PFT covers a grid cell. The mixture of multiple PFTs in a grid cell is not supported in TSMP. Furthermore, an urban land cover type should be included for many highly populated areas in Europe. Overall, the inclusion of CLM in TSMP has yet to reach its fullest potential. Coupling carbon fluxes and synchronizing the atmospheric concentration of CO_2 between the atmosphere and the land surface would be possible. Many improvements in the land component like the inclusion of harvesting depend on the inclusion of CLM version 5 in TSMP.

The improvement of atmospheric boundary data seems simple at first. The new reanalysis dataset ERA5 (Hersbach et al., 2020) improves resolution, available timesteps and physical simulation compared to ERA-Interim. Future regional simulations with TSMP can benefit from the new reanalysis. However, some limitations remain unchanged, as the regional simulation must always adapt to the moisture fluxes given by the boundary condition. Adaptation could lead to more ocean water evaporation and a positive precipitation bias over land with internal redistribution (Goergen and Kollet, 2020). Generally, it would be useful if the regional simulation could provide feedback to the global simulation, such as through establishing teleconnections at a large scale.

Despite the precipitation biases in regional climate simulations, many regional climate models are known to overestimate the intensity of heatwaves because of the lack of evapotranspiration data. In TSMP, heatwaves are less intense with an additional water supply from the water table, but a general wet and cold bias is evident in TSMP (Furusho-Percot et al., 2019, 2022). It might be helpful to apply bias correction to results obtained from TSMP similarly to other regional simulations (Casanueva et al., 2016). However, such a correction does not change the internal dynamics in the simulation. A solution could be a rigorous evaluation of soil moisture with remote-sensing products.

Other limitations involve processes that are absent from TSMP, such as interactions between the ocean and human influence. Early simulations incorporating human water use were performed regarding the heatwave in 2003 (Keune et al., 2018, 2019), but longer timespans are desirable.

6.3 Future Work

The mentioned limitations already hint at possible next steps for terrestrial simulations for TSMP. Possible steps are increasing the resolution, including new high-quality input datasets and new model versions that improve the simulation of physical processes. With the availability of ERA5 from 1950 onwards, evaluation simulations with TSMP can be run

for more than 70 years, much longer than any remote sensing products. In comparison, the simulations in this thesis were limited to 1989 to 2019.

The independence of TSMP simulations from satellite data is a strength. However, including data assimilation for several variables could improve the estimation of water resources. Total water storage anomalies derived from the GRACE satellite (Tapley et al., 2019) could be used to correct TSMP, especially when large biases in precipitation occur. For rainfall, a large net of high-resolution radar data is available over Europe, which could be used to correct the wet biases in TSMP.

Another option is to use machine learning tools for the subsurface component (Tahmasebi et al., 2020). While machine learning methods for the atmosphere are still in experimental development, there has been substantial progress in studies of porous media. The work of Ma et al. (2020, 2021) has shown that TSMP data can be used to predict water table depths at the European scale, but additional work is needed to incorporate this learning back into TSMP.

All three studies presented in this thesis offer possible extensions. Chapters 3 and 4 would have benefited from a larger ensemble size to render the statistical results more meaningful and to enable easier filtering for specific atmospheric conditions. Creating additional ensembles with different initial conditions, specifically wet ones, would provide more knowledge about the feedback processes. Finally, chapter 5 has the shortcoming of using only one sensitivity test. For more accurate statements about the interactions between the water table and precipitation, subsurface parameters must be varied to include additional values to enable a complete sensitivity study.

Regarding completely new studies with TSMP, it would be interesting to scrutinize floods, industrial groundwater abduction and groundwater changes with ongoing sea level rise. ParFlow has been used to study peak flows for the flood in Germany in July 2021 (Saadi et al., 2023), but no case studies have been conducted with a fully coupled TSMP. Floods are included in longer evaluation runs performed with TSMP, but there is no guarantee that the atmospheric conditions are adequately reproduced. The results in chapter 5 have shown that flood conditions can be less intensive, with a changed subsurface state, compared to the reference simulation. With a focus on a specific flood event like 2021, the simulation should be performed multiple times with different initial conditions to separate the chaotic atmospheric influence from the subsurface influence. The results could give insight regarding the importance of subsurface water storage for extreme floods and potential energy balance feedback.

Public fear regarding groundwater shortages has increased markedly with the ongoing droughts in recent years. The quantification of a robust trend in water resources is ongoing. However, de Graaf et al. (2019) showed that in parts of Central Europe, the limit of groundwater pumping will be reached in the middle of this century or earlier. Studies using TSMP could contribute to this debate through incorporating human groundwater pumping in agriculture and industry. The biggest obstacle to such studies is the lack

of data on human water usage. A solution could be the development of an algorithm that estimates groundwater pumping based on measurable factors such as days without precipitation.

Lastly, the rise in sea level driven by climate change interacts with groundwater and can lead to floods and the creation of new wetlands. Rotzoll and Fletcher (2013) found that a sea level rise of $0.6\,\mathrm{m}$ led to substantial groundwater flooding. A study using TSMP could help to examine this phenomenon on a large scale. Although TSMP does not include an ocean model, modifying the landmask and the ParFlow configuration to imitate a sea level rise is possible. The development of new wetlands could introduce new feedbacks in the terrestrial system.

Appendices

Appendix A

Information on the Assistance Received and Resources Used

The doctoral thesis I submitted is my own work and was prepared without unauthorized outside assistance. I have not included text passages, graphics or other materials from third parties or my own examination papers without identifying them. Only the sources and resources that I have indicated were used. All verbatim and non-verbatim citations from other works are identified in accordance with the citation rules for academic writing.

Appendix B

Acknowledgements

Completing this thesis would not have been possible without the help of my supervisor Stefan Kollet and many supportive members of our working group, including Carina Furusho-Percot, Klaus Goergen, Bibi Naz, Yueling Ma and Tobias Tesch and many others. I also have to thank Clemens Simmer for acting as the second reviewer and the other members of my committee, Jürgen Kusche and Silke Trömel.

I also have to thank my family, Gertrud, Martin, Rupert, Carolin and Norbert, for always being supportive.

Appendix C

List of Acronyms

AL Alps
BI British Isles
CEILING Cloud ceiling height
CLM Community Land Model
CLT Total cloud cover
CLW Total cloud water content
CMIP6 Coupled Model Intercomparison Project Phase 6
CORDEX European Coordinated Regional Downscaling Experiment
EA Eastern Europe
ECMWF European Centre for Medium-Range Weather Forecasts
ET Evapotranspiration
FAO Food and Agricultural Organization of the United Nations
FR France
GH Ground heat flux
GLHYMPS 2.0 GLobal HYdrogeology MaPS 2.0
GRACE Gravity Recovery and Climate Experiment
GRACE-FO Gravity Recovery and Climate Experiment-Follow-On
GRDC Global Runoff Data Center
GRT Groundwater response time
HPBL Height of planetary boundary layer
HOM Simulation run with homogeneous subsurface parameters
IP Iberian Peninsula
K Hydraulic conductivity
LA Land-atmosphere coupling
LCL Lifting condensation level
LF Net incoming longwave radiation
LH Latent heat flux
LW Incoming longwave radiation
MD Mediterranean

ME Mid-Europe
MODIS Moderate Resolution Imaging Spectroradiometer
NCAR National Center of Atmospheric Research
OASIS3 Ocean Sea Ice Soil
P Probability
PLS Partial least square regression
PMSL Pressure at sea level
PS Pressure at the lowest atmospheric level
PFT Plant functional type
PR Total atmospheric precipitation
PRESS Water pressure head in the subsurface
Q Humidity at the lowest atmospheric level
REF Reference simulation
RELHUM Relative humidity at the lowest atmospheric level
RNET Net radiation at the surface
S Total subsurface water storage
SAT Water saturation in the subsurface
SC Scandinavia
SH Sensible heat flux
SM-PR Soil moisture - precipitation coupling
SSR Net incoming shortwave radiation
SW Incoming shortwave radiation
TAS Temperature at the lowest atmospheric level
TRMM Tropical Rainfall Measuring Mission
TSMP Terrestrial System Modeling Platform
U Horizontal wind at the lowest atmospheric level
WTD Water table depth

List of Figures

List of Tables

Bibliography

Adams, K. H., Reager, J. T., Rosen, P., Wiese, D. N., Farr, T. G., Rao, S., Haines, B. J., Argus, D. F., Liu, Z., Smith, R., Famiglietti, J. S., and Rodell, M. (2022). Remote Sensing of Groundwater: Current Capabilities and Future Directions. *Water Resources Research*, pages 1–27.

Andersson, L., Wilk, J., Graham, L. P., Wikner, J., Mokwatlo, S., and Petja, B. (2020). Local early warning systems for drought - Could they add value to nationally disseminated seasonal climate forecasts? *Weather and Climate Extremes*, 28.

Ardilouze, C., Batté, L., Déqué, M., van Meijgaard, E., and van den Hurk, B. (2019). Investigating the impact of soil moisture on European summer climate in ensemble numerical experiments. *Climate Dynamics*, 52(7-8):4011–4026.

Arnal, L., Cloke, H. L., Stephens, E., Wetterhall, F., Prudhomme, C., Neumann, J., Krzeminski, B., and Pappenberger, F. (2018). Skilful seasonal forecasts of streamflow over Europe? *Hydrology and Earth System Sciences*, 22(4):2057–2072.

Ashby, S. F. and Falgout, R. D. (1996). A Parallel Multigrid Preconditioned Conjugate Gradient Algorithm for Groundwater Flow Simulations. *Nuclear Science and Engineering*, 124(1):145–159.

Baldauf, M., Seifert, A., Foerstner, J., Majewski, D., Raschendorfer, M., and Reinhardt, T. (2011). Operational Convective-Scale Numerical Weather Prediction with the COSMO Model: Description and Sensitivities. *Monthly Weather Review*, 139(12):3887–3905.

Barlage, M., Chen, F., Rasmussen, R., Zhang, Z., and Miguez-Macho, G. (2021). The Importance of Scale-Dependent Groundwater Processes in Land-Atmosphere Interactions Over the Central United States. *Geophysical Research Letters*, 48(5):1–10.

Barlage, M., Tewari, M., Chen, F., Miguez-Macho, G., Yang, Z. L., and Niu, G. Y. (2015). The effect of groundwater interaction in North American regional climate simulations with WRF/Noah-MP. *Climatic Change*, 129(3-4):485–498.

Bauer, P., Stevens, B., and Hazeleger, W. (2021). A digital twin of Earth for the green transition. *Nature Climate Change*, 11(2):80–83.

Betts, A. K. (2004). Understanding hydrometeorology using global models. *Bulletin of the American Meteorological Society*, 85(11):1673–1688.

Bisselink, B. and Dolman, A. J. (2008). Precipitation recycling: Moisture sources over Europe using ERA-40 data. *Journal of Hydrometeorology*, 9(5):1073–1083.

Blöschl, G., Nester, T., Komma, J., Parajka, J., and Perdigão, R. A. (2013). The June 2013 flood in the Upper Danube Basin, and comparisons with the 2002, 1954 and 1899 floods. *Hydrology and Earth System Sciences*, 17(12):5197–5212.

Boé, J. (2013). Modulation of soil moisture-precipitation interactions over France by large scale circulation. *Climate Dynamics*, 40(3-4):875–892.

Boergens, E., Güntner, A., Dobslaw, H., and Dahle, C. (2020). Quantifying the Central European Droughts in 2018 and 2019 With GRACE Follow-On. *Geophysical Research Letters*, 47(14):1–9.

Bonan, G. B., Oleson, K. W., Vertenstein, M., Levis, S., Zeng, X., Dai, Y., Dickinson, R. E., and Yang, Z. L. (2002). The land surface climatology of the community land model coupled to the NCAR community climate model. *Journal of Climate*, 15(22):3123–3149.

Börgel, F., Frauen, C., Neumann, T., and Meier, H. E. (2020). The Atlantic Multidecadal Oscillation controls the impact of the North Atlantic Oscillation on North European climate. *Environmental Research Letters*, 15(10).

Börker, J., Hartmann, J., Amann, T., and Romero-Mujalli, G. (2018). Terrestrial sediments of the earth: Development of a global unconsolidated sediments map database (gum). *Geochemistry, Geophysics, Geosystems*, 19(4):997–1024.

Bowden, J. H., Talgo, K. D., Spero, T. L., and Nolte, C. G. (2016). Assessing the Added Value of Dynamical Downscaling Using the Standardized Precipitation Index. *Advances in Meteorology*, 2016.

Brasseur, G. P., Jacob, D., and Schuck-Zöller, S. (2017). *Klimawandel in Deutschland: Entwicklung, Folgen, Risiken und Perspektiven*. Springer Nature.

Brooks, P. D., Gelderloos, A., Wolf, M. A., Jamison, L. R., Strong, C., Solomon, D. K., Bowen, G. J., Burian, S., Tai, X., Arens, S., Briefer, L., Kirkham, T., and Stewart, J. (2021). Groundwater-Mediated Memory of Past Climate Controls Water Yield in Snowmelt-Dominated Catchments. *Water Resources Research*, 57(10):1–15.

Brutsaert, W. (2005). *Hydrology – An Introduction*. Cambridge University Press.

Bucchignani, E. and Mercogliano, P. (2021). Performance evaluation of high-resolution simulations with COSMO over south Italy. *Atmosphere*, 12(1).

Campoy, A., Ducharne, A., Cheruy, F., Hourdin, F., Polcher, J., and Dupont, J. C. (2013). Response of land surface fluxes and precipitation to different soil bottom hydrological conditions in a general circulation model. *Journal of Geophysical Research Atmospheres*, 118(19):725–10.

Carballas, T., Macias, F., Diaz-Fierros, F., Carballas, M., and Fernandez-Urrutia, J. A. (1990). FAO-UNESCO soil map of the world. Revised legend. *Informes sobre Recursos Mundiales de Suelos (FAO)*.

Casanueva, A., Kotlarski, S., Herrera, S., Fernández, J., Gutiérrez, J. M., Boberg, F., Colette, A., Christensen, O. B., Goergen, K., Jacob, D., Keuler, K., Nikulin, G., Teichmann, C., and Vautard, R. (2016). Daily precipitation statistics in a EURO-CORDEX RCM ensemble: added value of raw and bias-corrected high-resolution simulations. *Climate Dynamics*, 47(3-4):719–737.

Chao, L., Zhang, K., Wang, J., Feng, J., and Zhang, M. (2021). A comprehensive evaluation of five evapotranspiration datasets based on ground and grace satellite observations: Implications for improvement of evapotranspiration retrieval algorithm. *Remote Sensing*, 13(12):1–18.

Christensen, J. H. and Christensen, O. B. (2007). A summary of the PRUDENCE model projections of changes in European climate by the end of this century. *Climatic Change*, 81(SUPPL. 1):7–30.

Christensen, J. H., Larsen, M. A., Christensen, O. B., Drews, M., and Stendel, M. (2019). Robustness of European climate projections from dynamical downscaling. *Climate Dynamics*, 53(7-8):4857–4869.

Collins, S. (2017). Incorporating groundwater flow in land surface models: literature review and recommendations for further work. *British Geological Survey Open Report*, OR/17/068:23.

Condon, L. E., Kollet, S., Bierkens, M. F., Fogg, G. E., Maxwell, R. M., Hill, M. C., Fransen, H. J. H., Verhoef, A., Van Loon, A. F., Sulis, M., and Abesser, C. (2021). Global Groundwater Modeling and Monitoring: Opportunities and Challenges. *Water Resources Research*, 57(12):1–27.

Cook, B. I., Puma, M. J., and Krakauer, N. Y. (2011). Irrigation induced surface cooling in the context of modern and increased greenhouse gas forcing. *Climate Dynamics*, 37(7-8):1587–1600.

Cornes, R. C., van der Schrier, G., van den Besselaar, E. J., and Jones, P. D. (2018). An Ensemble Version of the E-OBS Temperature and Precipitation Data Sets. *Journal of Geophysical Research: Atmospheres*, 123(17):9391–9409.

Cuthbert, M. O., Gleeson, T., Moosdorf, N., Befus, K. M., Schneider, A., Hartmann, J., and Lehner, B. (2019). Global patterns and dynamics of climate-groundwater interactions. *Nature Climate Change*, 9(2):137–141.

DAAC, L. P. (2004). Global 30 Arc-Second Elevation Data Set GTOPO30. Land Process Distributed Active Archive Center.

David, A., Martin, P., Buffett, B., Brovkin, V., Rahmstorf, S., and Ganopolski, A. (2004). The importance of ocean temperature to global biogeochemistry. *Earth and Planetary Science Letters*, 222(2):333–348.

Day, G. N. (1985). Extended streamflow forecasting using NWSRFS. *Journal of Water Resources Planning and Management*, 111(2):157–170.

de Graaf, I. E., Gleeson, T., (Rens) van Beek, L. P., Sutanudjaja, E. H., and Bierkens, M. F. (2019). Environmental flow limits to global groundwater pumping. *Nature*, 574(7776):90–94.

Decharme, B., Delire, C., Minvielle, M., Colin, J., Vergnes, J. P., Alias, A., Saint-Martin, D., Séférian, R., Sénési, S., and Voldoire, A. (2019). Recent Changes in the ISBA-CTRIP Land Surface System for Use in the CNRM-CM6 Climate Model and in Global Off-Line Hydrological Applications. *Journal of Advances in Modeling Earth Systems*, 11(5):1207–1252.

Dee, D. P., Uppala, S. M., Simmons, A. J., Berrisford, P., Poli, P., Kobayashi, S., Andrae, U., Balmaseda, M. A., Balsamo, G., Bauer, P., Bechtold, P., Beljaars, A. C. M., van de Berg, L., Bidlot, J., Bormann, N., Delsol, C., Dragani, R., Fuentes, M., Geer, A. J., Haimberger, L., Healy, S. B., Hersbach, H., Hólm, E. V., Isaksen, L., Kållberg, P., Köhler, M., Matricardi, M., McNally, A. P., Monge-Sanz, B. M., Morcrette, J.-J. J., Park, B.-K. K., Peubey, C., de Rosnay, P., Tavolato, C., Thépaut, J.-N. N., and Vitart, F. (2011). The ERA-Interim reanalysis: Configuration and performance of the data assimilation system. *Quarterly Journal of the Royal Meteorological Society*, 137(656):553–597.

Dirmeyer, P. A. (2000). Using a global soil wetness dataset to improve seasonal climate simulation. *Journal of Climate*, 13(16):2900–2922.

Dirmeyer, P. A., Balsamo, G., Blyth, E. M., Morrison, R., and Cooper, H. M. (2021). Land-Atmosphere Interactions Exacerbated the Drought and Heatwave Over Northern Europe During Summer 2018. *AGU Advances*, 2(2):1–16.

Dirmeyer, P. A., Wang, Z., Mbuh, M. J., and Norton, H. E. (2014). Intensified land surface control on boundary layer growth in a changing climate. *Geophysical Research Letters*, 41(4):1290–1294.

Diro, G. T., Sushama, L., Scinocca, J., and Jiao, Y. (2021). Impact of soil moisture on the dominant modes of North American temperature variability. *Climate Dynamics*, 56(5):1359–1370.

Doms, G. and Baldauf, M. (2021). Consortium for Small-Scale Modelling A Description of the Nonhydrostatic Regional COSMO-Model Part I : Dynamics and Numerics. *Deutscher Wetterdienst, Offenbach am Main*.

Doms, G., Förstner, J., Heise, E., Herzog, H.-J., Mironov, D., Raschendorfer, M., Reinhardt, T., Ritter, B., Schrodin, R., Schulz, J.-P., and Vogel, G. (2021). Consortium for

Small-Scale Modelling A Description of the Nonhydrostatic Regional COSMO Model Part II : Physical Parameterization. *Deutscher Wetterdienst, Offenbach am Main.*

Downing, R. A., Oakes, D. B., Wilkinson, W. B., and Wright, C. E. (1974). Regional Development of Groundwater Resources in Combination with Surface Water. *Journal of Hydrology*, 22:155-177.

Draper, C. and Reichle, R. H. (2019). Assimilation of satellite soil moisture for improved atmospheric reanalyses. *Monthly Weather Review*, 147(6):2163-2188.

Durand, F., Piecuch, C. G., Becker, M., Papa, F., Raju, S. V., Khan, J. U., and Ponte, R. M. (2019). Impact of Continental Freshwater Runoff on Coastal Sea Level. *Surveys in Geophysics*, 40(6):1437-1466.

Durkee, J., Degu, A. M., Hossain, F., Mahmood, R., Winchester, J., and Chronis, T. (2014). Investigating the effect of the "land between the lakes" on storm patterns. *Journal of Applied Meteorology and Climatology*, 53(6):1506-1524.

Famiglietti, J. S. and Ferguson, G. (2021). The hidden crisis beneath our feet. *Science*, 372(6540):344-345.

Fan, Y. (2015). Groundwater in the Earth's critical zone: Relevance to large-scale patterns and processes. *Water Resources Research*, 51(5):3052-3069.

Fang, Z., Bogena, H., Kollet, S., and Vereecken, H. (2016). Scale dependent parameterization of soil hydraulic conductivity in 3D simulation of hydrological processes in a forested headwater catchment. *Journal of Hydrology*, 536:365-375.

Fatichi, S., Vivoni, E. R., Ogden, F. L., Ivanov, V. Y., Mirus, B., Gochis, D., Downer, C. W., Camporese, M., Davison, J. H., Ebel, B., Jones, N., Kim, J., Mascaro, G., Niswonger, R., Restrepo, P., Rigon, R., Shen, C., Sulis, M., and Tarboton, D. (2016). An overview of current applications, challenges, and future trends in distributed process-based models in hydrology. *Journal of Hydrology*, 537:45-60.

Fekete, A. and Sandholz, S. (2021). Here comes the flood, but not failure? Lessons to learn after the heavy rain and pluvial floods in germany 2021. *Water (Switzerland)*, 13(21):1-20.

Fischer, E. M. and Knutti, R. (2016). Observed heavy precipitation increase confirms theory and early models. *Nature Climate Change*, 6(11):986-991.

Friedl, M. A., McIver, D. K., Hodges, J. C., Zhang, X. Y., Muchoney, D., Strahler, A. H., Woodcock, C. E., Gopal, S., Schneider, A., Cooper, A., Baccini, A., Gao, F., and Schaaf, C. (2002). Global land cover mapping from MODIS: Algorithms and early results. *Remote Sensing of Environment*.

Frye, J. D. and Mote, T. L. (2010). Convection initiation along soil moisture boundaries in the Southern Great Plains. *Monthly Weather Review*, 138(4):1140-1151.

Furusho-Percot, C., Goergen, K., Hartick, C., and Kollet, S. (2022). Groundwater Model Impacts Multiannual Simulations of Heat Waves. *Geophysical Research Letters*, 49(10).

Furusho-Percot, C., Goergen, K., Hartick, C., Kulkarni, K., Keune, J., and Kollet, S. (2019). Pan-European groundwater to atmosphere terrestrial systems climatology from a physically consistent simulation. *Scientific Data*, 6(1):320.

Gasper, F., Goergen, K., Shrestha, P., Sulis, M., Rihani, J., Geimer, M., and Kollet, S. (2014). Implementation and scaling of the fully coupled Terrestrial Systems Modeling Platform (TerrSysMP v1.0) in a massively parallel supercomputing environment - a case study on JUQUEEN (IBM Blue Gene/Q). *Geoscientific Model Development*, 7(5):2531–2543.

Gedney, N. and Cox, P. M. (2003). The sensitivity of global climate model simulations to the representation of soil moisture heterogeneity. *Journal of Hydrometeorology*, 4(6):1265–1275.

Geladi, P. and Kowalski, B. R. (1986). Partial least-squares regression: a tutorial. *Analytica chimica acta*, 185:1–17.

Gentine, P., Green, J. K., Guérin, M., Humphrey, V., Seneviratne, S. I., Zhang, Y., and Zhou, S. (2019). Coupling between the terrestrial carbon and water cycles - A review. *Environmental Research Letters*, 14(8).

Germann, U., Boscacci, M., Clementi, L., Gabella, M., Hering, A., Sartori, M., Sideris, I. V., and Calpini, B. (2022). Weather Radar in Complex Orography. *Remote Sensing*, 14(3):503.

Gilgen, A., Wilkenskjeld, S., Kaplan, J. O., Kühn, T., and Lohmann, U. (2019). Effects of land use and anthropogenic aerosol emissions in the Roman Empire. *Climate of the Past*, 15(5):1885–1911.

Giorgi, F., Jones, C., Asrar, G. R., and others (2009). Addressing climate information needs at the regional level: the CORDEX framework. *World Meteorological Organization (WMO) Bulletin*, 58(3):175.

Gleeson, T., Befus, K. M., Jasechko, S., Luijendijk, E., and Cardenas, M. B. (2016). The global volume and distribution of modern groundwater. *Nature Geoscience*, 9(2):161–164.

Goergen, K. and Kollet, S. (2020). Oceanic impacts on the atmospheric water balance in a European limited area climate model ensemble. *Scientific Reports*, pages 1–13.

Graf, A., Klosterhalfen, A., Arriga, N., Bernhofer, C., Bogena, H., Bornet, F., Brüggemann, N., Brümmer, C., Buchmann, N., Chi, J., Chipeaux, C., Cremonese, E., Cuntz, M., Dušek, J., El-Madany, T. S., Fares, S., Fischer, M., Foltýnová, L., Gharun, M., Ghiasi, S., Gielen, B., Gottschalk, P., Grünwald, T., Heinemann, G., Heinesch, B., Heliasz, M., Holst, J., Hörtnagl, L., Ibrom, A., Ingwersen, J., Jurasinski, G., Klatt, J., Knohl, A., Koebsch, F., Konopka, J., Korkiakoski, M., Kowalska, N., Kremer, P., Kruijt, B., Lafont, S., Léonard, J., De Ligne, A., Longdoz, B., Loustau, D., Magliulo, V., Mammarella, I.,

Manca, G., Mauder, M., Migliavacca, M., Mölder, M., Neirynck, J., Ney, P., Nilsson, M., Paul-Limoges, E., Peichl, M., Pitacco, A., Poyda, A., Rebmann, C., Roland, M., Sachs, T., Schmidt, M., Schrader, F., Siebicke, L., Šigut, L., Tuittila, E. S., Varlagin, A., Vendrame, N., Vincke, C., Völksch, I., Weber, S., Wille, C., Wizemann, H. D., Zeeman, M., and Vereecken, H. (2020). Altered energy partitioning across terrestrial ecosystems in the European drought year 2018: Energy partitioning in the drought 2018. *Philosophical Transactions of the Royal Society B: Biological Sciences*, 375(1810).

Grayson, R. B., Moore, I. D., and McMahon, T. A. (1992). Physically based hydrologic modeling: 2. Is the concept realistic? *Water Resources Research*, 28(10):2659–2666.

Greene, H., Leighton, H. G., and Stewart, R. E. (2011). Drought and associated cloud fields over the canadian prairie provinces. *Atmosphere - Ocean*, 49(4):356–365.

Gruber, A., Scanlon, T., Schalie, R. V. D., Wagner, W., and Dorigo, W. (2019). Evolution of the ESA CCI Soil Moisture climate data records and their underlying merging methodology. *Earth System Science Data*, 11:717–739.

Guo, Z., Dirmeyer, P. A., Koster, R. D., Sud, Y. C., Bonan, G., Oleson, K. W., Chan, E., Verseghy, D., Cox, P., Gordon, C. T., and others (2006). GLACE: the global land-atmosphere coupling experiment. Part II: analysis. *Journal of Hydrometeorology*, 7(4):611–625.

Gutowski, J. W., Giorgi, F., Timbal, B., Frigon, A., Jacob, D., Kang, H. S., Raghavan, K., Lee, B., Lennard, C., Nikulin, G., O'Rourke, E., Rixen, M., Solman, S., Stephenson, T., and Tangang, F. (2016). WCRP COordinated Regional Downscaling EXperiment (CORDEX): A diagnostic MIP for CMIP6. *Geoscientific Model Development*, 9(11):4087–4095.

Hao, Z., AghaKouchak, A., Nakhjiri, N., and Farahmand, A. (2014). Global integrated drought monitoring and prediction system. *Scientific data*, 1:140001.

Hao, Z., Hao, F., and Singh, V. P. (2016). A general framework for multivariate multi-index drought prediction based on Multivariate Ensemble Streamflow Prediction (MESP). *Journal of Hydrology*, 539:1–10.

Hao, Z., Singh, V. P., and Xia, Y. (2018). Seasonal Drought Prediction: Advances, Challenges, and Future Prospects. *Reviews of Geophysics*, 56(1):108–141.

Hari, V., Rakovec, O., Markonis, Y., Hanel, M., and Kumar, R. (2020). Increased future occurrences of the exceptional 2018–2019 Central European drought under global warming. *Scientific Reports*, 10(1):1–10.

Hartick, C., Furusho-Percot, C., Clark, M. P., and Kollet, S. (2022). An Interannual Drought Feedback Loop Affects the Surface Energy Balance and Cloud Properties Geophysical Research Letters. *Geophysical Research Letters*, 49(22).

Hartick, C., Furusho-Percot, C., Goergen, K., and Kollet, S. (2021). An Interannual Probabilistic Assessment of Subsurface Water Storage Over Europe Using a Fully Coupled Terrestrial Model. *Water Resources Research*, 57(1).

Hersbach, H., Bell, B., Berrisford, P., Hirahara, S., Horányi, A., Muñoz-Sabater, J., Nicolas, J., Peubey, C., Radu, R., Schepers, D., Simmons, A., Soci, C., Abdalla, S., Abellan, X., Balsamo, G., Bechtold, P., Biavati, G., Bidlot, J., Bonavita, M., De Chiara, G., Dahlgren, P., Dee, D., Diamantakis, M., Dragani, R., Flemming, J., Forbes, R., Fuentes, M., Geer, A., Haimberger, L., Healy, S., Hogan, R. J., Hólm, E., Janisková, M., Keeley, S., Laloyaux, P., Lopez, P., Lupu, C., Radnoti, G., de Rosnay, P., Rozum, I., Vamborg, F., Villaume, S., and Thépaut, J. N. (2020). The ERA5 global reanalysis. *Quarterly Journal of the Royal Meteorological Society*, 146(730):1999–2049.

Hirschi, M., Seneviratne, S. I., Alexandrov, V., Boberg, F., Boroneant, C., Christensen, O. B., Formayer, H., Orlowsky, B., and Stepanek, P. (2011). Observational evidence for soil-moisture impact on hot extremes in southeastern Europe. *Nature Geoscience*, 4(1):17–21.

Hohenegger, C., Brockhaus, P., Bretherton, C. S., and Schär, C. (2009). The soil moisture–precipitation feedback in simulations with explicit and parameterized convection. *Journal of Climate*, 22(19):5003–5020.

Hokkanen, J., Kollet, S., Kraus, J., Herten, A., Hrywniak, M., and Pleiter, D. (2021). Leveraging HPC accelerator architectures with modern techniques — hydrologic modeling on GPUs with ParFlow. *Computational Geosciences*, 25(5):1579–1590.

Hosseini-Moghari, S. M. and Araghinejad, S. (2015). Monthly and seasonal drought forecasting using statistical neural networks. *Environmental Earth Sciences*, 74(1):397–412.

Huang, H. Y. and Margulis, S. A. (2011). Investigating the impact of soil moisture and atmospheric stability on cloud development and distribution using a coupled large-eddy simulation and land surface model. *Journal of Hydrometeorology*, 12(5):787–804.

Humphrey, V. and Gudmundsson, L. (2019). GRACE-REC: a reconstruction of climate-driven water storage changes over the last century. *Earth System Science Data Discussions*, 11(3):1153–1170.

Humphrey, V., Zscheischler, J., Ciais, P., Gudmundsson, L., Sitch, S., and Seneviratne, S. I. (2018). Sensitivity of atmospheric CO2 growth rate to observed changes in terrestrial water storage. *Nature*, 560(7720):628–631.

Huscroft, J., Gleeson, T., Hartmann, J., and Börker, J. (2018). Compiling and Mapping Global Permeability of the Unconsolidated and Consolidated Earth: GLobal HYdrogeology MaPS 2.0 (GLHYMPS 2.0). *Geophysical Research Letters*, 45(4):1897–1904.

James, E. P., Alexander, C. R., Dowell, D. C., Weygandt, S. S., Benjamin, S. G., Manikin, G. S., Brown, J. M., Olson, J. B., Hu, M., Smirnova, T. G., Ladwig, T., Kenyon, J. S.,

and Turner, D. D. (2022). The High-Resolution Rapid Refresh (HRRR): An Hourly Updating Convection-Allowing Forecast Model. Part II: Forecast Performance. *Weather and Forecasting*, 37(8):1397–1417.

Jones, J. E. and Woodward, C. S. (2001). Newton-Krylov-multigrid solvers for large-scale, highly heterogeneous, variably saturated flow problems. *Advances in Water Resources*.

Kesselheim, S., Herten, A., Krajsek, K., Ebert, J., Jitsev, J., Cherti, M., Langguth, M., Gong, B., Stadtler, S., Mozaffari, A., Cavallaro, G., Sedona, R., Schug, A., Strube, A., Kamath, R., Schultz, M. G., Riedel, M., and Lippert, T. (2021). *JUWELS Booster – A Supercomputer for Large-Scale AI Research*, volume 12761 LNCS. Springer International Publishing.

Ketabchi, H., Mahmoodzadeh, D., Ataie-Ashtiani, B., and Simmons, C. T. (2016). Sea-level rise impacts on seawater intrusion in coastal aquifers: Review and integration. *Journal of Hydrology*, 535:235–255.

Keune, J., Gasper, F., Goergen, K., Hense, A., Shrestha, P., Sulis, M., and Kollet, S. (2016). Studying the influence of groundwater representations on land surface-atmosphere feedbacks during the European heat wave in 2003. *Journal of Geophysical Research: Atmospheres*, 121(22):13301–13325.

Keune, J., Sulis, M., Kollet, S., Siebert, S., and Wada, Y. (2018). Human Water Use Impacts on the Strength of the Continental Sink for Atmospheric Water. *Geophysical Research Letters*, 45(9):4068–4076.

Keune, J., Sulis, M., and Kollet, S. J. (2019). Potential Added Value of Incorporating Human Water Use on the Simulation of Evapotranspiration and Precipitation in a Continental-Scale Bedrock-to-Atmosphere Modeling System: A Validation Study Considering Observational Uncertainty. *Journal of Advances in Modeling Earth Systems*, pages 1959–1980.

Kidd, C., Takayabu, Y. N., Skofronick-Jackson, G. M., Huffman, G. J., Braun, S. A., Kubota, T., and Turk, F. J. (2020). The global precipitation measurement (GPM) mission. In *Satellite precipitation measurement*, pages 3–23. Springer.

Kløve, B., Ala-aho, P., Bertrand, G., Boukalova, Z., Ertürk, A., Goldscheider, N., Ilmonen, J., Karakaya, N., Kupfersberger, H., Kvœrner, J., Lundberg, A., Mileusnić, M., Moszczynska, A., Muotka, T., Preda, E., Rossi, P., Siergieiev, D., Šimek, J., Wachniew, P., Angheluta, V., and Widerlund, A. (2011). Groundwater dependent ecosystems. Part I: Hydroecological status and trends. *Environmental Science and Policy*, 14(7):770–781.

Kogan, F. and Guo, W. (2015). 2006–2015 mega-drought in the western USA and its monitoring from space data. *Geomatics, Natural Hazards and Risk*, 6(8):651–668.

Kollet, S., Gasper, F., Brdar, S., Goergen, K., Hendricks-Franssen, H. J., Keune, J., Kurtz, W., Küll, V., Pappenberger, F., Poll, S., Trömel, S., Shrestha, P., Simmer, C., and Sulis,

M. (2018). Introduction of an experimental terrestrial forecasting/monitoring system at regional to continental scales based on the terrestrial systems modeling platform (v1.1.0). *Water*, 10(11).

Kollet, S. J. and Maxwell, R. M. (2006). Integrated surface-groundwater flow modeling: A free-surface overland flow boundary condition in a parallel groundwater flow model. *Advances in Water Resources*, 29(7):945–958.

Kollet, S. J. and Maxwell, R. M. (2008). Capturing the influence of groundwater dynamics on land surface processes using an integrated, distributed watershed model. *Water Resources Research*, 44(2).

Koster, R. D., Guo, Z., Bonan, G., Chan, E., and Cox, P. (2004). Regions of Strong Coupling Between Soil Moisture and Precipitation. *Science*, 305(5687):1138–1140.

Koster, R. D., Guo, Z., Dirmeyer, P. A., Bonan, G., Chan, E., Cox, P., Davies, H., Gordon, C. T., Kanae, S., Kowalczyk, E., Lawrence, D., Liu, P., Lu, C. H., Malyshev, S., McAvaney, B., Mitchell, K., Mocko, D., Oki, T., Oleson, K. W., Pitman, A., Sud, Y. C., Taylor, C. M., Verseghy, D., Vasic, R., Xue, Y., and Yamada, T. (2006). GLACE: The Global Land-Atmosphere Coupling Experiment. Part I: Overview. *Journal of Hydrometeorology*, 7(4):590–610.

Koster, R. D., Mahanama, S. P., Yamada, T. J., Balsamo, G., Berg, A. A., Boisserie, M., Dirmeyer, P. A., Doblas-Reyes, F. J., Drewitt, G., Gordon, C. T., Guo, Z., Jeong, J. H., Lawrence, D. M., Lee, W. S., Li, Z., Luo, L., Malyshev, S., Merryfield, W. J., Seneviratne, S. I., Stanelle, T., Van Den Hurk, B. J., Vitart, F., and Wood, E. F. (2010). Contribution of land surface initialization to subseasonal forecast skill: First results from a multi-model experiment. *Geophysical Research Letters*, 37(2):1–6.

Krishnamurthy, V. (2019). Predictability of Weather and Climate. *Earth and Space Science*, 6(7):1043–1056.

Kuffour, B. N., Engdahl, N., Woodward, C., Condon, L., Kollet, S., and Maxwell, R. (2019). Simulating Coupled Surface-Subsurface Flows with ParFlow v3.5.0: Capabilities, applications, and ongoing developmentof an open-source, massively parallel, integrated hydrologic model. *Geoscientific Model Development Discussions*, pages 1–66.

Kumar, M., Duffy, C. J., and Salvage, K. M. (2009). A Second-Order Accurate, Finite Volume-Based, Integrated Hydrologic Modeling (FIHM) Framework for Simulation of Surface and Subsurface Flow. *Vadose Zone Journal*, 8(4):873–890.

Kurtz, W., He, G., Kollet, S. J., Maxwell, R. M., Vereecken, H., and Franssen, H.-J. H. (2016). TerrSysMP-PDAF version 1.0): a modular high-performance data assimilation framework for an integrated land surface-subsurface model. *Geoscientific Model Development*, 9(4):1341–1360.

Lee, J. M., Zhang, Y., and Klein, S. A. (2019). The effect of land surface heterogeneity and background wind on shallow cumulus clouds and the transition to deeper convection. *Journal of the Atmospheric Sciences*, 76(2):401–419.

Levizzani, V. and Cattani, E. (2019). Satellite remote sensing of precipitation and the terrestrial water cycle in a changing climate. *Remote Sensing*, 11(19).

Li, D., Wrzesien, M. L., Durand, M., Adam, J., and Lettenmaier, D. P. (2017). How much runoff originates as snow in the western United States, and how will that change in the future? *Geophysical Research Letters*, 44(12):6163–6172.

Liu, X., He, B., Guo, L., Huang, L., and Chen, D. (2020). Similarities and Differences in the Mechanisms Causing the European Summer Heatwaves in 2003, 2010, and 2018. *Earth's Future*, 8(4):1–11.

Lo, M. H. and Famiglietti, J. S. (2010). Effect of water table dynamics on land surface hydrologic memory. *Journal of Geophysical Research Atmospheres*, 115(22):1–12.

Long, A. J. and Mahler, B. J. (2013). Prediction, time variance, and classification of hydraulic response to recharge in two karst aquifers. *Hydrology and Earth System Sciences*, 17(1):281–294.

Lumbroso, D. and Gaume, E. (2012). Reducing the uncertainty in indirect estimates of extreme flash flood discharges. *Journal of Hydrology*, 414-415:16–30.

Lyons, T. W., Reinhard, C. T., and Planavsky, N. J. (2014). The rise of oxygen in Earth's early ocean and atmosphere. *Nature*, 506(7488):307–315.

Ma, Y., Montzka, C., Bayat, B., and Kollet, S. (2020). Using Long Short-Term Memory networks to connect water table depth anomalies to precipitation anomalies over Europe. *Hydrology and Earth System Sciences Discussions*, pages 1–30.

Ma, Y., Montzka, C., Bayat, B., and Kollet, S. (2021). An Indirect Approach Based on Long Short-Term Memory Networks to Estimate Groundwater Table Depth Anomalies Across Europe With an Application for Drought Analysis. *Frontiers in Water*, 3(November):1–13.

MacLeod, D., Cloke, H., Pappenberger, F., and Weisheimer, A. (2016). Evaluating uncertainty in estimates of soil moisture memory with a reverse ensemble approach. *Hydrology and Earth System Sciences*, 20(7):2737–2743.

Madadgar, S. and Moradkhani, H. (2013). A Bayesian Framework for Probabilistic Seasonal Drought Forecasting. *Journal of Hydrometeorology*, 14(6):1685–1705.

Mahmood, R., Pielke, R. A., Hubbard, K. G., Niyogi, D., Dirmeyer, P. A., Mcalpine, C., Carleton, A. M., Hale, R., Gameda, S., Beltrán-Przekurat, A., Baker, B., Mcnider, R., Legates, D. R., Shepherd, M., Du, J., Blanken, P. D., Frauenfeld, O. W., Nair, U. S., and Fall, S. (2014). Land cover changes and their biogeophysical effects on climate. *International Journal of Climatology*, 34(4):929–953.

Majewski, D., Liermann, D., Prohl, P., Ritter, B., Buchhold, M., Hanisch, T., Paul, G., Wergen, W., and Baumgardner, J. (2002). The operational global icosahedral-hexagonal gridpoint model GME: Description and high-resolution tests. *Monthly Weather Review*, 130(2):319–338.

Marshall, J. and Plumb, R. A. (1989). *Atmosphere, ocean and climate dynamics: an introductory text*. Academic Press.

Matte, D., Larsen, M. A. D., Christensen, O. B., and Christensen, J. H. (2019). Robustness and scalability of regional climate projections over Europe. *Frontiers in Environmental Science*, 7(JAN).

Maxwell, R. M. (2013). A terrain-following grid transform and preconditioner for parallel, large-scale, integrated hydrologic modeling. *Advances in Water Resources*, 53:109–117.

Maxwell, R. M., Condon, L. E., and Melchior, P. (2021). A physics-informed, machine learning emulator of a 2d surface water model: What temporal networks and simulation-based inference can help us learn about hydrologic processes. *Water (Switzerland)*, 13(24).

Meng, X. H., Evans, J. P., and McCabe, M. F. (2014). The influence of inter-annually varying albedo on regional climate and drought. *Climate Dynamics*, 42(3-4):787–803.

Miguez-Macho, G. and Fan, Y. (2012). The role of groundwater in the Amazon water cycle: 1. Influence on seasonal streamflow, flooding and wetlands. *Journal of Geophysical Research: Atmospheres*, 117(D15):n/a–n/a.

Miralles, D. G., Gentine, P., Seneviratne, S. I., and Teuling, A. J. (2019). Land-atmospheric feedbacks during droughts and heatwaves: state of the science and current challenges. *Annals of the New York Academy of Sciences*, 1436(1):19–35.

Mishra, A. K. and Desai, V. R. (2005). Drought forecasting using stochastic models. *Stochastic Environmental Research and Risk Assessment*, 19(5):326–339.

Mu, M., Pitman, A. J., De Kauwe, M. G., Ukkola, A. M., and Ge, J. (2022). How do groundwater dynamics influence heatwaves in southeast Australia? *Weather and Climate Extremes*, 37(May):100479.

Muñoz-Sabater, J., Dutra, E., Agustí-Panareda, A., Albergel, C., Arduini, G., Balsamo, G., Boussetta, S., Choulga, M., Harrigan, S., Hersbach, H., Martens, B., Miralles, D. G., Piles, M., Rodríguez-Fernández, N. J., Zsoter, E., Buontempo, C., and Thépaut, J. N. (2021). ERA5-Land: A state-of-the-art global reanalysis dataset for land applications. *Earth System Science Data*, 13(9):4349–4383.

Nguyen, H. H., Jeong, J., and Choi, M. (2019). Extension of cosmic-ray neutron probe measurement depth for improving field scale root-zone soil moisture estimation by coupling with representative in-situ sensors. *Journal of Hydrology*, 571:679–696.

Niedda, M. (2004). Upscaling hydraulic conductivity by means of entropy of terrain curvature representation. *Water Resources Research*, 40(4):1-16.

Oleson, K. W., Dai, Y., Bonan, G. B., Bosilovich, ., Dickinson, R. E., Dirmeyer, P. A., Hoffman, F., Houser, P. R., Levis, S., Niu, G., Thornton, P., Vertenstein, M., Yang, Z., Zeng, X., Dickenson, R., Dirmeyer, P. A., Hoffman, F., and Houser, P. R. (2004). Technical Description of the Community Land Model (CLM). *NCAR Technical Note*, NCAR/TN-46:186.

Oleson, K. W., Niu, G. Y., Yang, Z. L., Lawrence, D. M., Thornton, P. E., Lawrence, P. J., Stöckli, R., Dickinson, R. E., Bonan, G. B., Levis, S., Dai, A., and Qian, T. (2008). Improvements to the community land model and their impact on the hydrological cycle. *Journal of Geophysical Research: Biogeosciences*, 113(1).

Opie, S., Taylor, R., Brierley, C., Shamsudduha, M., and Cuthbert, M. (2020). Climate-groundwater dynamics inferred from GRACE and the role of hydraulic memory. *Earth System Dynamics Discussions*, pages 1-28.

Orlanski, I. (1975). A rational subdivision of scales for atmospheric processes. *Bulletin of the American Meteorological Society*, pages 527-530.

Pal, J. S. and Eltahir, E. A. (2001). Pathways relating soil moisture conditions to future summer rainfall within a model of the land-atmosphere system. *Journal of Climate*, 14(6):1227-1242.

Papa, F., Bala, S. K., Pandey, R. K., Durand, F., Gopalakrishna, V. V., Rahman, A., and Rossow, W. B. (2012). Ganga-Brahmaputra river discharge from Jason-2 radar altimetry: An update to the long-term satellite-derived estimates of continental freshwater forcing flux into the Bay of Bengal. *Journal of Geophysical Research: Oceans*, 117(11):1-13.

Pappenberger, F. and Beven, K. J. (2006). Ignorance is bliss: Or seven reasons not to use uncertainty analysis. *Water Resources Research*, 42(5).

Parry, S., Prudhomme, C., Wilby, R. L., and Wood, P. J. (2016). Drought termination: Concept and characterisation. *Progress in Physical Geography*, 40(6):743-767.

Peters, W., Bastos, A., Ciais, P., and Vermeulen, A. (2020). A historical, geographical and ecological perspective on the 2018 European summer drought. *Philosophical transactions of the Royal Society of London. Series B, Biological sciences*, 375(1810):20190505.

Peterson, T. J., Saft, M., Peel, M. C., and John, A. (2021). Watersheds may not recover from drought. *Science*, 372(6543):745-749.

Phillips, T. J. and Klein, S. A. (2014). Land-atmosphere coupling manifested in warm-season observations on the U.S. southern great plains. *Journal of Geophysical Research Atmospheres*, 119:509-528.

Rajan, N., Maas, S. J., and Cui, S. (2015). Extreme drought effects on summer evapotranspiration and energy balance of a grassland in the Southern Great Plains. *Ecohydrology*, 8(7):1194–1204.

Ramsauer, T., Weiß, T., and Marzahn, P. (2018). Comparison of the GPM IMERG Final Precipitation Product to RADOLAN Weather Radar Data over the Topographically and Climatically Diverse Germany. *Remote Sensing*, 10(2029).

Rasheed, M. W., Tang, J., Sarwar, A., Shah, S., Saddique, N., Khan, M. U., Khan, M. I., Nawaz, S., Shamshiri, R. R., Aziz, M., and Sultan, M. (2022). Soil Moisture Measuring Techniques and Factors Affecting the Moisture Dynamics : A Comprehensive Review. *Sustainability*, 14(11538).

Rast, M., Johannessen, J., and Mauser, W. (2014). Review of understanding of Earth's hydrological cycle: Observations, theory and modelling. *Surveys in Geophysics*, 35(3):491–513.

Reichstein, M., Camps-Valls, G., Stevens, B., Jung, M., Denzler, J., Carvalhais, N., and Prabhat (2019). Deep learning and process understanding for data-driven Earth system science. *Nature*, 566(7743):195–204.

Rhee, J. and Im, J. (2017). Meteorological drought forecasting for ungauged areas based on machine learning: Using long-range climate forecast and remote sensing data. *Agricultural and Forest Meteorology*.

Ritter, B. and Geleyn, J.-F. (1992). A Comprehensive Radiation Scheme for Numerical Weather Prediction Models with Potential Applications in Climate Simulations. *Monthly Weather Review*, 120(2):303–325.

Robinson, M. and Ward, R. C. (2017). *Hydrology: principles and processes*. Iwa Publishing.

Rockel, B., Will, A., and Hense, A. (2008). The regional climate model COSMO-CLM (CCLM). *Meteorologische Zeitschrift*, 17(4):347–348.

Romps, D. M. (2017). Exact expression for the lifting condensation level. *Journal of the Atmospheric Sciences*, 74(12):3891–3900.

Rotzoll, K. and Fletcher, C. H. (2013). Assessment of groundwater inundation as a consequence of sea-level rise. *Nature Climate Change*, 3(5):477–481.

Ryu, Y., Baldocchi, D. D., Ma, S., and Hehn, T. (2008). Interannual variability of evapotranspiration and energy exchange over an annual grassland in California. *Journal of Geophysical Research Atmospheres*, 113(9):1–16.

Saadi, M., Furusho-Percot, C., Belleflamme, A., Chen, J.-Y., Trömel, S., and Kollet, S. (2023). How uncertain are precipitation and peak flow estimates for the July 2021 flooding event? *Natural Hazards and Earth System Sciences*, 23(1):159–177.

Salvatier, J., Wiecki, T. V., and Fonnesbeck, C. (2016). Probabilistic programming in Python using PyMC3. *PeerJ Computer Science*, 2:1-24.

Samaniego, L., Thober, S., Kumar, R., Wanders, N., Rakovec, O., Pan, M., Zink, M., Sheffield, J., Wood, E. F., and Marx, A. (2018). Anthropogenic warming exacerbates European soil moisture droughts. *Nature Climate Change*, 8(5):421-426.

Schalge, B., Haefliger, V., Kollet, S., and Simmer, C. (2019). Improvement of surface runoff in the hydrological model ParFlow by a scale-consistent river parameterization. *Hydrological Processes*, 33(14):2006-2019.

Schamm, K., Ziese, M., Becker, A., Finger, P., Meyer-Christoffer, A., Schneider, U., Schröder, M., and Stender, P. (2014). Global gridded precipitation over land: a description of the new GPCC First Guess Daily product. *Earth System Science Data*, 6:49-60.

Seneviratne, S. I., Corti, T., Davin, E. L., Hirschi, M., Jaeger, E. B., Lehner, I., Orlowsky, B., and Teuling, A. J. (2010). Investigating soil moisture-climate interactions in a changing climate: A review. *Earth-Science Reviews*, 99(3-4):125-161.

Shangguan, W., Hengl, T., Mendes de Jesus, J., Yuan, H., and Dai, Y. (2017). Mapping the global depth to bedrock for land surface modeling. *Journal of Advances in Modeling Earth Systems*, 9:65-68.

Sheffield, J., Wood, E. F., Chaney, N., Guan, K., Sadri, S., Yuan, X., Olang, L., Amani, A., Ali, A., Demuth, S., and Ogallo, L. (2013). A Drought Monitoring and Forecasting System for Sub-Sahara African Water Resources and Food Security. *Bulletin of the American Meteorological Society*, 95(6):861-882.

Shrestha, P., Sulis, M., Masbou, M., Kollet, S., and Simmer, C. (2014). A Scale-Consistent Terrestrial Systems Modeling Platform Based on COSMO, CLM, and ParFlow. *Monthly Weather Review*, 142(9):3466-3483.

Shukla, S., Sheffield, J., Wood, E. F., and Lettenmaier, D. P. (2013). On the sources of global land surface hydrologic predictability. *Hydrology and Earth System Sciences*, 17(7):2781-2796.

Solaraju-Murali, B., Caron, L. P., Gonzalez-Reviriego, N., and Doblas-Reyes, F. J. (2019). Multi-year prediction of European summer drought conditions for the agricultural sector. *Environmental Research Letters*, 14(12).

Soulsby, C., Scheliga, B., Neill, A., Comte, J. C., and Tetzlaff, D. (2021). A longer-term perspective on soil moisture, groundwater and stream flow response to the 2018 drought in an experimental catchment in the Scottish Highlands. *Hydrological Processes*, 35(6):1-16.

Staal, A., Flores, B. M., Aguiar, A. P. D., Bosmans, J. H., Fetzer, I., and Tuinenburg, O. A. (2020). Feedback between drought and deforestation in the Amazon. *Environmental Research Letters*, 15(4):44024.

Stampoulis, D., Reager, J. T., David, C. H., Andreadis, K. M., Famiglietti, J. S., Farr, T. G., Trangsrud, A. R., Basilio, R. R., Sabo, J. L., Osterman, G. B., Lundgren, P. R., and Liu, Z. (2019). Model-data fusion of hydrologic simulations and GRACE terrestrial water storage observations to estimate changes in water table depth. *Advances in Water Resources*, 128:13–27.

Staudinger, M. and Seibert, J. (2014). Predictability of low flow - An assessment with simulation experiments. *Journal of Hydrology*, 519(PB):1383–1393.

Stegehuis, A. I., Vautard, R., Ciais, P., Teuling, A. J., Jung, M., and Yiou, P. (2013). Summer temperatures in Europe and land heat fluxes in observation-based data and regional climate model simulations. *Climate Dynamics*, 41(2):455–477.

Stephan, K., Klink, S., and Schraff, C. (2008). Assimilation of radar-derived rain rates into the convective-scale model COSMO-DE at DWD. *Quarterly Journal of the Royal Meteorological Society*, 134(July):1315–1326.

Stern, H. and Davidson, N. E. (2015). Trends in the skill of weather prediction at lead times of 1-14 days. *Quarterly Journal of the Royal Meteorological Society*, 141(692):2726–2736.

Stumpp, C. and Kammerer, G. (2022). The Vadose Zone—A Semi-Aquatic Ecosystem. In Mehner, T. and Tockner, K., editors, *Encyclopedia of Inland Waters (Second Edition)*, pages 331–338. Elsevier, Oxford, second edi edition.

Su, H. and Dickinson, R. E. (2017). On the spatial gradient of soil moisture-precipitation feedback strength in the April 2011 drought in the southern Great Plains. *Journal of Climate*, 30(3):829–848.

Sutanto, S. J. and Van Lanen, H. A. (2022). Catchment memory explains hydrological drought forecast performance. *Scientific Reports*, 12(1):1–11.

Swenson, S. and Wahr, J. (2006). Post-processing removal of correlated errors in GRACE data. *Geophysical Research Letters*, 33(8):1–4.

Tahmasebi, P., Kamrava, S., Bai, T., and Sahimi, M. (2020). Machine learning in geo- and environmental sciences: From small to large scale. *Advances in Water Resources*, 142:103619.

Tang, Q. and Oki, T. (2016). *Terrestrial water cycle and climate change: Natural and human-induced impacts*, volume 221. John Wiley & Sons.

Tapley, B. D., Watkins, M. M., Flechtner, F., Reigber, C., Bettadpur, S., Rodell, M., Sasgen, I., Famiglietti, J. S., Landerer, F. W., Chambers, D. P., Reager, J. T., Gardner, A. S., Save, H., Ivins, E. R., Swenson, S. C., Boening, C., Dahle, C., Wiese, D. N., Dobslaw, H., Tamisiea, M. E., and Velicogna, I. (2019). Contributions of GRACE to understanding climate change. *Nature Climate Change*, 9(5):358–369.

Taylor, C. M., Parker, D. J., and Harris, P. P. (2007). An observational case study of mesoscale atmospheric circulations induced by soil moisture. *Geophysical Research Letters*, 34(15):2–7.

Teuling, A. J., Seneviratne, S. I., Williams, C., and Troch, P. A. (2006). Observed timescales of evapotranspiration response to soil moisture. *Geophysical Research Letters*, 33(23):1–5.

Tiedtke, M. (1989). A comprehensive mass flux scheme for cumulus parameterization in large-scale models.

Toreti A., Bavera D., Acosta Navarro J., Cammalleri C., de Jager A., Di Ciollo C.i, Hrast Essenfelder A., Maetens W., Masante D., Magni D., Mazzeschi M., and Spinoni J. (2022). Drought in Europe August 2022. *Publications Office of the European Union*.

Tsai, W.-P., Feng, D., Pan, M., Beck, H., Lawson, K., Yang, Y., Liu, J., and Shen, C. (2021). From calibration to parameter learning: Harnessing the scaling effects of big data in geoscientific modeling. *Nature Communications*, 12(1).

Turco, M., Ceglar, A., Prodhomme, C., Soret, A., Toreti, A., and Doblas-Reyes Francisco, J. (2017). Summer drought predictability over Europe: Empirical versus dynamical forecasts. *Environmental Research Letters*, 12(8).

Valcke, S. (2013). The OASIS3 coupler: a European climate modelling community software. *Geoscientific Model Development*, 6(2):373–388.

Van Der Ent, R. J. and Tuinenburg, O. A. (2017). The residence time of water in the atmosphere revisited. *Hydrology and Earth System Sciences*, 21(2):779–790.

Vereecken, H., Amelung, W., Bauke, S. L., Bogena, H., Brüggemann, N., Montzka, C., Vanderborght, J., Bechtold, M., Blöschl, G., Carminati, A., Javaux, M., Konings, A. G., Kusche, J., Neuweiler, I., Or, D., Steele-Dunne, S., Verhoef, A., Young, M., and Zhang, Y. (2022). Soil hydrology in the Earth system. *Nature Reviews Earth and Environment*.

Viviroli, D., Kummu, M., Meybeck, M., Kallio, M., and Wada, Y. (2020). Increasing dependence of lowland populations on mountain water resources. *Nature Sustainability*, 3(11):917–928.

Vogel, M. M., Zscheischler, J., and Seneviratne, S. I. (2018). Varying soil moisture-atmosphere feedbacks explain divergent temperature extremes and precipitation projections in central Europe. *Earth System Dynamics*, 9(3):1107–1125.

Vogt, J. V., Naumann, G., Masante, D., Spinoni, J., Cammalleri, C., Erian, W., Pischke, F., Pulwarty, R., and Barbosa, P. (2018). *Drought Risk Assessment and Management. A conceptual framework*. EUR 29464 EN, Publications Office of the European Union.

Von Asmuth, J. R. and Knotters, M. (2004). Characterising groundwater dynamics based on a system identification approach. *Journal of Hydrology*, 296(1-4):118–134.

Wada, Y., Van Beek, L. P., Wanders, N., and Bierkens, M. F. (2013). Human water consumption intensifies hydrological drought worldwide. *Environmental Research Letters*, 8(3).

Walko, R. L., Band, L. E., Baron, J., Kittel, T. G. F., Lammers, R., Lee, T. J., Ojima, D., Pielke, R. A., Taylor, C., Tague, C., Tremback, C. J., Vidale, P. L., Walko, R. L., Band, L. E., Baron, J., Kittel, T. G. F., Lammers, R., Lee, T. J., Ojima, D., Sr., R. A. P., Taylor, C., Tague, C., Tremback, C. J., and Vidale, P. L. (2000). Coupled Atmosphere-Biophysics-Hydrology Models for Environmental Modeling. *Journal of Applied Meteorology*, 39(6):931–944.

Wanner, H., Brönnimann, S., Casty, C., Gyalistras, D., Luterbacher, J., Schmutz, C., Stephenson, D., , and Xoplaki, E. (2001). NORTH ATLANTIC OSCILLATION - CONCEPTS AND STUDIES Everyone living in Europe knows that different winters have different characterist- ics . For example , the winters between 1975 and 1995 were generally mild and there was little snow in Central Europe , w. *Surveys in Geophysics*, 22(4):321–382.

Waters, C. N., Zalasiewicz, J., Summerhayes, C., Barnosky, A. D., Poirier, C., Gałuszka, A., Cearreta, A., Edgeworth, M., Ellis, E. C., Ellis, M., Jeandel, C., Leinfelder, R., McNeill, J. R., Richter, D. D. B., Steffen, W., Syvitski, J., Vidas, D., Wagreich, M., Williams, M., Zhisheng, A., Grinevald, J., Odada, E., Oreskes, N., and Wolfe, A. P. (2016). The Anthropocene is functionally and stratigraphically distinct from the Holocene. *Science*, 351(6269).

Watkins, M. M., Wiese, D. N., Yuan, D.-N., Boening, C., and Landerer, F. W. (2015). Improved methods for observing Earth's time variable mass distribution with GRACE using spherical cap mascons. *Journal of Geophysical Research: Solid Earth*, 120(4):2648–2671.

Wood, A. W. and Lettenmaier, D. P. (2008). An ensemble approach for attribution of hydrologic prediction uncertainty. *Geophysical Research Letters*, 35(14):1–5.

Wood, A. W., Maurer, E. P., Kumar, A., and Lettenmaier, D. P. (2002). Long-range experimental hydrologic forecasting for the eastern United States. *Journal of Geophysical Research: Atmospheres*, 107(20):6–1.

Wood, E. F., Sivapalan, M., Beven, K., and Band, L. (1988). Effects of spatial variability and scale with implications to hydrologic modeling. *Journal of Hydrology*, 102(1-4):29–47.

Wunsch, A., Liesch, T., and Broda, S. (2022). Deep learning shows declining groundwater levels in Germany until 2100 due to climate change. *Nature Communications*, 13(1):1–13.

Yin, J., Albertson, J. D., Rigby, J. R., and Porporato, A. (2015). Land and atmospheric controls on initiation and intensity of moist convection: CAPE dynamics and LCL crossings. *Water Resources Research*, 51:8476–8493.

York, J. P., Person, M., Gutowski, W. J., and Winter, T. C. (2002). Putting aquifers into atmospheric simulation models: an example from the Mill Creek Watershed, northeastern Kansas. *Advances in Water Resources*, 25(2):221–238.

Yuan, J., Stein, M. L., and Kopp, R. E. (2020). The Evolving Distribution of Relative Humidity Conditional Upon Daily Maximum Temperature in a Warming Climate. *Journal of Geophysical Research: Atmospheres*, 125(19).

Yuan, X., Roundy, J. K., Wood, E. F., and Sheffield, J. (2015a). Seasonal forecasting of global hydrologic extremes : System development and evaluation over GEWEX basins. *Bulletin of the American Meteorological Society*, 96(11):1895–1912.

Yuan, X., Wood, E. F., Chaney, N. W., Sheffield, J., Kam, J., Liang, M., and Guan, K. (2013a). Probabilistic Seasonal Forecasting of African Drought by Dynamical Models. *Journal of Hydrometeorology*, 14(6):1706–1720.

Yuan, X., Wood, E. F., and Ma, Z. (2015b). A review on climate-model-based seasonal hydrologic forecasting: physical understanding and system development. *Wiley Interdisciplinary Reviews: Water*, 2(5):523–536.

Yuan, X., Wood, E. F., Roundy, J. K., and Pan, M. (2013b). CFSv2-Based seasonal hydroclimatic forecasts over the conterminous United States. *Journal of Climate*, 26(13):4828–4847.

Zängl, G., Reinert, D., Rípodas, P., and Baldauf, M. (2015). The ICON (ICOsahedral Non-hydrostatic) modelling framework of DWD and MPI-M: Description of the non-hydrostatic dynamical core. *Quarterly Journal of the Royal Meteorological Society*, 141(687):563–579.

Zeng, D., Yuan, X., and Roundy, J. K. (2019). Effect of teleconnected land-atmosphere coupling on northeast China persistent drought in spring-summer of 2017. *Journal of Climate*, 32(21):7403–7420.

Zeng, X., Zhao, M., and Dickinson, R. E. (1998). Intercomparison of bulk aerodynamic algorithms for the computation of sea surface fluxes using TOGA COARE and TAO data. *Journal of Climate*, 11(10):2628–2644.

Zhang, W., Luo, M., Gao, S., Chen, W., Hari, V., and Khouakhi, A. (2021). Compound Hydrometeorological Extremes: Drivers, Mechanisms and Methods. *Frontiers in Earth Science*, 9(October):1–20.

Zhou, Q., Leng, G., and Peng, J. (2018). Recent changes in the occurrences and damages of floods and droughts in the United States. *Water (Switzerland)*, 10(9):27–30.

Zhou, S., Williams, A. P., Lintner, B. R., Berg, A. M., Zhang, Y., Keenan, T. F., Cook, B. I., Hagemann, S., Seneviratne, S. I., and Gentine, P. (2021). Soil moisture–atmosphere feedbacks mitigate declining water availability in drylands. *Nature Climate Change*, 11(January).

Zhou, Y., Wu, D., Lau, W. K., and Tao, W. K. (2016). Scale dependence of land-atmosphere interactions in wet and dry regions as simulated with NU-WRf over the southwestern and South-Central United States. *Journal of Hydrometeorology*, 17(8):2121-2136.

Zink, M., Pommerencke, J., Kumar, R., Thober, S., Samaniego, L., and Marx, A. (2016). The German Drought Monitor. *Environmental Research Letters*, 17:5625.

Zipper, S. C., Keune, J., and Kollet, S. J. (2019). Land use change impacts on European heat and drought: Remote land-atmosphere feedbacks mitigated locally by shallow groundwater. *Environmental Research Letters*.